

MAGNETOOPTICAL STUDIES OF SMALL-GAP
SEMICONDUCTORS: $\text{Hg}_{1-x}\text{Cd}_x\text{Te}$ AND InSb

by

Margaret H. Weiler

A.B., Radcliffe College (1962)

M.S., University of Maine (1964)

SUBMITTED IN PARTIAL FULFILLMENT
OF THE REQUIREMENTS FOR THE
DEGREE OF

DOCTOR OF PHILOSOPHY

at the

MASSACHUSETTS INSTITUTE OF TECHNOLOGY

June 1977

Signature of Author..... Signature redacted.....
Department of Physics, May 3, 1977

Certified by..... Signature redacted..... Signature redacted.....
Thesis Supervisors

Accepted by..... Signature redacted.....
Chairman, Departmental Committee
on Graduate Students



MAGNETOOPTICAL STUDIES OF SMALL-GAP
SEMICONDUCTORS: $\text{Hg}_{1-x}\text{Cd}_x\text{Te}$ AND InSb

by

Margaret H. Weiler

Submitted to the Department of Physics on May 3, 1977, in partial fulfillment of the requirements for the degree of Doctor of Philosophy.

ABSTRACT

Magneto-optical studies have been made of two small-gap semiconductors, $\text{Hg}_{1-x}\text{Cd}_x\text{Te}$ and InSb. For InSb we have made a group-theoretical determination of the allowed band parameters, including three not previously defined. We show that the harmonics of cyclotron resonance observed experimentally are induced by the warping and inversion asymmetry effects usually neglected in the quasi Ge model for this material.

We have performed magnetoreflexion experiments on a series of single-crystal specimens of the $\text{Hg}_{1-x}\text{Cd}_x\text{Te}$ alloy system, for alloy compositions $0.175 \leq x \leq 0.269$ in the small-gap semiconductor region. These experiments have been interpreted to yield the parameters of the quasi Ge model: $\gamma_1 = 2.5 \pm 0.4$, $\gamma_2 = -0.3 \pm 0.2$, $\gamma_3 = 0.5 \pm 0.1$, $\kappa = -1.2 \pm 0.1$ and $F = -0.7 \pm 0.3$, using $\Delta = 1$ eV, with E_g and E_p determined from a two-parameter fit to each set of data giving $E_p = 17.9 \pm 0.2$ eV and values of the energy gap which fit reasonably well to $E_g(x, T) = -0.31 + 1.88x + (1-2x) 5 \times 10^{-4} T(\text{K})$ eV at temperatures $T = 24\text{K}$ and 91K .

Thesis Supervisors:

Benjamin Lax, Professor, Department of Physics
Roshan L. Aggarwal, Senior Research Scientist, Department of Physics

TABLE OF CONTENTS

	Page
ABSTRACT.	2
TABLE OF CONTENTS.	3
LIST OF FIGURES.	5
LIST OF TABLES.	7
I. INTRODUCTION.	8
A. InSb.	8
B. $\text{Hg}_{1-x}\text{Cd}_x\text{Te}$	10
II. $\vec{k} \cdot \vec{p}$ THEORY FOR ZINCBLLENDE SEMICONDUCTORS.	16
A. Zincblende Hamiltonian to Second Order in \vec{k}	16
B. Quasi Ge Model in a Magnetic Field.	24
III. SELECTION RULES FOR WARPING AND INVERSION ASYMMETRY INDUCED CYCLOTRON-HARMONIC TRANSITIONS IN InSb.	40
A. Warping and Inversion Asymmetry Perturbations.	42
B. Selection Rules for Cyclotron Harmonic Transitions	46
C. Comparison with Experiments	56
D. Discussion.	59
IV. MAGNETOREFLECTION EXPERIMENTS ON $\text{Hg}_{1-x}\text{Cd}_x\text{Te}$	62
A. Samples.	63
B. Optical Apparatus.	68
C. Magnetoreflexion Spectra.	72
D. Fan Charts.	81
V. BAND PARAMETERS OF $\text{Hg}_{1-x}\text{Cd}_x\text{Te}$	106
A. Parameter Fitting Techniques	107

TABLE OF CONTENTS (continued)

	Page
B. Determination of γ_1 , γ_2 , γ_3 , and κ	111
C. Determination of E_g , E_p and F	115
D. Discussion.	119
VI. CONCLUSION	129
APPENDIX A. PARAMETER ESTIMATES	131
B. DERIVATIVES OF TRANSITION ENERGIES	139
C. COMPUTER PROGRAMS	143
ACKNOWLEDGEMENTS	186
BIOGRAPHICAL NOTE	187

LIST OF FIGURES

	Page
Fig. I-1	Hg _{1-x} Cd _x Te Bands at the Γ Point 11
Fig. II-1	Zincblende Semiconductor Energy Bands 17
Fig. II-2	Coordinate Transformation in a Magnetic Field \vec{H} 26
Fig. II-3	Intra-conduction-band Transitions 36
Fig. II-4	Interband Transitions 37
Fig. IV-1	Hg _{1-x} Cd _x Te Cuton Wavelength vs. Alloy Composition 65
Fig. IV-2	Spectrophotometer Curves for Samples 804 and 805 66
Fig. IV-3	Optical Apparatus for Magnetoreflexion 69
Fig. IV-4	Calculated Magnetoreflexion Spectra 71
Fig. IV-5	Magnetoreflexion Spectra for InSb 73
Fig. IV-6	Magnetoreflexion Spectra for Hg _{.787} Cd _{.213} Te, T = 24K 74
Fig. IV-7	Magnetoreflexion Spectra for Hg _{.787} Cd _{.213} Te, T = 91 K 75
Fig. IV-8	Magnetoreflexion Spectra for InSb, $\vec{H} \parallel [001]$ 76
Fig. IV-9	Magnetoreflexion Spectra for InSb, $\vec{H} \parallel [111]$ 77
Fig. IV-10	Magnetoreflexion Spectra for Hg _{.78} Cd _{.22} Te, $\vec{H} \parallel [001]$ 78
Fig. IV-11	Magnetoreflexion Spectra for Hg _{.789} Cd _{.211} Te, $\vec{H} \parallel [111]$ 79
Figs. IV-12a - 12t.	Fan Charts for Hg _{1-x} Cd _x Te Samples 82
Figs. IV-13a - 13b.	Fan Charts for InSb 103

LIST OF FIGURES (continued)

		Page
Fig. V-1	Determination of $E[a^-(1)] - E[a^-(3)]$	113
Fig. V-2	Determination of F	116
Fig. V-3	E_p vs. x for $Hg_{1-x}Cd_xTe$	121
Fig. V-4	Energy Gap vs. x for $Hg_{1-x}Cd_xTe$	123
Fig. V-5	Conduction Band-edge Effective Mass vs. x . . .	124
Fig. V-6	Conduction Band-edge g-Factor vs. x	125

LIST OF TABLES

		Page
II-1	Comparison of Basis States with Previous Work . . .	20
II-2	Parameters of the $\vec{k} \cdot \vec{p}$ Hamiltonian among the Γ_6 , Γ_7 and Γ_8 Band-edge States	23
II-3	$\vec{k} \cdot \vec{p}$ Hamiltonian for a Zincblende Semiconductor	25
II-4	Rotation matrix U for the Coordinate Trans- formation in Fig. II-2	28
II-5	The Quasi Ge Model Hamiltonians	30
III-1	Perturbation Hamiltonian	43
III-2	Matrices for the Inversion Asymmetry Parameter G	47
III-3	Matrices for the Inversion Asymmetry Parameter N_2	48
III-4	Matrices for the Inversion Asymmetry Parameter N_3	49
III-5	Couplings among the Quasi Ge States	53
III-6	Intra-conduction-band Transitions in InSb.	55
III-7	Comparison of the Selection Rules with Experiment	57
IV-1	Physical and Electrical Characteristics of $\text{Hg}_{1-x}\text{Cd}_x\text{Te}$ Samples	64
V-1	Interband Transitions Identified for $\text{Hg}_{1-x}\text{Cd}_x\text{Te}$	108
V-2	Results for the Heavy-hole Mass Parameter γ_H	114
V-3	E_g and E_p for $\text{Hg}_{1-x}\text{Cd}_x\text{Te}$ Samples at $T=24\text{K}$	117
V-4	E_g and E_p for $\text{Hg}_{1-x}\text{Cd}_x\text{Te}$ Samples at $T=91\text{K}$	118

I. INTRODUCTION

This thesis investigation has been concerned with two materials, $\text{Hg}_{1-x}\text{Cd}_x\text{Te}$ and InSb , which belong to the class of materials known as the small-gap semiconductors. Such materials are of technological interest because the conduction electrons have very small effective masses and large g -factors and, consequently, have large mobilities and, among other interesting properties, large cross sections for spin-flip Raman scattering. The semiconductors in this class which crystallize in the zincblende structure, as do $\text{Hg}_{1-x}\text{Cd}_x\text{Te}$ and InSb , are of interest for detector applications because of their direct energy gaps, at the center of the Brillouin zone, and because of the high purity with which they can be grown.

A. InSb

InSb is a compound III-V semiconductor which has for some time been a prototype of both small-gap and zincblende semiconductors. It is available in samples of extremely high quality. It is used for the detection of infrared and far infrared radiation,¹ and is the material most used for the spin-flip Raman laser.² It is perhaps the most-studied semiconductor (with the exception of Ge), starting with the early cyclotron resonance experiments,³ and culminating with the work of Pidgeon and Brown⁴ and Pidgeon and Groves.⁵ They developed a theoretical model for the energies of the conduction and valence bands in an applied magnetic field in terms of a number of adjustable parameters. They used the results of their interband magnetoabsorption, magnetoreflexion and Faraday rotation experiments to determine these parameters. Although there are discrepancies between the values of the parameters obtained from these interband measurements and those obtained from intra-conduction-band^{6,7}

and intra-valence-band⁸ cyclotron resonance experiments, the validity of the model is generally accepted.

An important exception has been the observation in InSb of a number of harmonics of the conduction band cyclotron resonance transition, most recently by Favrot, Aggarwal and Lax.⁹ Although in principle these could have been understood in terms of the so-called warping effects first studied in Ge,¹⁰ and the inversion asymmetry effects which are important for zincblende materials,^{11,12} the only calculation of the selection rules for these transitions¹³ was restricted to one orientation of magnetic field with respect to the crystal axes and did not agree with the earlier experiments in unspecified orientations.¹⁴ These effects were shown by Pidgeon and Groves⁵ to induce extra interband transitions, primarily in the [111] orientation, which they used to determine the small warping and inversion asymmetry parameters. The anisotropy of the cyclotron harmonic transitions was finally emphasized by the experiments of Favrot et al.,⁹ in the three orientations [001], [110] and [111].

The objective of our study of InSb was a theoretical determination of the selection rules for these cyclotron harmonic transitions, with the ultimate objective being a determination of the parameters of the warping and inversion asymmetry effects from a comparison of the theoretical and experimental intensities. Our investigation has demonstrated that these harmonic transitions are, indeed, induced by the warping and inversion asymmetry effects, with absorption strengths of the correct order of magnitude. The selection rules agree with the experiments of Favrot et al.⁹ except for one unpredicted experimental transition. Because of this exception, we have not attempted a detailed determination of the warping and inversion asymmetry parameters. This must await an understanding of this extra transition, and would be facilitated by more

careful studies of the absorption strengths.

In the course of our investigation we found that the model of Pidgeon and Brown⁴ was incomplete; we have made a group-theoretical analysis including the full effects of electron spin, and have found three new parameters, including two inversion asymmetry parameters. Thus our investigation has laid the groundwork for further refinements of our understanding of the zincblende semiconductors.

B. $\text{Hg}_{1-x}\text{Cd}_x\text{Te}$

$\text{Hg}_{1-x}\text{Cd}_x\text{Te}$ denotes a system of ternary alloys of the II-VI materials HgTe and CdTe. These all form single crystals in the zincblende structure, with a lattice parameter which varies slightly, and nearly linearly, from 6.46 Å at $x = 0$ (HgTe) to 6.48 Å at $x = 1$ (CdTe). These alloys are of particular interest because the energy gap varies with alloy composition as illustrated in Fig. I-1. For $x \geq 0.17$ (depending on the temperature) the bands have the normal structure of a zincblende semiconductor such as InSb, with a Γ_6 conduction band, a degenerate Γ_8 valence band and a Γ_7 split-off band; CdTe has a rather large energy gap $E_g \approx 1.6$ eV. For $x \leq 0.16$ the Γ_6 band is submerged below the Γ_8 band which now becomes both the conduction and valences bands which are degenerate at $\vec{k} = 0$. This band structure was established for HgTe by Groves, Brown and Pidgeon,¹⁵ with an energy "gap" $E_g \equiv E(\Gamma_6) - E(\Gamma_8) \approx -0.3$ eV.

For $x \geq 0.16$ $\text{Hg}_{1-x}\text{Cd}_x\text{Te}$ forms a truly "small-gap" semiconductor, with arbitrarily small gap and band-edge effective mass. For a given application, one can select the best material, for example, for detectors with a given response curve,^{16, 17} by growing material with the appropriate alloy composition.

Another important application for this variable gap is the spin-flip Raman laser.²

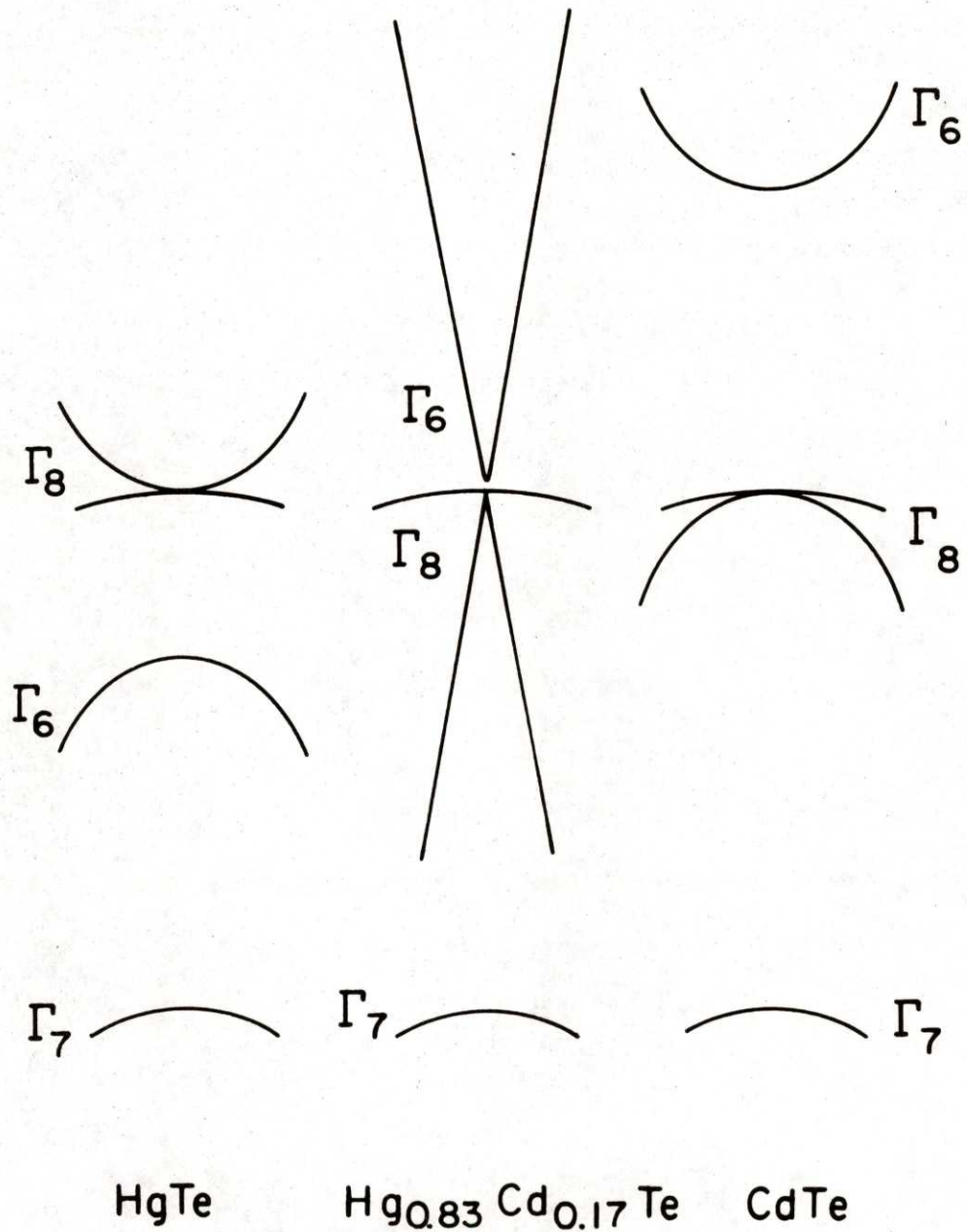


Fig. I-1. $\text{Hg}_{1-x}\text{Cd}_x\text{Te}$ bands at the Γ point.

The cross section for electronic Raman scattering is resonant when the laser pump photon energy is near the band gap energy,^{18, 19} and since the CO₂ laser is a powerful source of infrared radiation, Hg_{1-x}Cd_xTe chosen with a gap at about 10 μm, in a spin-flip Raman laser, may prove to be an extremely intense source of tunable infrared radiation.²⁰

The fundamental properties of Hg_{1-x}Cd_xTe alloys were reviewed by Harman.²¹ More recently, the energy gap was shown to vary almost linearly with x and with temperature by Schmit and Stelzer¹⁷ from detector cutoff wavelengths. However, their data show deviations from their fitted curves for sample temperatures below 100 K and for energy gaps below 100 meV. Magneto-optical studies have been made for a few values of alloy composition: interband magnetoreflexion for $x = 0.16$ ²² and 0.17 ,²³ and intra-conduction-band cyclotron and combined resonance for $x = 0.203$ ²⁴ and 0.204 .²⁵ Values of the energy gap deduced from these experiments tended to be somewhat lower than those found by Schmit and Stelzer,¹⁷ and values of the interband coupling energy E_p ranged from about 17 to 20 eV. A knowledge of these parameters is necessary to predict the electronic properties of these alloys for a given application. Until the recent work of Guldner et al.,²⁶ no attempt had been made to determine other parameters, such as the higher-band effective mass parameters, for this material.

The objective of our study of the Hg_{1-x}Cd_xTe system was to make a systematic determination of the band parameters, especially the energy gap, over a range of alloy compositions spanning the small-gap semiconductor region which is of technological interest. We have carried out interband magnetoreflexion measurements on ten specimens of Hg_{1-x}Cd_xTe, with $0.175 \leq x \leq 0.269$, at both liquid helium (4 K) and liquid nitrogen (77 K) temperatures. We have obtained band parameters by fitting transition energies calculated using the

theoretical model developed for InSb, to the positions of our magnetorefectivity peaks. Our results include more accurate and systematic values for E_g and E_p , as well as improved values for most of the higher-band parameters.

During the course of our investigation we became aware of similar work by Guldner et al.,²⁶ who carried out magnetoabsorption experiments for $0 < x < 0.3$. They deduce quite different values for E_p and the valence band parameters. They do not give their results as a function of alloy composition, only of E_g , and most of their results are for the semimetallic region ($E_g < 0$). We will give a detailed comparison of our results with those of Guldner et al.²⁶

We were unable to observe any extra transitions induced by warping and inversion asymmetry, such as were used by Pidgeon and Groves⁵ to determine these parameters for InSb. The accuracy of our results was limited by the inhomogeneity of the alloy composition of our samples, which caused our reflectivity lines to be broad. More accurate results must await improvements in the techniques for growing this material.

This thesis is divided into six Chapters. In Chapter II we give the basic theory for zincblende semiconductors, developing the quasi Ge model which we will use for both InSb and $\text{Hg}_{1-x}\text{Cd}_x\text{Te}$. In Chapter III we present our results for InSb, using the terms usually neglected in the quasi Ge model as perturbations which induce the cyclotron harmonic transitions. In Chapter IV we describe our experiments on $\text{Hg}_{1-x}\text{Cd}_x\text{Te}$, which we analyze in terms of the quasi Ge model in Chapter V. Chapter VI includes a summary of our results and suggestions for future work.

REFERENCES

1. K.F. Hulme, in Materials used in Semiconductor Devices, C.A. Hogarth, ed. (Interscience Publishers, New York, 1965), p. 115.
2. C.K.N. Patel and E.D. Shaw, *Phys. Rev. Letters* 24, 451 (1970).
3. G. Dresselhaus, A.F. Kip, C. Kittel and G. Wagoner, *Phys. Rev.* 98, 556 (1955).
4. C.R. Pidgeon and R.N. Brown, *Phys. Rev.* 146, 575 (1966).
5. C.R. Pidgeon and S.H. Groves, *Phys. Rev.* 186, 824 (1969).
6. E.J. Johnson and D.H. Dickey, *Phys. Rev.* B1, 2676 (1970).
7. B.D. McCombe, S.G. Bishop and R. Kaplan, *Phys. Rev. Letters* 18, 748 (1967).
8. R. Ranvaud, Ph.D. Thesis, Brown University (1973).
9. G.F. Favrot, R.L. Aggarwal and B. Lax, *Solid State Commun.* 18, 577 (1976).
10. R.N. Dexter, H.J. Zeiger and B. Lax, *Phys. Rev.* 104, 637 (1956);
H.J. Zeiger, B. Lax and R.N. Dexter, *Phys. Rev.* 105, 495 (1957).
11. G. Dresselhaus, *Phys. Rev.* 100, 580 (1955).
12. E.O. Kane, *J. Phys. Chem. Solids* 1, 249 (1957).
13. R.L. Bell and K.T. Rogers, *Phys. Rev.* 152, 746 (1966).
14. M.H. Weiler, R.L. Aggarwal and B. Lax, *Solid State Commun.* 14, 299 (1974).
15. S.H. Groves, R.N. Brown and C.R. Pidgeon, *Phys. Rev.* 161, 779 (1967).
16. P.W. Kruse, *Appl. Optics* 4, 687 (1965).
17. J.L. Schmit and E.L. Stelzer, *J. Appl. Phys.* 40, 4865 (1969).
18. P.A. Wolff, *Phys. Rev. Letters* 16, 225 (1966); Y. Yafet, *Phys. Rev.* 152, 858 (1966).

19. A. Mooradian, S.R.J. Brueck and F.A. Blum, *Appl. Phys. Letters* 17, 481 (1970).
20. J.P. Sattler, B.A. Weber and J. Nemanich, *Appl. Phys. Letters* 25, 491 (1974).
21. T.C. Harman, in Physics and Chemistry of II-VI Compounds, M. Aven and J.S. Prener, eds. (Wiley, New York, 1967), p. 769.
22. A.J. Strauss, T.C. Harman, J.G. Mavroides, D.H. Dickey and M.S. Dresselhaus, Report of the International Conference on the Physics of Semiconductors, A.C. Strickland, ed. (The Institute of Physics and The Physical Society, London, 1962), p. 703.
23. S.H. Groves, T.C. Harman and C.R. Pidgeon, *Solid State Commun.* 9, 451 (1971).
24. B.D. McCombe, R.J. Wagner and G.A. Prinz, *Solid State Commun.* 8, 1687 (1970).
25. M.A. Kinch and D.D. Buss, *J. Phys. Chem. Solids Suppl.* 32, 461 (1971).
26. Y. Guldner, C. Rigaux, A. Mycielski and Y. Couder, Proc. 13th International Conf. on the Physics of Semiconductors, F.G. Fumi, ed. (Tipographia Marves, Rome, 1976), p. 1175.

II. $\vec{k} \cdot \vec{p}$ THEORY FOR ZINCBLLENDE SEMICONDUCTORS

In this Chapter we develop a method for calculating the conduction and valence band energies for the small-gap zincblende semiconductors. The $\vec{k} \cdot \vec{p}$ Hamiltonian is obtained in Sec. A to second order in \vec{k} and to first order in the applied magnetic field \vec{H} , as a matrix coupling the Γ_6 ($J=1/2$) conduction band, the Γ_8 ($J=3/2$) light and heavy hole bands, and the Γ_7 ($J=1/2$) spin-orbit split-off valence band. This is developed in Sec. B into the quasi Ge model which enables one to make numerical calculations for the energies of the conduction and valence band Landau levels in a magnetic field. These energies will be compared in Chapt. V with the results of our magnetoreflexion experiments on $\text{Hg}_{1-x}\text{Cd}_x\text{Te}$. This model is obtained by neglecting a number of small terms, proportional to the so-called warping and inversion asymmetry parameters, which are shown in Chapt. III to induce the cyclotron harmonic transitions which have been observed in InSb.

A. Zincblende Hamiltonian to Second Order in \vec{k}

In order to obtain the $\vec{k} \cdot \vec{p}$ matrix Hamiltonian for a zincblende semiconductor, that is for the set of coupled bands illustrated in Fig. II-1, there have been two different approaches based on group-theoretical techniques. In the first approach^{1,2} one finds interband matrix elements $\vec{p}_{\alpha\beta}$ of the $\vec{k} \cdot \vec{p}$ perturbation Hamiltonian $\hbar\vec{k} \cdot \vec{p}_{\alpha\beta}/m$, and also of the spin-orbit Hamiltonian. For the case of InSb, Kane² enumerated all possible combinations of these matrix elements to second order in \vec{k} among the single-group basis states transforming as Γ_1 (conduction band S) and Γ_4 (valence bands X, Y and Z) of the T_d group. The first order matrix elements $\vec{p}_{\alpha\beta}$, and second-order combinations involving intermediate states belonging to different representations

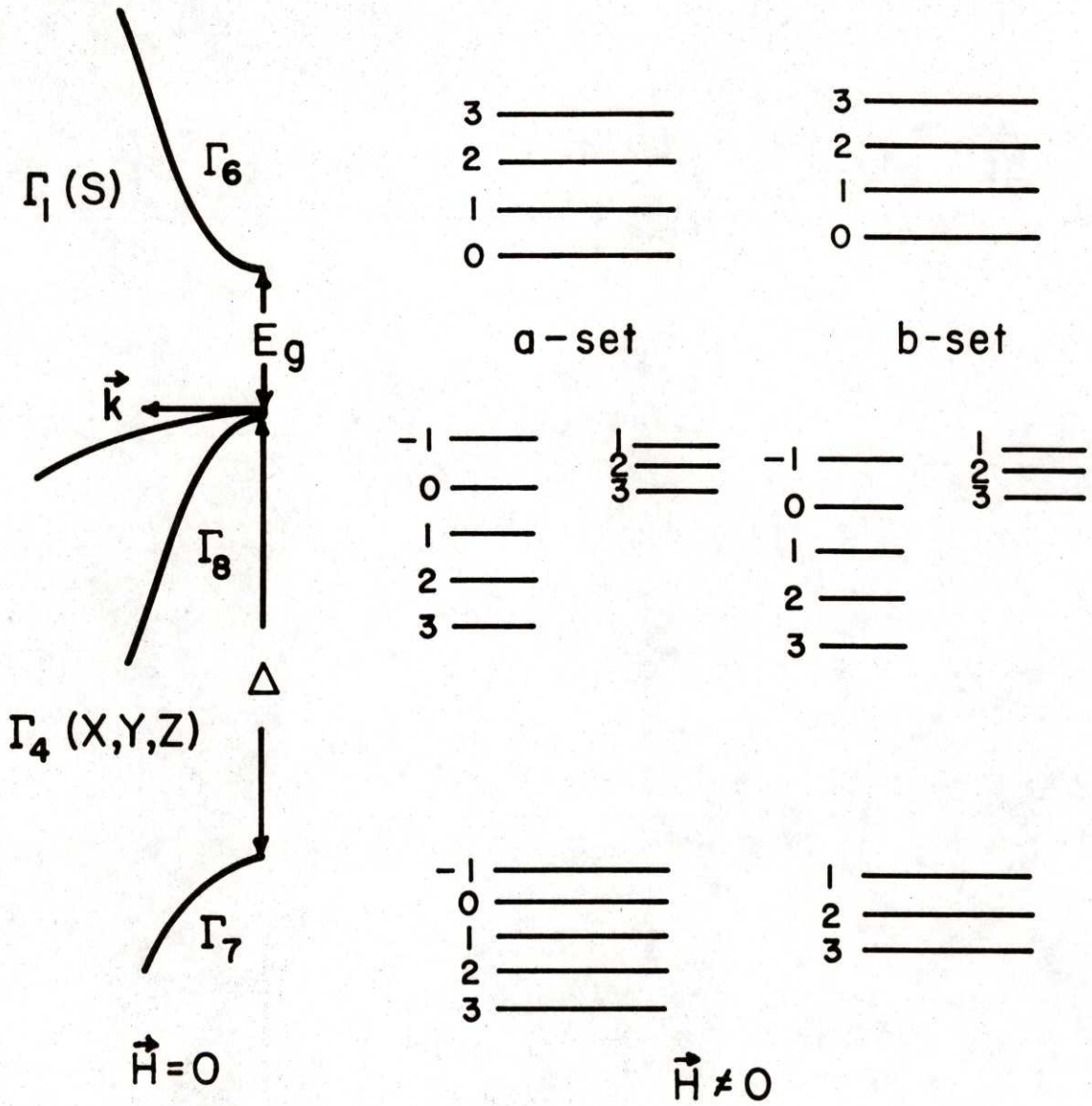


Fig. II-1. Zincblende semiconductor energy bands, illustrating the dependence on crystal momentum \vec{k} ($\vec{H}=0$) and, in an applied magnetic field \vec{H} , the coupled sets of Landau levels in the quasi Ge model.

of the T_d single group, were adjustable parameters of the perturbation Hamiltonian. This Hamiltonian was expressed in terms of linear combinations of the functions X, Y, and Z and of the spin-functions \uparrow and \downarrow , which diagonalize the spin-orbit interaction. This Hamiltonian involves matrix elements coupling the various basis states including adjustable parameters multiplying functions to second order in \vec{k} . A second approach to obtaining this Hamiltonian was made by Luttinger,³ who used a group-theoretical analysis to find all allowed matrix elements of \vec{k} and $\vec{k} \times \vec{k}$ among the valence band states transforming as the Γ_8 representation of the double group. His result involved adjustable parameters which were linear combinations of those of Kane,² but included an additional parameter, q, which is non-zero only in the presence of spin-orbit splittings of the intermediate states. Luttinger's results were extended by Roth et al.⁴ to include the Γ_7 split-off band. Pidgeon and Brown⁵ included the Γ_6 conduction band in their analysis, combining the results of Kane and of Roth et al. The use of this model in the analysis of magneto-optical investigations was reviewed in detail by Aggarwal.⁶

In this Chapter we use the second approach to obtain a complete set of parameters for the coupled Γ_6 , Γ_7 and Γ_8 bands and find three new parameters in addition to those of Refs. 2 and 4, which have the same origin as Luttinger's parameter q.³ Our group theoretical treatment makes use of the Koster, Dimmock, Wheeler and Statz (KDWS) tables of coupling coefficients.⁷ Although their basis functions are not stated explicitly, we find these by comparing our resulting matrix with those of Refs. 2 and 4. This set of basis functions is given below, in terms of the basis functions used by Kane.²

a-set

$$|1\rangle = \psi_{1/2, 1/2}^6 = S\uparrow$$

$$|3\rangle = \psi_{3/2, 3/2}^8 = -\frac{i}{\sqrt{2}} (X + iY)\uparrow$$

$$|5\rangle = \psi_{3/2, -1/2}^8 = \frac{i}{\sqrt{6}} [(X - iY)\uparrow + 2Z\downarrow]$$

$$|7\rangle = \psi_{1/2, -1/2}^7 = -\frac{i}{\sqrt{3}} [(X - iY)\uparrow - Z\downarrow]$$

b-set

(II-1)

$$|2\rangle = \psi_{1/2, -1/2}^6 = S\downarrow$$

$$|6\rangle = \psi_{3/2, 1/2}^8 = -\frac{i}{\sqrt{6}} [(X + iY)\downarrow - 2Z\uparrow]$$

$$|4\rangle = \psi_{3/2, -3/2}^8 = \frac{i}{\sqrt{2}} (X - iY)\downarrow$$

$$|8\rangle = \psi_{1/2, 1/2}^7 = -\frac{i}{\sqrt{3}} [(X + iY)\downarrow + Z\uparrow]$$

In Table II-1 this set is compared to those used in previous work. The states $|3\rangle$, $|4\rangle$, $|5\rangle$ and $|6\rangle$ are the same, except for an overall factor of $(-i)$, as those used by Pidgeon and Groves.⁸ These four states form a representation of the $J = 3/2(\Gamma_8)$ valence band, and, as stated by Pidgeon and Groves, the $4 \times 4 \vec{k} \cdot \vec{p}$ matrices involving these states agree with those given by Luttinger.³ The valence band states are equal to those of Eqs. (23) and (A-3) of Roth, Lax and Zwerdling⁴ except for an overall factor of $(-i)$ and an additional factor of (-1) in states $|4\rangle$ and $|6\rangle$, so that our a-set matrices for the valence band (states $|3\rangle$, $|5\rangle$ and $|7\rangle$) will agree with the equations in the Appendix of Ref. 4, but the b-set matrix will have opposite signs in the off-diagonal elements of the last

TABLE II-1. Comparison of the basis states with previous work. For the last column, $\alpha = \exp(i\pi/8)$ and the states v_1 through v_8 comprise the basis set of Ref. 6 after the transformations in Eqs. (73-77) of Ref. 6.

	PRESENT WORK	REFERENCE				
		8	4	9	5	6
a-set	$ 1\rangle$			θ_1^π	$u_{1,0}(\vec{r})$	$\alpha^2 v_1$
	$ 3\rangle$	$-i u_{3,0}(\vec{r})$	$-i u_{1,0}$	θ_3^π	$-i u_{3,0}(\vec{r})$	$\alpha^2 v_3$
	$ 5\rangle$	$-i u_{5,0}(\vec{r})$	$-i u_{2,0}$	θ_5^π	$i u_{5,0}(\vec{r})$	$-\alpha^2 v_5$
	$ 7\rangle$		$-i u_{6,0}$	θ_7^π	$u_{7,0}(\vec{r})$	$\alpha^2 v_7$
b-set	$ 2\rangle$			θ_2^π	$-i u_{2,0}(\vec{r})$	$\alpha^2 v_2$
	$ 6\rangle$	$-i u_{6,0}(\vec{r})$	$i u_{3,0}$	$-\theta_6^\pi$	$-u_{6,0}(\vec{r})$	$\alpha^2 v_6$
	$ 4\rangle$	$-i u_{4,0}(\vec{r})$	$i u_{4,0}$	θ_4^π	$u_{4,0}(\vec{r})$	$-\alpha^2 v_4$
	$ 8\rangle$		$-i u_{5,0}$	θ_8^π	$-i u_{8,0}(\vec{r})$	$\alpha^2 v_8$

row and column. The states $|1\rangle$ through $|8\rangle$ are identical with a set used by Groves, Pidgeon, Ewald and Wagner,⁹ except for a factor of (-1) in state $|6\rangle$. Thus the $J = 3/2$ subset of Ref. 9 does not give the same matrices as those in Ref. 3.

Finally, the states $|1\rangle$ through $|8\rangle$ are related to those of Pidgeon and Brown⁵ and of Aggarwal⁶ as indicated in the last two columns of Table II-1. Our results for the $8 \times 8 \vec{k} \cdot \vec{p}$ Hamiltonian will be related to those of Ref. 5 by a unitary transformation. This transformation is nearly the same as the one given by Aggarwal⁶ from work by Reine.¹⁰ The resulting 4×4 matrices for the a and b sets are real. Apart from overall factors, our states differ from those of Ref. 6 by a factor of (-1) for the states $|4\rangle$ and $|5\rangle$, which gives a factor of (-1) in the off-diagonal elements in the third row and third column of each 4×4 matrix.

As can be seen from the above discussion, our basis states are not identical to those of any of the important papers on the quasi Ge model. However, it is also clear that this previous work involves several inconsistent basis sets. The considerations involved in choosing our set were: (1) to make the 4×4 matrices for the a and b sets real; (2) to agree with the widely-available KDWS tables;⁷ (3) to agree with the most extensive previous work in the quasi Ge model (a) Luttinger,³ (b) Roth, Lax and Zwerdling,⁴ (c) Pidgeon and Brown,⁵ and (d) Aggarwal.⁶ Our set satisfies (1), (2) and (3a); it differs slightly from (3b) to satisfy (2), from (3c) to satisfy (1), and from (3d) to satisfy (3a).

The character tables for the T_d group are given by Dresselhaus,¹¹ and by KDWS⁷ on p. 88. It should be pointed out that the definition of Γ_4 and Γ_5 are reversed and that the column S_4 in Ref. 17 and $I \times C_4$ in Ref. 11 should

have the same character, which means that the definitions of Γ_6 and Γ_7 are also reversed. The spin-1/2 basis set belongs to the KDWS Γ_7 or Dresselhaus Γ_6 representation. We will use the Dresselhaus notation. Using the KDWS tables of coupling coefficients for the T_d group, we find the matrices involving terms to second order in \vec{k} among these basis functions. For example, two terms in $\vec{k} \times \vec{k}$ are $F_3^1 = 2k_z^2 - k_x^2 - k_y^2$ and $F_3^2 = \sqrt{3}(k_x^2 - k_y^2)$ which belong to the two-fold Γ_3 representation. The matrix elements of these functions among the Γ_6 , Γ_7 and Γ_8 states are proportional to the complex conjugates of the table entries on p. 91 of KDWS. The resulting matrices must be Hermitian and be invariant under time reversal. These conditions require certain parameters to be either zero or else purely real or imaginary.

All the real, independent parameters found in this manner are listed in Table II-2. We find matrices for all the previously-defined parameters. The $\Gamma_8 \times \Gamma_8$ parameters $\gamma_1, \gamma_2, \gamma_3, \kappa$ and q were defined by Luttinger.³ $\gamma_1, \gamma_2, \gamma_3$ and κ were shown by Roth, Lax and Zwerdling⁴ also to involve the split-off band Γ_7 when one starts with single-group representations. In the full double-group picture the $\Gamma_7 \times \Gamma_7$ and $\Gamma_7 \times \Gamma_8$ parameters are independent of the $\Gamma_8 \times \Gamma_8$ ones and are denoted by $\gamma_1', \gamma_2', \gamma_3', \kappa'$ and κ'' . The conduction band (Γ_6) effective mass parameter F , the "linear-k" parameter C for Γ_8 and the $\Gamma_6 \times \Gamma_8$ parameters P and G were defined by Dresselhaus,¹¹ Kane² and Dresselhaus, Kip and Kittel¹ in terms of single-group basis states; the $\Gamma_6 \times \Gamma_7$ and $\Gamma_7 \times \Gamma_8$ parameters are denoted by C', P' and G' . We also obtain three new parameters, N_1, N_2 and N_3 . N_1 contributes to the conduction band g-factor, similar to κ in the valence bands; N_2 and N_3 represent additional couplings between the Γ_6 conduction band and the Γ_8 valence bands. In Appendix A we show that these new parameters, like q , arise from the

TABLE II-2. Parameters of the $\vec{k} \cdot \vec{p}$ Hamiltonian among the Γ_6 , Γ_7 and Γ_8 band-edge states.

$f(\vec{k})$	k_x			$\{k_y, k_z\}$	$i[k_y, k_z]$
	k_y	\vec{k}^2	$2k_z^2 - k_x^2 - k_y^2$	$\{k_z, k_x\}$	$i[k_z, k_x]$
	k_z		$\sqrt{3}(k_x^2 - k_y^2)$	$\{k_x, k_y\}$	$i[k_x, k_y]$
$\langle \Gamma_6 f(\vec{k}) \Gamma_6 \rangle$		F			N_1
$\langle \Gamma_8 f(\vec{k}) \Gamma_8 \rangle$	C	γ_1	γ_2	γ_3	χ, ϱ
$\langle \Gamma_7 f(\vec{k}) \Gamma_7 \rangle$		γ'_1			χ'
$\langle \Gamma_6 f(\vec{k}) \Gamma_8 \rangle$	P		N_2	G	N_3
$\langle \Gamma_6 f(\vec{k}) \Gamma_7 \rangle$	P'			G'	
$\langle \Gamma_7 f(\vec{k}) \Gamma_8 \rangle$	C'		γ'_2	γ'_3	χ''

spin-orbit splitting of higher bands.

The parameters q and $\mu = (\gamma_3 - \gamma_2)/2$ are the so-called Ge warping parameters because, if these were zero, in a material like Ge with inversion symmetry, the energy bands would be isotropic or independent of the direction of \vec{k} . The parameters C , G , N_2 and N_3 are the so-called inversion asymmetry parameters because they are zero in materials like Ge with inversion symmetry but nonzero in the zincblende materials.

The complete 8×8 matrix \mathcal{H} for the parameters listed in Table II-2 is given in Table II-3, which also includes the band-edge energies E_g and Δ relative to the Γ_8 valence band, and the parts of the free electron terms not included in the definitions of γ_1 and κ .³ Other terms used in Table II-3 are:

$$\begin{aligned}
 k^2 &\equiv k_x^2 + k_y^2 + k_z^2, \quad k^\pm \equiv k_x \pm ik_y \\
 F_3^1 &\equiv 2k_z^2 - k_x^2 - k_y^2, \quad F_3^2 \equiv \sqrt{3}(k_x^2 - k_y^2) \\
 F_4^\pm &\equiv \{k_z, k^\pm\} \equiv (k_z k^\pm + k^\pm k_z), \quad F_4^Z = \{k_x, k_y\} \\
 H_Z &= i[k_x, k_y], \quad H^\pm = \pm [k^\pm, k_z] \quad .
 \end{aligned}
 \tag{II-2}$$

For simplicity, Table II-3 is given in atomic units $\hbar = m = 1$.

B. Quasi Ge Model in a Magnetic Field

For a magnetic field \vec{H} in an arbitrary direction defined by the spherical polar angles θ and ϕ , we perform the following coordinate transformation illustrated in Fig. II-2:

TABLE II-3. $\vec{k} \cdot \vec{p}$ Hamiltonian for a zincblende semiconductor. The terms used are defined in Eqs. (II-1, 2). The upper triangle is the Hermitian conjugate of the lower triangle.

E_g					11)					
$+(F+\frac{1}{2})\vec{k}^2$										
$+(N_2+\frac{1}{2})H_z$										
$-\frac{1}{\sqrt{2}}Pk^-$	$-\frac{1}{2}\gamma_1\vec{k}^2$									
$+\frac{1}{\sqrt{2}}GF_4^+$	$+\frac{1}{2}\gamma_2F_3^2$				13)					
$+\frac{1}{2}N_3H^+$	$-\frac{3}{2}(\alpha+\frac{7}{8})H_z$									
$-\frac{1}{\sqrt{6}}Pk^+$	$\frac{1}{2}\gamma_2F_3^2$	$-\frac{1}{2}\gamma_1\vec{k}^2$								
$+\frac{1}{\sqrt{6}}GF_4^-$	$+\frac{i\sqrt{3}}{2}\gamma_3F_4^2$	$-\frac{1}{2}\gamma_2F_3^2$			15)					
$+\frac{\sqrt{3}}{2}N_3H^-$	$+Ck_z$	$+\frac{1}{2}(\alpha+\frac{7}{8})H_z$								
$\frac{1}{\sqrt{3}}P'k^+$	$\frac{1}{\sqrt{2}}\gamma_2'F_3^2$	$-\frac{1}{\sqrt{2}}\gamma_2'F_3^2$	$-\Delta$							
$-\frac{1}{\sqrt{3}}G'F_4^-$	$-i\frac{\sqrt{3}}{2}\gamma_3'F_4^2$	$-\frac{1}{\sqrt{2}}(\alpha+1)H_z$	$-\frac{1}{2}\gamma_1'\vec{k}^2$							
	$+\frac{1}{\sqrt{2}}C'k_z$	$+(\alpha+\frac{1}{2})H_z$			17)					
$(N_2+\frac{1}{2})H^+$	$N_2F_3^2$	$-\frac{\sqrt{3}}{3}Pk_z$	$-\frac{1}{\sqrt{3}}P'k_z$	E_g						
	$+N_3H_z$	$+i\frac{\sqrt{3}}{3}GF_4^2$	$+\frac{i}{\sqrt{3}}G'F_4^2$	$+(F+\frac{1}{2})\vec{k}^2$						
		$-N_2F_3^2$	$+\frac{1}{\sqrt{3}}G'F_4^2$	$-(N_2+\frac{1}{2})H_z$						
$-\frac{\sqrt{3}}{3}Pk_z$	$\frac{\sqrt{3}}{2}\gamma_3F_4^+$	$\frac{\sqrt{3}}{2}Ck^+$	$\frac{3}{\sqrt{8}}\gamma_3'F_4^-$	$\frac{1}{\sqrt{6}}Pk^-$	$-\frac{1}{2}\gamma_1\vec{k}^2$					
$-i\frac{\sqrt{3}}{3}GF_4^2$	$-\frac{1}{2}Ck^-$	$-(\alpha+\frac{5}{8})H^-$	$-\frac{\sqrt{3}}{8}C'k^+$	$+\frac{1}{\sqrt{6}}GF_4^+$	$-\frac{1}{2}\gamma_2F_3^2$					
$+N_2F_3^2$	$-\frac{\sqrt{3}}{2}(\alpha+\frac{7}{8})H^+$	$+\frac{1}{\sqrt{8}}(\alpha+1)H^-$	$-\frac{\sqrt{3}}{2}N_3H^+$	$-\frac{\sqrt{3}}{2}N_3H^+$	$-\frac{1}{2}(\alpha+\frac{7}{8})H_z$					
$-N_2F_3^2$	$-\frac{\sqrt{3}}{2}Ck^+$	$-\frac{\sqrt{3}}{2}\gamma_3F_4^+$	$-\frac{\sqrt{3}}{8}\gamma_3'F_4^+$	$-\frac{1}{\sqrt{2}}Pk^+$	$\frac{1}{2}\gamma_2F_3^2$	$-\frac{1}{2}\gamma_1\vec{k}^2$				
$+N_3H_z$	$-\frac{3}{4}qH^-$	$-\frac{1}{2}Ck^-$	$-\frac{1}{\sqrt{8}}C'k^-$	$+\frac{1}{\sqrt{2}}GF_4^-$	$i\frac{\sqrt{3}}{2}\gamma_3F_4^2$	$+\frac{1}{2}\gamma_2F_3^2$				
		$-\frac{\sqrt{3}}{2}(\alpha+\frac{7}{8})H^+$	$-\frac{\sqrt{3}}{8}(\alpha+1)H^+$	$-\frac{1}{2}N_3H^-$	$-Ck_z$	$+\frac{3}{2}(\alpha+\frac{7}{8})H_z$				
$\frac{1}{\sqrt{3}}P'k_z$	$-\frac{\sqrt{3}}{8}\gamma_3'F_4^+$	$\frac{3}{\sqrt{8}}\gamma_3'F_4^-$			$\frac{1}{\sqrt{3}}P'k^-$	$\frac{1}{\sqrt{2}}\gamma_2'F_3^2$	$\frac{1}{\sqrt{2}}\gamma_2'F_3^2$	$-\Delta$		
$+\frac{i}{\sqrt{3}}G'F_4^2$	$+\frac{1}{\sqrt{8}}C'k^-$	$+\frac{1}{\sqrt{8}}C'k^+$	$-(\alpha+\frac{1}{2})H^-$	$+\frac{1}{\sqrt{3}}G'F_4^+$	$-\frac{1}{\sqrt{2}}(\alpha+1)H_z$	$-\frac{i\sqrt{3}}{2}\gamma_3'F_4^2$	$-\frac{1}{2}\gamma_1'\vec{k}^2$	$-\frac{1}{2}\gamma_2'\vec{k}^2$		
	$+\frac{\sqrt{3}}{8}(\alpha+1)H^+$	$-\frac{1}{\sqrt{8}}(\alpha+1)H^-$				$+\frac{1}{\sqrt{2}}C'k_z$	$-(\alpha+\frac{1}{2})H_z$			

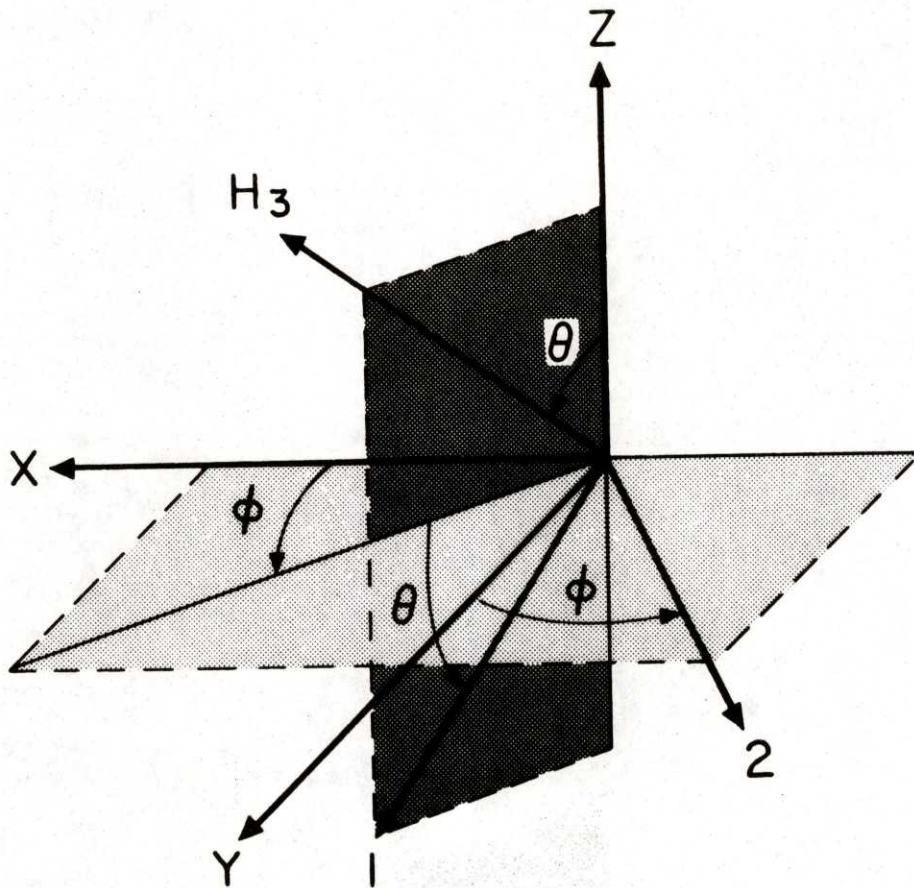


Fig. II-2. Coordinate transformation in a magnetic field \vec{H} ; (X, Y, Z) are the cubic crystal axes, and (1, 2, 3) are the new axes with $\vec{H} \parallel 3$.

$$\begin{aligned}
k_x &= \cos \theta \cos \phi k_1 - \sin \phi k_2 + \cos \phi \sin \theta k_3 \\
k_y &= \cos \theta \sin \phi k_1 + \cos \phi k_2 + \sin \phi \sin \theta k_3 \\
k_z &= -\sin \theta k_1 + \cos \theta k_3
\end{aligned} \tag{II-3}$$

A similar transformation was given by Luttinger³ for the case $\phi = 45^\circ$ which confines the magnetic field to the $(1\bar{1}0)$ crystal plane. The new coordinate axes (1, 2, 3) are shown in Fig. II-2, where the magnetic field is along the 3-axis. The corresponding rotation of the basis states results in a transformation of the $\vec{k} \cdot \vec{p}$ Hamiltonian according to $\mathcal{K}(\theta, \phi) = U^\dagger \mathcal{K} U$ where U is given in Table II-4. We then set

$$k_1 = \frac{1}{\lambda\sqrt{2}}(a + a^\dagger), \quad k_2 = \frac{i}{\lambda\sqrt{2}}(a - a^\dagger), \quad k_3 \equiv k_H \tag{II-4}$$

where $\lambda \equiv (\hbar c/eH)^{1/2}$ is the Landau radius, c is the velocity of light, $\hbar k_H$ is the component of the momentum along the direction of the applied magnetic field, and a^\dagger, a are raising and lowering operators for harmonic oscillator functions ϕ_n :

$$a^\dagger \phi_n = \sqrt{n+1} \phi_{n+1}, \quad a \phi_n = \sqrt{n} \phi_{n-1}, \tag{II-5}$$

$$N \phi_n \equiv a^\dagger a \phi_n = n \phi_n$$

and

$$[a, a^\dagger] \equiv a a^\dagger - a^\dagger a = 1 \tag{II-6}$$

TABLE II-4. Rotation matrix U for the coordinate transformation in Fig. II-2, with $S \equiv \sin \theta/2$, $C \equiv \cos \theta/2$ and $\alpha \equiv \exp(i\phi/2)$.

$C\alpha^*$	0	0	0	$-S\alpha^*$	0	0	0	11>
0	$C^3\alpha^{*3}$	$\sqrt{3}S^2C\alpha^{*3}$	0	0	$-\sqrt{3}SC^2\alpha^{*3}$	$-S^3\alpha^{*3}$	0	13>
0	$\sqrt{3}SC\alpha$	$(1-3S^2)C\alpha$	0	0	$(3C^2-1)S\alpha$	$-\sqrt{3}SC^2\alpha$	0	15>
0	0	0	$C\alpha$	0	0	0	$S\alpha$	17>
$S\alpha$	0	0	0	$C\alpha$	0	0	0	12>
0	$\sqrt{3}SC^2\alpha^*$	$-(3C^2-1)S\alpha^*$	0	0	$(1-3S^2)C\alpha^*$	$\sqrt{3}S^2C\alpha^*$	0	16>
0	$S^3\alpha^3$	$\sqrt{3}SC^2\alpha^3$	0	0	$\sqrt{3}SC\alpha^3$	$C^3\alpha^3$	0	14>
0	0	0	$-S\alpha^*$	0	0	0	$C\alpha^*$	18>

The resulting $\mathcal{K}(\theta)$ separates into two 4×4 matrices for the a and b sets

$$\mathcal{K}(\theta) \approx \begin{bmatrix} \mathcal{K}_a & 0 \\ 0 & \mathcal{K}_b \end{bmatrix} \quad (\text{II-7})$$

if one neglects terms proportional to k_H , q , C , G , N_2 and N_3 and most terms proportional to the warping parameter $\mu \equiv \frac{1}{2}(\gamma_3 - \gamma_2)$. One can include some warping by way of two valence-band effective mass parameters

$$\gamma' \equiv \gamma_3 + (\gamma_2 - \gamma_3) f(\theta, \phi) \quad (\text{II-8})$$

$$\gamma'' \equiv \frac{1}{3}\gamma_2 + \frac{2}{3}\gamma_3 + \frac{1}{6}(\gamma_2 - \gamma_3) f(\theta, \phi)$$

where

$$f(\theta, \phi) \equiv \left(\frac{3\cos^2\theta - 1}{2} \right)^2 + \frac{3}{4}\cos^2 2\phi \sin^4 \theta \quad (\text{II-9})$$

These parameters were defined previously,³ for the case $\phi = 45^\circ = \pi/4$, corresponding to the magnetic field \vec{H} in the $(1\bar{1}0)$ plane, which makes the second term in Eq. (II-9) equal to zero. The average of this term over all angles θ and ϕ is $1/5$, which is equal to that of the first term, so that $\overline{f(\theta, \phi)} = 2/5$.

The 4×4 matrices \mathcal{K}_a and \mathcal{K}_b in Eq. (II-7) are displayed in Table II-5, where the terms involving γ_1 , γ' , and γ'' in the fourth rows and columns are included in the single-group approximation $P' \approx P$, $\gamma_1' \approx \gamma_1$, etc. Also in Table II-5, P is included using the interband energy $E_p \equiv 2mP^2/\hbar^2$, and $\beta \equiv eh/2mc$ is the Bohr magneton. Table II-5 is now in ordinary energy

TABLE II-5. The quasi Ge model Hamiltonians.

 $\mathcal{H}_a:$

$$\left[\begin{array}{cccc}
 E_g + [(2N+1)F + N_2 + N + 1]2\beta H & \sqrt{\beta H E_p} a^\dagger & -\sqrt{\frac{1}{3}\beta H E_p} a & \sqrt{\frac{2}{3}\beta H E_p} a & |1\rangle \\
 \sqrt{\beta H E_p} a & -[(2N+1)(\gamma, +\gamma') + 3\kappa]\beta H & 2\sqrt{3}\gamma''\beta H a^2 & -2\sqrt{6}\gamma''\beta H a^2 & |3\rangle \\
 -\sqrt{\frac{1}{3}\beta H E_p} a^\dagger & 2\sqrt{3}\gamma''\beta H a^{+2} & -[(2N+1)(\gamma, -\gamma') - \kappa]\beta H & \sqrt{2}[(2N+1)\gamma' - \kappa - 1]\beta H & |5\rangle \\
 \sqrt{\frac{2}{3}\beta H E_p} a^\dagger & -2\sqrt{6}\gamma''\beta H a^{+2} & \sqrt{2}[(2N+1)\gamma' - \kappa - 1]\beta H & -\Delta - [(2N+1)\gamma, -2\kappa - 1]\beta H & |7\rangle
 \end{array} \right]$$

 $\mathcal{H}_b:$

$$\left[\begin{array}{cccc}
 E_g + [(2N+1)F - N_2 + N]2\beta H & \sqrt{\frac{1}{3}\beta H E_p} a^\dagger & -\sqrt{\beta H E_p} a & \sqrt{\frac{2}{3}\beta H E_p} a^\dagger & |2\rangle \\
 \sqrt{\frac{1}{3}\beta H E_p} a & -[(2N+1)(\gamma, -\gamma') + \kappa]\beta H & 2\sqrt{3}\gamma''\beta H a^2 & -\sqrt{2}[(2N+1)\gamma' + \kappa + 1]\beta H & |6\rangle \\
 -\sqrt{\beta H E_p} a^\dagger & 2\sqrt{3}\gamma''\beta H a^{+2} & -[(2N+1)(\gamma, +\gamma') - 3\kappa]\beta H & 2\sqrt{6}\gamma''\beta H a^{+2} & |4\rangle \\
 \sqrt{\frac{2}{3}\beta H E_p} a & -\sqrt{2}[(2N+1)\gamma' + \kappa + 1]\beta H & 2\sqrt{6}\gamma''\beta H a^2 & -\Delta - [(2N+1)\gamma, +2\kappa + 1]\beta H & |8\rangle
 \end{array} \right]$$

units since E_g , Δ , E_p and βH have the dimensions of energy and F , κ , N_1 and the γ 's are dimensionless.

The Hamiltonians of Table II-5 are equivalent¹² to those of Pidgeon and Brown⁵ [their Eqs. (10) and (11)] when account is taken of the different basis sets as indicated in Table II-1. Table II-5 is also equivalent to Eqs. (B-9) and (B-10) of Roth, Lax and Zwerdling⁴ for the Γ_8 and Γ_7 band energies except, as indicated in Table II-1, for a sign change in the matrix elements involving the Γ_7 , b-set state.

The solutions to the Schrödinger equations

$$\begin{aligned} \mathcal{H}_a |a\rangle &= E_a |a\rangle \\ \mathcal{H}_b |b\rangle &= E_b |b\rangle \end{aligned} \quad (\text{II-10})$$

are of the form

$$|a(n)\rangle = \begin{bmatrix} a_1^n \phi_n \\ a_3^n \phi_{n-1} \\ a_5^n \phi_{n+1} \\ a_7^n \phi_{n+1} \end{bmatrix}, \quad |b(n)\rangle = \begin{bmatrix} b_2^n \phi_n \\ b_6^n \phi_{n-1} \\ b_4^n \phi_{n+1} \\ b_8^n \phi_{n-1} \end{bmatrix} \quad (\text{II-11})$$

with $n \geq -1$ and with $a_1^{-1} = b_2^{-1} = a_3^{-1} = a_3^0 = b_6^{-1} = b_6^0 = b_8^{-1} = b_8^0 \equiv 0$. For $n \geq 1$ there are eight independent solutions $|a(n)\rangle$, $|b(n)\rangle$ for each n , which are denoted, in order of decreasing energy, conduction band [$|a^c(n)\rangle$, $|b^c(n)\rangle$], heavy hole [$|a^-(n)\rangle$, $|b^-(n)\rangle$], light hole [$|a^+(n)\rangle$, $|b^+(n)\rangle$] and split-off band [$|a^s(n)\rangle$, $|b^s(n)\rangle$]. These states are illustrated in Fig. II-1. Although a number

of authors^{3, 4, 13, 14} have given approximate analytical solutions for the states $|a(n)\rangle$, $|b(n)\rangle$ and the corresponding energies $E[a(n)]$, $E[b(n)]$, the numerical solutions obtained by Pidgeon and Brown⁵ were necessary to give an accurate fit to their interband magneto-optical experiments in InSb.

Aggarwal⁶ has given approximate solutions for the conduction and valence band energies from Eqs. (II-10), which are useful for understanding the effects of the various parameters. We have extended these to include some terms proportional to N_1 and also to q (see next Chapter). The conduction band energies are, to first order in H ,

$$\begin{aligned} E[a^c(n)] &\approx E_g + (n + \frac{1}{2})\hbar\omega_c + \frac{1}{2}g_c\beta H \\ E[b^c(n)] &\approx E_g + (n + \frac{1}{2})\hbar\omega_c - \frac{1}{2}g_c\beta H \end{aligned} \quad (\text{II-12})$$

where $\omega_c = eH/m_c c$ and

$$\begin{aligned} \frac{m}{m_c} &\equiv 1 + 2F + \frac{1}{3}E_p \left(\frac{2}{E_g} + \frac{1}{E_g + \Delta} \right) \\ g_c &\equiv 2 + 4N_1 - \frac{2}{3}E_p \left(\frac{1}{E_g} - \frac{1}{E_g + \Delta} \right) \end{aligned} \quad (\text{II-13})$$

The valence band energies are, for $n \geq 1$

$$\begin{aligned} E[a^\pm(n)] &\approx -2\beta H \left\{ (n + \frac{1}{2})\gamma_1^L - \gamma^L + \frac{1}{2}\kappa^L + (\frac{5}{8} + f)q \right. \\ &\quad \left. \pm \sqrt{[\gamma_1^L - (n + \frac{1}{2})\gamma^L - \kappa^L - \frac{1}{2}(\frac{9}{2} - f)]^2 + 3n(n+1)(\gamma^L)^2} \right\} \\ E[b^\pm(n)] &\approx -2\beta H \left\{ (n + \frac{1}{2})\gamma_1^L + \gamma^L - \frac{1}{2}\kappa^L - (\frac{5}{8} + f)q \right. \\ &\quad \left. \pm \sqrt{[\gamma_1^L + (n + \frac{1}{2})\gamma^L - \kappa^L - \frac{1}{2}(\frac{9}{2} - f)q]^2 + 3n(n+1)(\gamma^L)^2} \right\} \end{aligned} \quad (\text{II-14})$$

where $f \equiv f(\theta, \phi)$ and γ_1^L , γ'^L , etc., are the parameters originally defined by Luttinger³:

$$\begin{aligned}\gamma_1^L &\equiv \frac{1}{3} \frac{E_p}{E_g} + \gamma_1 \\ \gamma'^L &\equiv \frac{1}{6} \frac{E_p}{E_g} + \gamma' \\ \gamma''^L &\equiv \frac{1}{6} \frac{E_p}{E_g} + \gamma'' \\ \kappa^L &\equiv \frac{1}{6} \frac{E_p}{E_g} + \kappa\end{aligned}\tag{II-15}$$

For large n , the energy differences in Eqs. (II-14) are approximately equal to $E \approx -2\beta Hm/m_{\pm}$ where the effective masses for the light and heavy hole bands are given by

$$\frac{m}{m_{\pm}} = \frac{1}{3} \frac{E_p}{E_g} + \gamma_1 \pm \sqrt{\left(\frac{1}{6} \frac{E_p}{E_g} + \gamma'\right)^2 + 3\left(\frac{1}{6} \frac{E_p}{E_g} + \gamma''\right)^2}\tag{II-16}$$

For $E_p/E_g \gg \gamma', \gamma''$ this gives

$$\begin{aligned}\frac{m}{m_+} &\approx \frac{2}{3} \frac{E_p}{E_g} + \gamma_1 + \frac{1}{2}(\gamma' + 3\gamma'') \\ \frac{m}{m_-} &\approx \gamma_1 - \frac{1}{2}(\gamma' + 3\gamma'')\end{aligned}\tag{II-17}$$

Thus for large E_p/E_g the light hole band is nearly the mirror image of the conduction band (equal but opposite curvature or mass), and the heavy hole band has a large effective mass ($\sim \gamma_1^{-1}$) which is sensitive to the warping effects contained in γ' and γ'' . The conduction band effective mass and g-factor in Eqs. (II-13) contain the higher-band contributions F and N_1

which also were considered by Johnson and Dickey.¹⁵

The strongest allowed optical transitions among the states of Eqs. (II-11) are those proportional to the interband matrix element P ; that is, we find the optical perturbation \mathcal{K}'_{ω} by replacing \vec{k} by $\vec{k} + \frac{e\vec{A}}{\hbar c}$ in the matrix for P , where \vec{A} is the light vector potential in the radiation gauge. The resulting transition matrix elements are

$$\begin{aligned}
 \langle a(n') | \mathcal{K}'_{\omega} | a(n) \rangle &= \frac{eE}{\omega} \sqrt{\frac{E_p}{6m}} \left\{ [\sqrt{3} a_3^{n'} a_1^n - a_1^{n'} (a_5^n - \sqrt{2} a_7^n)] \right. \\
 &\quad \left. \cdot \hat{e}_-^{\delta_{n',n+1}} + [n \leftrightarrow n'] \hat{e}_+^{\delta_{n',n-1}} \right\} \\
 \langle b(n') | \mathcal{K}'_{\omega} | b(n) \rangle &= \frac{eE}{\omega} \sqrt{\frac{E_p}{6m}} \left\{ [(b_6^{n'} + \sqrt{2} b_8^{n'}) b_2^n - \sqrt{3} b_2^{n'} b_4^n] \right. \\
 &\quad \left. \cdot \hat{e}_-^{\delta_{n',n+1}} + [n \leftrightarrow n'] \hat{e}_+^{\delta_{n',n-1}} \right\} \\
 \langle b(n') | \mathcal{K}'_{\omega} | a(n) \rangle &= -\frac{eE}{\omega} \sqrt{\frac{E_p}{6m}} \left[b_2^{n'} (\sqrt{2} a_5^n + a_7^n) \right. \\
 &\quad \left. + (\sqrt{2} b_6^{n'} - b_8^{n'}) a_1^n \right] \hat{e}_3^{\delta_{n',n+1}}
 \end{aligned} \tag{II-18}$$

where E is the optical electric field. \hat{e}_+ and \hat{e}_- are the unit polarization vectors $(\hat{e}_1 \pm i \hat{e}_2)/\sqrt{2}$ for, respectively, right and left circular polarization σ_R, σ_L transverse to the magnetic field \vec{H} , and \hat{e}_3 is a unit polarization vector parallel to \vec{H} usually referred to as the π or $\vec{E} \parallel \vec{H}$ polarization. Thus the selection rules for both inter- and intra-band transitions (before renumbering of the valence bands) are

$$\begin{aligned}
 \sigma_L : & \quad a_n \rightarrow a_{n+1} , \quad b_n \rightarrow b_{n+1} \\
 \sigma_R : & \quad a_n \rightarrow a_{n-1} , \quad b_n \rightarrow b_{n-1} \\
 \pi : & \quad a_n \rightarrow b_{n+1} , \quad b_n \rightarrow a_{n-1}
 \end{aligned}
 \tag{II-19}$$

The selection rules for interband transitions given by Roth et al.⁴ and by Pidgeon and Brown⁵ were, for σ_L and σ_R , $\Delta n = 0$ and -2 rather than $+1$ and -1 respectively. This is because they renumbered all valence band states $n \rightarrow n+1$ so that the state numbers n correspond to the harmonic oscillator number of one of the larger terms (the coefficient of state $|5\rangle$ or $|4\rangle$ in Eqs. (II-11)). We do not renumber the valence band states, so that each set of states n are coupled in the quasi Ge model.⁹

For the intra-conduction-band transitions illustrated in Fig. II-3, the σ_L transition occurs at the cyclotron frequency $\omega \approx \omega_c$, and the π transition at the "combined resonance" frequency $\omega \approx \omega_c + \omega_s$,¹⁶ where ω_s is the spin-flip frequency given by $\hbar\omega_s = g_c\beta H$. The interband transitions illustrated in Fig. II-4 occur as series of oscillations corresponding to transitions from the light- and heavy-hole ladders to the conduction band ladders.

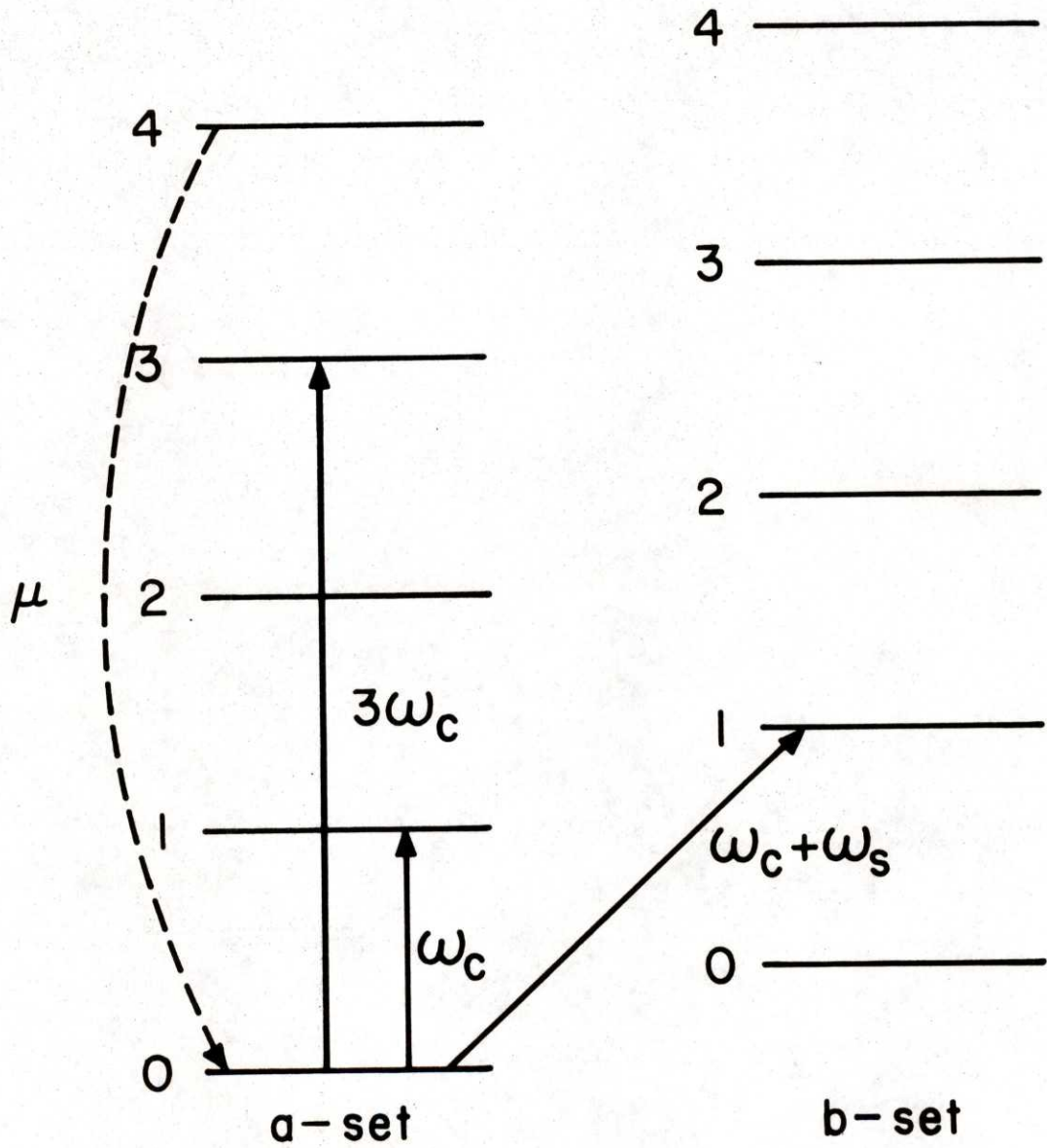


Fig. II-3. Intra-conduction band transitions allowed in the quasi Ge model (ω_c and $\omega_c + \omega_s$) and induced by warping ($3\omega_c$).

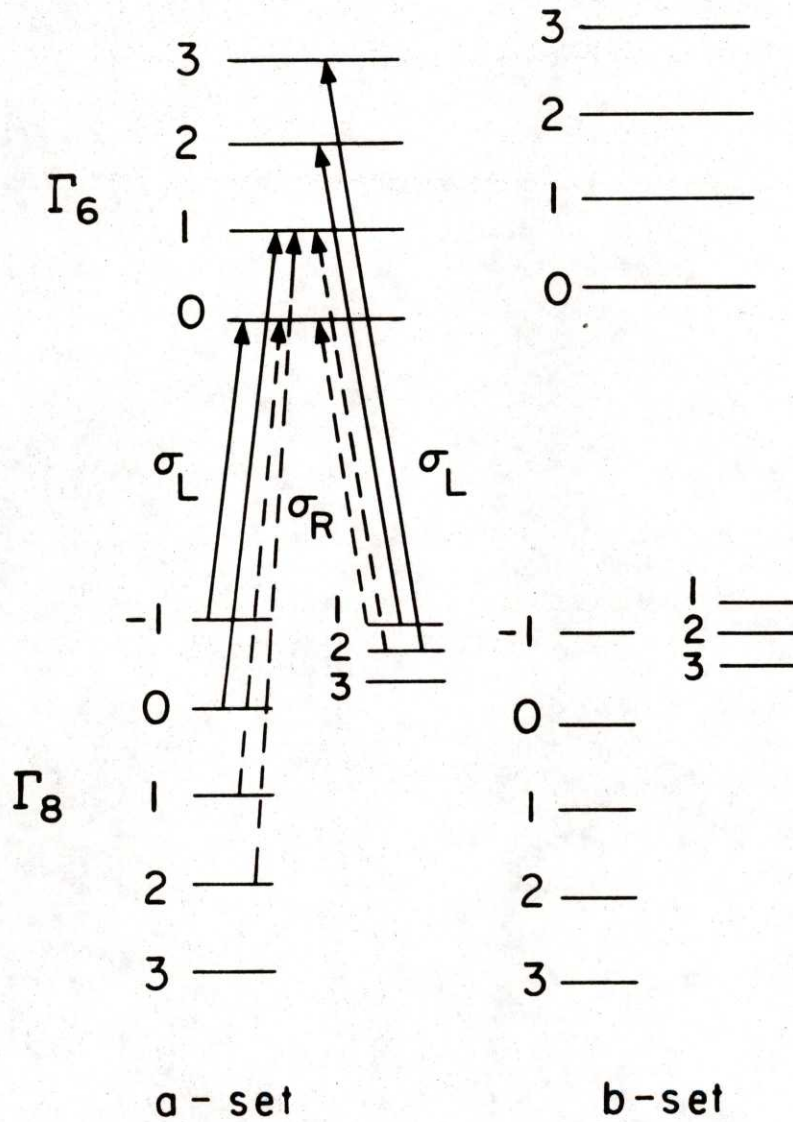


Fig. II-4. Interband transitions allowed in the quasi Ge model. A similar set of transitions connects the b-set levels.

REFERENCES

1. G. Dresselhaus, A.F. Kip and C. Kittel, Phys. Rev. 98, 368 (1955).
2. E.O. Kane, J. Phys. Chem. Solids 1, 249 (1957).
3. J.M. Luttinger, Phys. Rev. 102, 1030 (1956).
4. L.M. Roth, B. Lax and S. Zwerdling, Phys. Rev. 114, 90 (1959).
5. C.R. Pidgeon and R.N. Brown, Phys. Rev. 146, 575 (1966).
6. R.L. Aggarwal, in "Semiconductors and Semimetals" (R.K. Willardson and A.C. Beer, eds.). Vol. 9, p. 151 (1972).
7. G.F. Koster, J.O. Dimmock, R.G. Wheeler and H. Statz, "Properties of the Thirty-Two Point Groups" (MIT Press, Cambridge, 1966).
8. C.R. Pidgeon and S.H. Groves, Phys. Rev. 186, 824 (1969).
9. S.H. Groves, C.R. Pidgeon, A.W. Ewald and R.J. Wagner, J. Phys. Chem. Solids 31, 2031 (1970).
10. M. Reine, Ph.D. Thesis, Massachusetts Institute of Technology (1970);
M. Reine, R.L. Aggarwal and B. Lax, Phys. Rev. B5, 3033 (1972).
11. G. Dresselhaus, Phys. Rev. 100, 580 (1955).
12. However, Eq. (10) of Ref. 5 contains errors in the (3,7) and (7,3) matrix elements: the signs are incorrect and γ' should read γ'' . The sign error was included in Ref. 6. Fortunately, for small-gap materials, at least, the calculated energies are only slightly altered. These errors were also discovered recently by R.S. Kim and S. Narita, Phys. Stat. Sol. (b) 73, 741 (1976).
13. R. Bowers and Y. Yafet, Phys. Rev. 115, 1165 (1959); Y. Yafet, Phys. Rev. 115, 1172 (1959).
14. P. Kacman and W. Zawadzki, Phys. Stat. Sol. (b) 47, 629 (1971).

15. E.J. Johnson and D.H. Dickey, Phys. Rev. B1, 2676 (1970).
16. B.D. McCombe, S.G. Bishop and R. Kaplan, Phys. Rev. Letters 18, 748 (1967).

III. SELECTION RULES FOR WARPING AND INVERSION ASYMMETRY INDUCED CYCLOTRON-HARMONIC TRANSITIONS IN InSb

As the result of many magneto-optical investigations, most electronic properties of InSb are reasonably well understood in terms of the quasi Ge model presented in the preceding Chapter. An important exception has been a number of observations in n-type InSb of the second and third harmonics of cyclotron resonance, denoted by $2\omega_c$ and $3\omega_c$,¹⁻⁶ as well as the spin-shifted harmonic denoted by $2\omega_c + \omega_s$.⁶ These transitions have been observed along with the allowed combined resonance $\omega_c + \omega_s$ transition,¹ and the LO-phonon-assisted resonances $\omega_c + \omega_{LO}$, $2\omega_c + \omega_{LO}$, etc.^{2,3} The latter have been explained by the theoretical work of Enck, Saleh and Fan,² and of Bass and Levinson.⁷ Bell and Rogers⁸ obtained selection rules for warping and inversion-asymmetry induced harmonic transitions, for an applied magnetic field \vec{H} parallel to a [001] crystal axis. Favrot, Aggarwal and Lax⁶ recently reported that the intensity of these transitions exhibits marked anisotropy with respect to the crystal orientation relative to the applied magnetic field, in addition to its dependence on the optical polarization. In this Chapter we obtain the selection rules for cyclotron harmonic transitions induced by warping and inversion asymmetry for the magnetic field applied along the crystal axes [001], [110] and [111].⁹ These selection rules are consistent with the experimental results with one important exception. Favrot et al.⁶ observed a strong $2\omega_c$ absorption for the light polarization vector $\vec{E} \perp \vec{H}$ with $\vec{H} \parallel [001]$. This is not predicted either by us or by Bell and Rogers,⁸ or by the recent work of Zawadzki and Wlasak¹⁰ for this orientation.

The main effect of the small terms neglected in the quasi Ge model of

Chapter II is to allow extra weak optical transitions. For $k_H = 0$ the warping terms μ and q allow third-harmonic transitions $a(n) \rightarrow a(n+3)$ denoted by $3\omega_c$, as observed for the heavy holes in Ge.¹¹ The inversion-asymmetry parameters C , G , N_2 and N_3 allow the second-harmonic transitions $a(n) \rightarrow a(n+2)$ denoted by $2\omega_c$ and $a(n) \rightarrow b(n+2)$ denoted by $2\omega_c + \omega_s$. For $k_H \neq 0$ the warping terms also induce second-harmonic transitions,¹¹ and the inversion asymmetry terms induce third-harmonic transitions. The optical polarizations in which these extra transitions occur depend on the orientation of the crystal axes relative to the applied magnetic field. Similar effects were shown by Pidgeon and Groves¹² to induce extra interband transitions, primarily for $\vec{H} \parallel [111]$.

The mechanism for the warping-induced $3\omega_c$ transition is illustrated in Fig. II-3, in addition to the allowed transitions ω_c and $\omega_c + \omega_s$. For certain orientations of the crystal relative to the applied magnetic field, a term proportional to the warping parameter μ couples the $a(4)$ level to the $a(0)$ ground state in the conduction band, giving the $a(0)$ level an admixture of the $a(4)$ wave function. Then the optical matrix element $a(4) \rightarrow a(3)$ for $\vec{E}_\perp \vec{H}$ also gives a weaker transition $a(0) \rightarrow a(3)$, denoted by $3\omega_c$, as illustrated.

The strength of these extra transitions is found by calculating the optical matrix elements among the levels of the quasi Ge model, including the warping and inversion asymmetry perturbations as first-order corrections to the wavefunctions. In Sec. A below we obtain expressions for the warping and inversion asymmetry perturbations, and in Sec. B we calculate the transition matrix elements from these perturbations, and the resulting selection rules for intraband transitions for the magnetic field in the three principal directions [001], [110] and [111]. These selection rules are compared with the experimental results in Sec. C. Our results are summarized in Sec. D.

A. Warping and Inversion Asymmetry Perturbations, for \vec{H} in the $(1\bar{1}0)$ Plane

The terms not included in the quasi Ge Hamiltonian of Table II-5 divide into three categories: (i) terms proportional to k_H and k_H^2 ; (ii) the warping terms proportional to $\mu = \frac{1}{2}(\gamma_3 - \gamma_2)$ and q ; and (iii) the inversion asymmetry terms proportional to C , G , and the new parameters N_2 and N_3 . All of these extra terms, from applying the unitary transformation of Table II-4 to the Hamiltonian matrix of Table II-3, are given in Table III-1. The terms involving k_H are proportional to the effective mass parameters F , γ_1 , and γ' , and to

$$\gamma''' \equiv \frac{2}{3}\gamma_2 + \frac{1}{3}\gamma_3 - \frac{2}{3}(\gamma_2 - \gamma_3) f(\theta, \phi) \quad . \quad (\text{III-1})$$

For consideration of the other terms in Table III-1, we now consider only the case $\phi = 45^\circ$, which corresponds to \vec{H} in the $(1\bar{1}0)$ crystal plane, including the three principal directions $[001]$, $[110]$, and $[111]$ which were studied by Favrot et al.⁶ (see Fig. II-2). The warping terms are proportional to

$$\begin{aligned} \mu_1 &\equiv -\frac{3}{2}\mu\beta H(3c^2-1) \left[s^2(a^2 + a'^2) - 2\sqrt{2} sc\lambda k_H(a+a') \right] \\ \mu_2 &\equiv \frac{\sqrt{3}}{2}\mu\beta H \left\{ s^2(3c^2-1)(2N+1-2\lambda^2 k_H^2) - (c^2-3)(3c^2-1)a^2 \right. \\ &\quad \left. + 2\sqrt{2} sc\lambda k_H [(5-3c^2)a - (3c^2-1)a'] \right\} \\ \mu_3 &\equiv -\sqrt{3}\mu\beta H \left\{ sc[(3c^2-1)(2N+1-2\lambda^2 k_H^2) - (5-3c^2)a^2 + (3c^2-1)a'^2] \right. \\ &\quad \left. + 2\sqrt{2} s^2(3c^2-1)\lambda k_H a \right\} \end{aligned} \quad (\text{III-2})$$

where $c \equiv \cos \theta$, $s \equiv \sin \theta$, and to

$$\begin{aligned}
q_1 &\equiv -\frac{3}{4}q\beta H(3c^4 - 2c^2 + 8) & q_4 &\equiv -\frac{3}{4}q\beta Hsc(3c^2 - 5) \\
q_2 &\equiv -\frac{3\sqrt{3}}{4}q\beta Hs^2(3c^2 - 1) & q_5 &\equiv -\frac{1}{4}q\beta H(27c^4 - 18c^2 - 10) \\
q_3 &\equiv \frac{3\sqrt{3}}{4}q\beta Hsc(3c^2 - 1) & q_6 &\equiv -\frac{9}{8}q\beta Hsc(3c^2 - 1)
\end{aligned} \tag{III-3}$$

The terms from Eqs. (II-2) and (II-3) in the $\Gamma_8 \times \Gamma_8$ portions of Table III-1 (involving states $|3\rangle - |6\rangle$) are identical to those given by Luttinger,¹³ but with the opposite signs throughout since Luttinger's equations involved hole energies. Table III-1 includes additional couplings proportional to μ between the Γ_8 and Γ_7 bands.

The inversion asymmetry terms are proportional to

$$\begin{aligned}
c_1 &\equiv \frac{\sqrt{6}}{8} \frac{C}{\lambda} s(3c^2 - 1)(a - a^\dagger) \\
c_2 &\equiv \frac{\sqrt{2}}{8} \frac{C}{\lambda} [5s(3c^2 - 1)a^\dagger - 3s(1 + c^2)a - 2\sqrt{2}c(3c^2 - 1)\lambda k_H] \\
c_3 &\equiv \frac{\sqrt{2}}{8} \frac{C}{\lambda} [12s^2ca^\dagger + 2c(3c^2 - 1)a - \sqrt{2}s(3c^2 - 1)\lambda k_H] \\
c_4 &\equiv \frac{\sqrt{6}}{8} \frac{C}{\lambda} [2c(3c^2 - 1)a^\dagger + 3\sqrt{2}s(1 + c^2)\lambda k_H] \\
c_5 &\equiv \frac{1}{4} \frac{C}{\lambda} [s(3c^2 - 1)a^\dagger + 3s(1 + c^2)a - \sqrt{2}c(3c^2 - 1)\lambda k_H] \\
c_6 &\equiv -\frac{\sqrt{3}}{4} \frac{C}{\lambda} [s(3c^2 - 1)(a + a^\dagger) + 3\sqrt{2}s^2c\lambda k_H] \\
c_7 &\equiv \frac{1}{4} \frac{C}{\lambda} [3s^2ca^\dagger - c(3c^2 - 1)a - \sqrt{2}s(3c^2 - 1)\lambda k_H]
\end{aligned} \tag{III-4}$$

$$g_1 \equiv \frac{G\beta H}{\sqrt{2}} [-s(3c^2-1)(2N+1-2\lambda^2 k_H^2 + a^2) - 3s(1+c^2)a^{+2} \\ - 6\sqrt{2}s^2 c \lambda k_H a + 2\sqrt{2}c(3c^2-1)\lambda k_H a^+] \quad (\text{III-5})$$

$$g_2 \equiv \frac{2G\beta H}{\sqrt{6}} [3s^2 c(2N+1-2\lambda^2 k_H^2) - c(3c^2-1)(a^2 + a^{+2}) \\ - 2\sqrt{2}s(3c^2-1)\lambda k_H(a + a^+)]$$

$$e_1 \equiv \frac{1}{2}N_2\beta H[-s(3c^2-1)(2N+1-2\lambda^2 k_H^2 + 3a^2) + 3s(1+c^2)a^{+2} - 12\sqrt{2}s^2 c \lambda k_H a]$$

$$e_2 \equiv -\sqrt{3}N_2\beta H[c(3c^2-1)(a^2 - a^{+2}) + \sqrt{2}s(3c^2-1)\lambda k_H(a - a^+)] \quad (\text{III-6})$$

$$e_3 \equiv -N_2\beta H[c(3c^2-1)(2N+1-2\lambda^2 k_H^2) - 6s^2 c a^{+2} + 3\sqrt{2}s(1+c^2)\lambda k_H a \\ + 3\sqrt{2}s(3c^2-1)\lambda k_H a^+]$$

and to

$$f_1 \equiv N_3\beta Hs(3c^2-1)$$

$$f_2 \equiv -3\sqrt{3}N_3\beta Hs^2 c \quad (\text{III-7})$$

$$f_3 \equiv -N_3\beta Hc(3c^2-1)$$

The portions of the matrix in Table III-1 for couplings within the Γ_8 band proportional to C [Eqs. (III-4)] for these three orientations, and for $k_H = 0$, are

the same as those given by Pidgeon and Groves¹² with an overall sign change since they, like Luttinger,¹³ consider hole energies. Similarly, their result for q for $\vec{H} \parallel [111]$ is identical to ours [Eqs. (III-3)] with the sign reversed. However, our result for μ [Eqs. (III-2)] for $\vec{H} \parallel [111]$ is identical to that of Pidgeon and Groves with no sign change, so that their results for the μ matrix differ in sign from that of Luttinger. Our results, as indicated above, agree with that of Luttinger with an overall sign change.

In Tables III-2 through III-4 we list the matrices for G , N_2 , and N_3 , for $k_H = 0$ and for the three principal orientations. The matrices proportional to the other parameters have been given elsewhere.¹²⁻¹⁴

B. Selection Rules for Cyclotron-Harmonic Transitions

Bell and Rogers⁸ calculated transition strengths for intraband optical transitions, for $\vec{H} \parallel [001]$ only, by diagonalizing the Hamiltonian of Table II-3 in the single group basis set, without the parameter q and the new parameters N_1 , N_2 and N_3 . Because this Hamiltonian couples an infinitely large number of oscillator functions ϕ_n , they obtained numerical solutions by diagonalizing two 120×120 truncated matrices. In addition to the fundamental cyclotron resonance ω_c for the σ_L polarization and the combined resonance $\omega_c + \omega_s$ for the π polarization, they found that the following intra-conduction-band optical transitions were weakly allowed:

TABLE III-2. Matrices for the inversion asymmetry parameter G.

$$\vec{H} \parallel [001]:$$

	$ 3\rangle$	$ 5\rangle$	$ 6\rangle$	$ 4\rangle$	
$i\sqrt{\frac{8}{3}} G\beta H$	0	0	$a^2 + a^{+2}$	0	$ 1\rangle$
	0	$a^2 + a^{+2}$	0	0	$ 2\rangle$

$$\vec{H} \parallel [110]:$$

$\frac{i}{\sqrt{6}} G\beta H$	$-\sqrt{3}(2N+1 - 3a^2 + a^{+2})$	$2N+1 + a^2 - 3a^{+2}$	0	0	$ 1\rangle$
	0	0	$-(2N+1 + a^{+2} - 3a^2)$	$\sqrt{3}(2N+1 - 3a^{+2} + a^2)$	$ 2\rangle$

$$\vec{H} \parallel [111]:$$

$i\sqrt{\frac{8}{3}} G\beta H$	$\sqrt{6}a^2$	$-\sqrt{2}a^{+2}$	$-(2N+1)$	0	$ 1\rangle$
	0	$-(2N+1)$	$\sqrt{2}a^2$	$-\sqrt{6}a^{+2}$	$ 2\rangle$

TABLE III-3. Matrices for the inversion asymmetry parameter N_2 .

$$\vec{H}_{\parallel} [001]:$$

$$2iN_2\beta H \begin{array}{cccc} |3\rangle & |5\rangle & |6\rangle & |4\rangle \\ \left[\begin{array}{cccc} 0 & 0 & -\sqrt{3}(a^2 - a^{+2}) & 2N+1 \\ 2N+1 & \sqrt{3}(a^2 - a^{+2}) & 0 & 0 \end{array} \right] \begin{array}{l} |1\rangle \\ |2\rangle \end{array} \end{array}$$

$$\vec{H}_{\parallel} [110]:$$

$$\frac{i}{2} N_2 \beta H \begin{array}{cccc} \left[\begin{array}{cccc} -(2N+1) & -\sqrt{3}(2N+1) & 0 & 0 \\ +3a^2 + 3a^{+2}) & +3a^2 + 3a^{+2}) & & \\ 0 & 0 & \sqrt{3}(2N+1) & 2N+1 \\ & & +3a^2 + 3a^{+2}) & +3a^2 + 3a^{+2}) \end{array} \right] \begin{array}{l} |1\rangle \\ |2\rangle \end{array} \end{array}$$

$$\vec{H}_{\parallel} [111]:$$

$$i\sqrt{\frac{8}{3}} N_2 \beta H \begin{array}{cccc} \left[\begin{array}{cccc} -a^2 & -\sqrt{3}a^{+2} & 0 & -\sqrt{2}a^2 \\ -\sqrt{2}a^{+2} & 0 & \sqrt{3}a^2 & a^{+2} \end{array} \right] \begin{array}{l} |1\rangle \\ |2\rangle \end{array} \end{array}$$

TABLE III-4. Matrices for the inversion asymmetry parameter N_3 .

$$\begin{array}{l}
 \vec{H} \parallel [001]: \\
 2iN_3\beta H \begin{array}{c} \left[\begin{array}{cccc} |3\rangle & |5\rangle & |6\rangle & |4\rangle \\ 0 & 0 & 0 & 1 \\ -1 & 0 & 0 & 0 \end{array} \right] \begin{array}{l} |1\rangle \\ |2\rangle \end{array} \end{array} \\
 \\
 \vec{H} \parallel [110]: \\
 iN_3\beta H \begin{array}{c} \left[\begin{array}{cccc} 1 & -\sqrt{3} & 0 & 0 \\ 0 & 0 & -\sqrt{3} & 1 \end{array} \right] \begin{array}{l} |1\rangle \\ |2\rangle \end{array} \end{array} \\
 \\
 \vec{H} \parallel [111]: \\
 2iN_3\beta H \begin{array}{c} \left[\begin{array}{cccc} 0 & 0 & 1 & 0 \\ 0 & -1 & 0 & 0 \end{array} \right] \begin{array}{l} |1\rangle \\ |2\rangle \end{array} \end{array}
 \end{array}$$

$$\begin{aligned}
\sigma_L : \quad & a_n \rightarrow b_n & (\omega_s) \\
& b_n \rightarrow a_{n+2} & (2\omega_c - \omega_s) \\
\sigma_R : \quad & a_n \rightarrow b_{n+2} & (2\omega_c + \omega_s) \\
& a_n \rightarrow a_{n+3} & (3\omega_c) \\
\pi : \quad & a_n \rightarrow a_{n+2} & (2\omega_c) \\
& b_n \rightarrow a_{n+3} & (3\omega_c - \omega_s)
\end{aligned} \tag{III-8}$$

They showed that these were the result of warping and inversion asymmetry effects. We use a perturbation treatment to find the intraband selection rules for $\vec{H} \parallel [110]$ and $[111]$ and well as $[001]$, as outlined below.

Using the Hamiltonian \mathcal{K}' in Table III-1 as a perturbation in the basis states of Eq. (II-11), we find new states

$$|a'(n)\rangle = |a(n)\rangle + \sum_{n'} \sum_{j=a,b} \frac{\langle j(n') | \mathcal{K}' | a(n) \rangle}{E[j(n')] - E[a(n)]} |j(n')\rangle \tag{III-9}$$

And similarly for $|b'(n)\rangle$, where we consider only conduction band states $a=a^c$ and $b=b^c$ and coupled states $j=a^c, b^c$. Since the couplings of Eq. (III-9) are all very small compared to the energy differences, it was not necessary to include the energy corrections. The actual expressions for these couplings are very lengthy. As illustration, we given, for $\vec{H} \parallel [001]$ and $k_H = 0$

$$\begin{aligned}
\langle j(n') | \mathcal{H}' | a(n) \rangle = & 2\sqrt{3}\mu\beta H \{ \sqrt{(n+2)(n+3)} a_3^{n'} (a_5^n - \sqrt{2} a_7^n) \delta_{n', n+4} \\
& + \sqrt{(n-1)(n-2)} (a_5^{n'} - \sqrt{2} a_7^{n'}) a_3^n \delta_{n', n-4} \} \delta_{j, a} \\
& + \frac{iC}{2\lambda} \{ \sqrt{3(n+2)} [b_6^{n'} (\sqrt{2} a_5^n - a_7^n) + b_8^{n'} a_5^n] \delta_{n', n+3} \\
& + [\sqrt{n-1} (\sqrt{2} b_6^{n'} - b_8^{n'}) a_3^n + \sqrt{6n} b_4^{n'} a_3^n \\
& + \sqrt{n+1} b_4^{n'} (\sqrt{2} a_5^n + a_7^n)] \delta_{n', n-1} \} \delta_{j, b} \\
& + \frac{2iG\beta H}{\sqrt{3}} \{ \sqrt{n+2} [\sqrt{n+3} b_2^{n'} (\sqrt{2} a_5^n + a_7^n) \\
& - \sqrt{n+1} (\sqrt{2} b_6^{n'} - b_8^{n'}) a_1^n] \delta_{n', n+3} \quad \text{(III-10)} \\
& + \sqrt{n} [\sqrt{n+1} b_2^{n'} (\sqrt{2} a_5^n + a_7^n) \\
& - \sqrt{n-1} (\sqrt{2} b_6^{n'} - b_8^{n'}) a_1^n] \delta_{n', n-1} \} \delta_{j, b} \\
& - 2iN_2\beta H \{ \sqrt{3(n+2)} (\sqrt{n+3} b_2^{n'} a_5^n - \sqrt{n+1} b_6^{n'} a_1^n) \delta_{n', n+3} \\
& - [b_2^{n'} ((2n-1)a_3^n + \sqrt{3n(n+1)} a_5^n) \\
& - ((2n+1)b_4^{n'} + \sqrt{3n(n-1)} b_6^{n'}) a_1^n] \delta_{n', n-1} \} \delta_{j, b} \\
& - 2iN_3\beta H \{ b_2^{n'} a_3^n + b_4^{n'} a_1^n \} \delta_{n', n-1} \delta_{j, b}
\end{aligned}$$

with a similar expression for $\langle j(n') | \mathcal{K}_\omega' | b(n) \rangle$. All such couplings, proportional to the warping and inversion asymmetry parameters, are summarized in Table III-5.

Using these coupled states, the allowed optical transitions originating in the state $a(n)$ are proportional to the square of the matrix element $\langle f'(n') | \mathcal{K}_\omega' | a'(n) \rangle$ which becomes

$$\begin{aligned} \langle f'(n') | \mathcal{K}_\omega' | a'(n) \rangle &= \langle f(n') | \mathcal{K}_\omega' | a(n) \rangle \\ &+ \sum_{n''} \sum_{j=a,b} \left[\frac{\langle f(n') | \mathcal{K}_\omega' | j(n') \rangle \langle j(n') | \mathcal{K}_\omega' | a(n) \rangle}{E[j(n'')] - E[a(n)]} \right. \\ &\left. + \frac{\langle f(n') | \mathcal{K}_\omega' | j(n') \rangle \langle j(n'') | \mathcal{K}_\omega' | a(n) \rangle}{E[f(n')] - E[j(n'')] } \right] \quad \text{(III-11)} \end{aligned}$$

with a similar expression for transitions originating in the state $b(n)$. The summation runs over all intermediate states in the conduction band. The first term in Eq. III-11 represents an "allowed" transition. The matrix elements of \mathcal{K}_ω' proportional to P are given in Eqs. (II-18), and all matrix elements are calculated using the approximate numerical solutions Eqs. (II-11) to Eqs. (II-10). \mathcal{K}_ω' also includes terms proportional to the warping and inversion asymmetry parameters.

Equations (III-10) and (III-11) illustrate the difference between the intra-band transitions considered in detail in the next section, and the interband transitions considered by Pidgeon and Groves.¹² For conduction band states, the coefficients a_1^n and b_2^n in Eqs. (II-11) are large, and the others small, but

TABLE III-5. Couplings among the quasi Ge states, proportional to the warping and inversion asymmetry parameters, for $k_H = 0$ and extra couplings for $k_H \neq 0$.

		$k_H = 0$	$k_H \neq 0$
$\vec{H} \parallel [001]$	μ	$a_n \dots a_{n\pm 4}$ $b_n \dots b_{n\pm 4}$	
	\mathcal{G}		
	C	$a_n \dots b_{n-1, n+3}$	$a_n \dots a_{n\pm 2}$ $b_n \dots b_{n\pm 2}$
	G	$a_n \dots b_{n-1, n+3}$	$a_n \dots a_{n\pm 2}$ $b_n \dots b_{n\pm 2}$
	N_2	$a_n \dots b_{n-1, n+3}$	
$\vec{H} \parallel [110]$	N_3	$a_n \dots b_{n-1}$	
	μ	$a_n \dots a_{n\pm 2, n\pm 4}$ $b_n \dots b_{n\pm 2, n\pm 4}$	$a_n \dots b_{n-1, n+3}$
	\mathcal{G}	$a_n \dots a_{n\pm 2}$ $b_n \dots b_{n\pm 2}$	
	C	$a_n \dots a_{n\pm 1, n\pm 3}$ $b_n \dots b_{n\pm 1, n\pm 3}$	$a_n \dots b_n, n\pm 2$
	G	$a_n \dots a_{n\pm 1, n\pm 3}$ $b_n \dots b_{n\pm 1, n\pm 3}$	$a_n \dots b_n, n\pm 2$
	N_2	$a_n \dots a_{n\pm 1, n\pm 3}$ $b_n \dots b_{n\pm 1, n\pm 3}$	$a_n \dots b_n, n\pm 2$
$\vec{H} \parallel [111]$	N_3	$a_n \dots a_{n\pm 1}$ $b_n \dots b_{n\pm 1}$	
	μ	$a_n \dots b_{n-2, n+4}$	$a_n \dots a_{n\pm 3}$ $b_n \dots b_{n\pm 3}$
	\mathcal{G}	$a_n \dots b_{n-2}$	
	C	$a_n \dots a_{n\pm 3}$ $a_n \dots b_{n+1}$ $b_n \dots b_{n\pm 3}$	$a_n \dots b_{n-2}$
	G	$a_n \dots a_{n\pm 3}$ $a_n \dots b_{n+1}$ $b_n \dots b_{n\pm 3}$	
	N_2	$a_n \dots a_{n\pm 3}$ $a_n \dots b_{n+1}$ $b_n \dots b_{n\pm 3}$	$a_n \dots b_{n-2}$
N_3	$a_n \dots b_{n+1}$		

for valence band states a_3^n and a_5^n , or b_4^n and b_6^n , are large, particularly for heavy-hole states, and a_1^n and b_2^n are small. Thus, if $a(n)$ and the coupled state $j(n')$ in Eq. (III-10) are hole states as is the case for the transitions observed by Pidgeon and Groves, then the coefficients of G , N_2 and N_3 in this equation are smaller, roughly by an order of magnitude, than that of C , so that their analysis did not need to include effects of G , N_2 and N_3 . For conduction-band matrix elements, on the other hand, the coefficients of G , N_2 and N_3 become comparable to that of C , so that all four parameters must be considered.

The intra-conduction band transitions allowed in Eq. (III-11) by the couplings in Table III-5 are listed in Table III-6. We use the notation of Eq. (III-8): a transition from a_n to a_{n+m} is denoted by $m\omega_c$; from a_n to b_{n+m} by $m\omega_c + \omega_s$, and from b_n to a_{n+m} by $m\omega_c - \omega_s$. We would like to point out that, in fact, the conduction band Landau levels are not equally spaced, so that the transitions are not precisely harmonic transitions; we use the $m\omega_c$ notation for convenience. In Table III-6 we have grouped together the transitions induced by warping (μ and q) and by inversion asymmetry (C, G, N_2, N_3) and have included the allowed transitions as well. For $\vec{H} \parallel [001]$ and $k_H = 0$ our results are consistent with those of Bell and Rogers,⁸ summarized in Eq. (III-8).

A calculation of selection rules for the cyclotron harmonic transitions has recently been made for the $\vec{H} \parallel [001]$ orientation by Zawadzki and Wlasak.¹⁰ Their analysis includes transitions proportional to the parameters μ , C , and G , but not q , N_2 or N_3 . Their perturbation treatment is similar to ours, but includes some additional weaker transitions allowed to second order in the warping, inversion asymmetry and $k_H \neq 0$ effects. Zawadzki and Wlasak obtain

TABLE III-6. Intra-conduction-band transitions in InSb, for $k_H = 0$ and extra transitions for $k_H \neq 0$, for optical polarizations σ_L , σ_R , and π , both allowed (A) and induced by warping (W) and inversion asymmetry (I).

		$k_H = 0$			$k_H \neq 0$		
		σ_L	σ_R	π	σ_L	σ_R	π
ALL ORIENTATIONS	A	ω_c		$\omega_c + \omega_s$	$2\omega_c + \omega_s$	ω_s	
	W	$5\omega_c$	$3\omega_c$	$\omega_c - \omega_s,$ $5\omega_c + \omega_s$			
	I	$\omega_s, 2\omega_c - \omega_s,$ $4\omega_c + \omega_s$	$2\omega_c + \omega_s$	$2\omega_c$	$3\omega_c$	ω_c	$\omega_c - \omega_s,$ $3\omega_c + \omega_s$
$\vec{H} \parallel [001]$	W	$3\omega_c, 5\omega_c$	$\omega_c, 3\omega_c$	$\omega_c - \omega_s,$ $3\omega_c \pm \omega_s,$ $5\omega_c + \omega_s$	$\omega_s, 2\omega_c - \omega_s,$ $4\omega_c + \omega_s$	$2\omega_c + \omega_s$	$2\omega_c$
	I	$2\omega_c, 4\omega_c$	$2\omega_c$	$\omega_s, 2\omega_c \pm \omega_s,$ $4\omega_c + \omega_s$	$\omega_c \pm \omega_s,$ $3\omega_c \pm \omega_s$	$\omega_c \pm \omega_s$	$\omega_c, 3\omega_c$
	W	$3\omega_c - \omega_s,$ $5\omega_c + \omega_s$	$\omega_c - \omega_s,$ $3\omega_c + \omega_s$	$3\omega_c$	$4\omega_c$	$2\omega_c$	$2\omega_c - \omega_s,$ $4\omega_c + \omega_s$
$\vec{H} \parallel [110]$	I	$2\omega_c + \omega_s,$ $4\omega_c$	$\omega_s, 2\omega_c$	$2\omega_c - \omega_s,$ $4\omega_c + \omega_s$	$3\omega_c - \omega_s$	$\omega_c - \omega_s$	$3\omega_c$
	W	$3\omega_c - \omega_s,$ $5\omega_c + \omega_s$	$\omega_c - \omega_s,$ $3\omega_c + \omega_s$	$3\omega_c$	$4\omega_c$	$2\omega_c$	$2\omega_c - \omega_s,$ $4\omega_c + \omega_s$
	I	$2\omega_c + \omega_s,$ $4\omega_c$	$\omega_s, 2\omega_c$	$2\omega_c - \omega_s,$ $4\omega_c + \omega_s$	$3\omega_c - \omega_s$	$\omega_c - \omega_s$	$3\omega_c$
$\vec{H} \parallel [111]$	W	$3\omega_c - \omega_s,$ $5\omega_c + \omega_s$	$\omega_c - \omega_s,$ $3\omega_c + \omega_s$	$3\omega_c$	$4\omega_c$	$2\omega_c$	$2\omega_c - \omega_s,$ $4\omega_c + \omega_s$
	I	$2\omega_c + \omega_s,$ $4\omega_c$	$\omega_s, 2\omega_c$	$2\omega_c - \omega_s,$ $4\omega_c + \omega_s$	$3\omega_c - \omega_s$	$\omega_c - \omega_s$	$3\omega_c$
	W	$3\omega_c - \omega_s,$ $5\omega_c + \omega_s$	$\omega_c - \omega_s,$ $3\omega_c + \omega_s$	$3\omega_c$	$4\omega_c$	$2\omega_c$	$2\omega_c - \omega_s,$ $4\omega_c + \omega_s$

for $\vec{H} \parallel [001]$ the transitions we list in Table III-6, and, in addition, other transitions: $6\omega_c (\pi)$, $4\omega_c \pm \omega_s$ and $8\omega_c \pm \omega_s$ (σ_L and σ_R) allowed by a combination of μ and C effects, and also $4\omega_c (\pi)$, $2\omega_c \pm \omega_s$ and $6\omega_c \pm \omega_s$ (σ_L and σ_R) allowed by μ and $k_H \neq 0$. We expect these transitions, which arise only in a third-order perturbation treatment, to be considerably weaker than those in Table III-6.

Our quantum-mechanical calculation confirms the results of Zeiger, Lax and Dexter,¹¹ who obtained the intensities of the harmonics of heavy-hole cyclotron resonance in Ge and Si from a semiclassical Boltzman treatment. They found that the third-harmonic intensity should be zero for $\vec{E} \perp \vec{H} \parallel [111]$ and for $\vec{E} \parallel \vec{H} \parallel [001]$ and $[110]$, and the second-harmonic intensity, allowed for $k_H \neq 0$, should be zero for $\vec{E} \perp \vec{H} \parallel [001]$ and $[110]$ and for $\vec{E} \parallel \vec{H} \parallel [001]$ and $[111]$; these selection rules are consistent with Table III-6, where $\vec{E} \perp \vec{H}$ induces both σ_L and σ_R transitions.

C. Comparison with Experiments

Experimentally, only the lowest-energy harmonic transitions $2\omega_c$, $2\omega_c + \omega_s$ and $3\omega_c$, from the ground state $a^c(0)$, have been identified.¹⁻⁶ The experimental results of Favrot et al.⁶ are compared in Table III-7 with the results in Table III-6 for $k_H = 0$. As can be seen, the predicted selection rules for these transitions are confirmed experimentally, with one important exception. Favrot et al. observed a strong transition at $2\omega_c$ for $\vec{E} \perp \vec{H} \parallel [001]$ which is not explained by our calculations, even for $k_H \neq 0$. They also found very weak absorptions in the $\vec{E} \parallel \vec{H}$ polarization, for example, $3\omega_c$ for $\vec{H} \parallel [110]$, and somewhat stronger absorptions at $2\omega_c + \omega_s$ for $\vec{H} \parallel [001]$ and $[111]$ axes,

TABLE III-7. Comparison of the theoretical selection rules with the experimental results of Favrot, Aggarwal and Lax.⁶

		$\vec{E} \perp \vec{H}$	$\vec{E} \parallel \vec{H}$
$\vec{H} \parallel [001]$	THEORY	$2\omega_c + \omega_s, 3\omega_c$	$2\omega_c$
	EXP	$2\omega_c, 2\omega_c + \omega_s, 3\omega_c$	$2\omega_c$
$\vec{H} \parallel [110]$	THEORY	$2\omega_c, 3\omega_c$	$2\omega_c + \omega_s$
	EXP	$2\omega_c, 3\omega_c$	$2\omega_c + \omega_s$
$\vec{H} \parallel [111]$	THEORY	$2\omega_c, 2\omega_c + \omega_s$	$3\omega_c$
	EXP	$2\omega_c, 2\omega_c + \omega_s$	$3\omega_c$

which are not yet understood. It is evident from the spectra of Ref. 6 that population effects ($k_H \neq 0$) are not important, since the strongest $k_H \neq 0$ line predicted in Table III-6, $2\omega_c + \omega_s$ for $\vec{E}_\perp \vec{H}$ in all orientations, is not observed for $\vec{E}_\perp \vec{H} \parallel [110]$. The results of Favrot et al.⁶ were recently confirmed over the wavelength region ~ 7.5 to $18 \mu\text{m}$ by K. Lee,¹⁵ for $\vec{H} \parallel [110]$ and $[111]$ axes, except that Lee did not observe the weak $2\omega_c + \omega_s$ line for $\vec{E} \parallel \vec{H} \parallel [111]$.

A recent calculation by Miyake¹⁶ of impurity cyclotron-resonance harmonics suggests a possible explanation for the $2\omega_c$, $\vec{E}_\perp \vec{H} \parallel [001]$ transition observed by Favrot et al.⁶ If the ground state electron occupies an impurity state associated with the $a^c(0)$ Landau level, the impurity potential acts as a perturbation which allows the electron to make transitions to all $a^c(n)$ levels, $n \geq 1$. Miyake's calculations indicate that the strongest harmonic is the second ($n=2$ or $2\omega_c$), about 10 times stronger than the third harmonic. Thus the impurity potential could have a strong effect on the $2\omega_c$ absorption but have only a small effect on the $3\omega_c$ absorption. It would be useful to repeat the experiments of Ref. 6 at different carrier concentrations, since for the value $n_e \approx 2 \times 10^{16} \text{ cm}^{-3}$ used by Favrot et al.,⁶ a significant number of carriers should not have frozen¹⁷ into impurity levels at $H \approx 90 \text{ kG}$ where they observed the $2\omega_c$ peak. For higher carrier concentrations the effect of impurity perturbation would be weaker relative to the warping and inversion asymmetry perturbations.

McCombe et al.¹ observed cyclotron resonance absorption at ω_c as well as the harmonics $2\omega_c$ and $3\omega_c$ in n-type InSb for the "inactive" sense of circular polarization σ_R . They interpreted these results in terms of electron-plasmon interaction. This interpretation was disputed by Blinowski and Mycielski¹⁸ and defended by Quinn et al.¹⁹ A more likely interpretation is that these are

warping and inversion-asymmetry induced transitions. McCombe et al.¹ do not specify the sample orientation; if they had $\vec{H} \parallel [110]$ one would predict from Table III-6 for $k_H = 0$, weak transitions for σ_L at $2\omega_c$, $3\omega_c$, $4\omega_c$ and $5\omega_c$, and for σ_R at ω_c , $2\omega_c$ and $3\omega_c$. The σ_L transitions were evidently obscured by the overabsorbed cyclotron resonance transition, but the σ_R transitions follow these selection rules. Thus one does not necessarily have to invoke the electron-plasmon coupling in order to explain the "inactive-mode" cyclotron resonance.

D. Discussion

To summarize the results of our work on InSb, we have arrived at an understanding of most of the cyclotron harmonic transitions. It should be possible, once the $2\omega_c$, $\vec{E} \perp \vec{H} \parallel [001]$ transition is understood, to use a comparison of the calculated and observed intensities for the predicted transitions to determine the six small parameters μ , q , C , G , N_2 , and N_3 . Preliminary calculations using the parameter estimates in App. A give roughly the same order of magnitude as the observed intensities. Thus, with the exception of the $2\omega_c$, $\vec{E} \perp \vec{H} \parallel [001]$ transition, the cyclotron harmonic transitions in InSb have been shown to be induced by the warping and inversion asymmetry effects.

REFERENCES

1. B.D. McCombe, R.J. Wagner, S. Teitler and J.J. Quinn, Phys. Rev. Letters 28, 37 (1972).
2. R.C. Enck, A.L. Saleh and H.Y. Fan, Phys. Rev. 182, 790 (1969).
3. E.J. Johnson and D.H. Dickey, Phys. Rev. B1, 2676 (1970).
4. R.B. Dennis, R.A. Wood, C.R. Pidgeon, S.D. Smith, and J.W. Smith, J. Phys. C5, L23 (1972).
5. M.H. Weiler, R.L. Aggarwal and B. Lax, Solid State Commun. 14, 299 (1974).
6. G. Favrot, R.L. Aggarwal and B. Lax, Solid State Commun. 18, 577 (1976).
7. F.G. Bass and I.B. Levinson, Zh. Eksp. Teor. Fiz. 49, 914 (1965) [Eng. transl. Soviet Physics JETP 22, 635 (1966)].
8. R.L. Bell and K.T. Rogers, Phys. Rev. 152, 746 (1966).
9. M.H. Weiler, R.L. Aggarwal and B. Lax, Bul. Am. Phys. Soc. 21, 429 (1976).
10. W. Zawadzki and J. Wlasak, J. Phys. C. 9, L663 (1976).
11. R.N. Dexter, H.J. Zeiger and B. Lax, Phys. Rev. 104, 637 (1956);
H.J. Zeiger, B. Lax and R.N. Dexter, Phys. Rev. 105, 495 (1957).
12. C.R. Pidgeon and S.H. Groves, Phys. Rev. 186, 824 (1969).
13. J.M. Luttinger, Phys. Rev. 102, 1030 (1956).
14. Y. Ohmura, J. Phys. Soc. Japan 25, 740 (1968).
15. K. Lee, B.S. Thesis, Massachusetts Institute of Technology (1976).
16. S.J. Miyake, J. Phys. Soc. Japan 35, 551 (1973).
17. O. Beckman, E. Hanamura and L.J. Neuringer, Phys. Rev. Letters 18, 773 (1967).

18. J. Blinowski and J. Mycielski, Phys. Letters 50A, 88 (1974).
19. J.J. Quinn, B.D. McCombe, K.L. Ngai and T.L. Reineke, Phys. Letters 54A, 161 (1975).

IV. MAGNETOREFLECTION EXPERIMENTS ON $\text{Hg}_{1-x}\text{Cd}_x\text{Te}$

Our studies of $\text{Hg}_{1-x}\text{Cd}_x\text{Te}$ are based on the extensive work of Pidgeon, Groves and their collaborators on InSb,^{1,2} α -Sn,³ HgTe,⁴ and $\text{Hg}_{0.84}\text{Cd}_{0.16}\text{Te}$.⁵ This work was, in turn, based on experimental and theoretical techniques developed for studies of Ge.^{6,7} The large number of interband transitions observed in magnetoabsorption of thin samples,^{1,6,7} and magnetoreflexion,²⁻⁵ provided a wealth of information with which to determine the electronic band parameters of these materials.

Magnetoabsorption experiments require extremely thin samples, which are subject to strain, with the rapid increase in the background absorption above the band edge limiting the spectral range which can be studied. Magnetoreflexion effects, on the other hand, are much weaker and often difficult to observe. Therefore a number of differential magnetoreflexion techniques have been developed, which were reviewed by Aggarwal.⁸ One of these techniques, stress modulation, was used by Reine⁹ in his studies of GaSb and GaAs. Fortunately, we were able to observe extensive magnetoreflexion structure for our $\text{Hg}_{1-x}\text{Cd}_x\text{Te}$ samples, so that modulation techniques were not necessary.

In this Chapter we describe the details of our experiments on $\text{Hg}_{1-x}\text{Cd}_x\text{Te}$, describing the samples in Sec. A and the optical apparatus in Sec. B. In Sec. C we present some typical magnetoreflexion spectra, giving in Sec. D our results for the photon energy and magnetic field positions of the interband transitions observed for each of our samples. These results will be interpreted in Chapter V in terms of the quasi Ge model developed in Chapter II.

A. Samples

The samples of $\text{Hg}_{1-x}\text{Cd}_x\text{Te}$, as received from Cominco, Inc., consisted of single-crystal slices approximately 12 to 15 mm in diameter and 0.5 mm thick. Each slice had been annealed to lower its carrier concentration and to enhance the homogeneity of its alloy composition. Most samples were oriented with reflecting faces normal to [001] or [111] crystal axes. Upon receipt, each slice was photographed using the extended-spot Laue technique to check for grain boundaries, and two slices were found in this way to be polycrystalline. These were returned to Cominco. The orientation of each slice was determined by x-ray diffraction.

The characteristics of each sample are given in Table IV-1. The nominal alloy composition, carrier concentration and Hall mobility were stated by Cominco. The alloy composition x was also determined either by microprobe measurements which were kindly performed on most of our samples by Mary Finn at Lincoln Laboratory, or, for the other samples, using the room-temperature transmission observed with an infrared spectrophotometer. The last three columns of Table IV-1 give the orientation and/or the angles θ and ϕ (corresponding to Fig. II-2) of the reflecting face normal.

The spectrophotometer determination of the alloy composition made use of the curve shown in Fig. IV-1, which was supplied to us by Cominco, giving the alloy composition x as a function of the "cut-on" wavelength. The determination of this wavelength from a spectrophotometer curve is illustrated in Fig. IV-2, which shows spectra for samples 804 and 805 which had been cut from nearby positions on the same ingot. The microprobe result $x = 0.269$ for sample 804 corresponds in Fig. IV-1 to a "cut-on" wavelength of $5.4 \mu\text{m}$,

TABLE IV-1. Physical and electrical characteristics of $\text{Hg}_{1-x}\text{Cd}_x\text{Te}$ samples.

SAMPLE NO.	NML ALLOY COMPOSITION X		77 K:		ORIENTATION			
	NOMINAL	MICROPROBE	SPECTROPHOTOMETER	CARRIER CONCENTRATION	HALL MOBILITY	AXIS	θ	ϕ
796	.20	.213 ± .004		$1.3 \times 10^{14} \text{ cm}^{-3}$	$8.9 \times 10^5 \text{ cm}^2/\text{Vs}$		70°	30°
798	.20	.182 ± .015		4.5	1.4	[111]	54.7	45
800	.26	.248 ± .014		3.2	0.8		39	42
801	.22	.196 ± .013		8.7	2.1		82	32
802	.20	.175 ± .013		1.1	2.2	[001]	0	45
804	.30	.269 ± .017		2.1	0.5	[001]	0	45
805	.30		.265 ± .005	2.1	0.5	[001]	0	45
806	.26		.247 ± .005	1.1	0.7	[001]	0	45
809	.23		.220 ± .005	2.4	1.1	[001]	0	45
810	.23		.221 ± .005	2.8	1.1	[111]	54.7	45

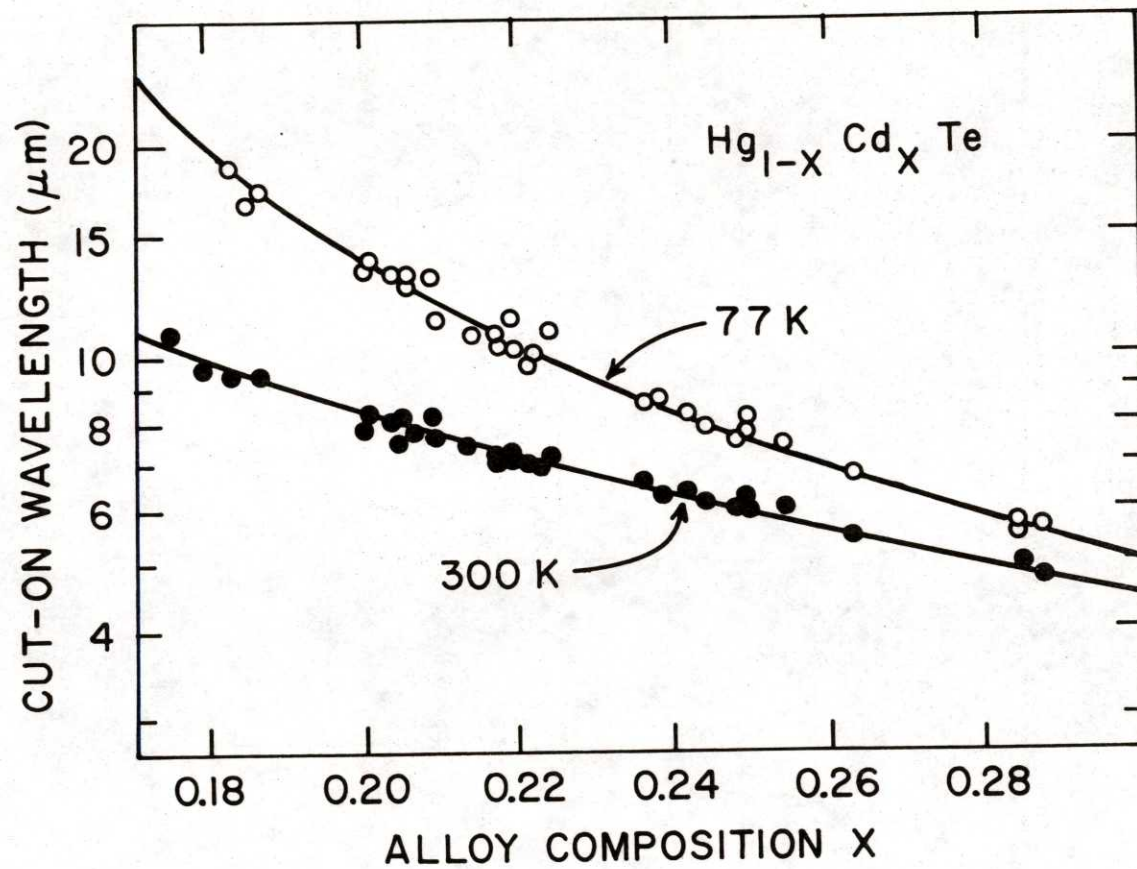


Fig. IV-1. $\text{Hg}_{1-x}\text{Cd}_x\text{Te}$ cuton wavelength vs. alloy composition, at temperatures $T = 77\text{K}$ and 300K .

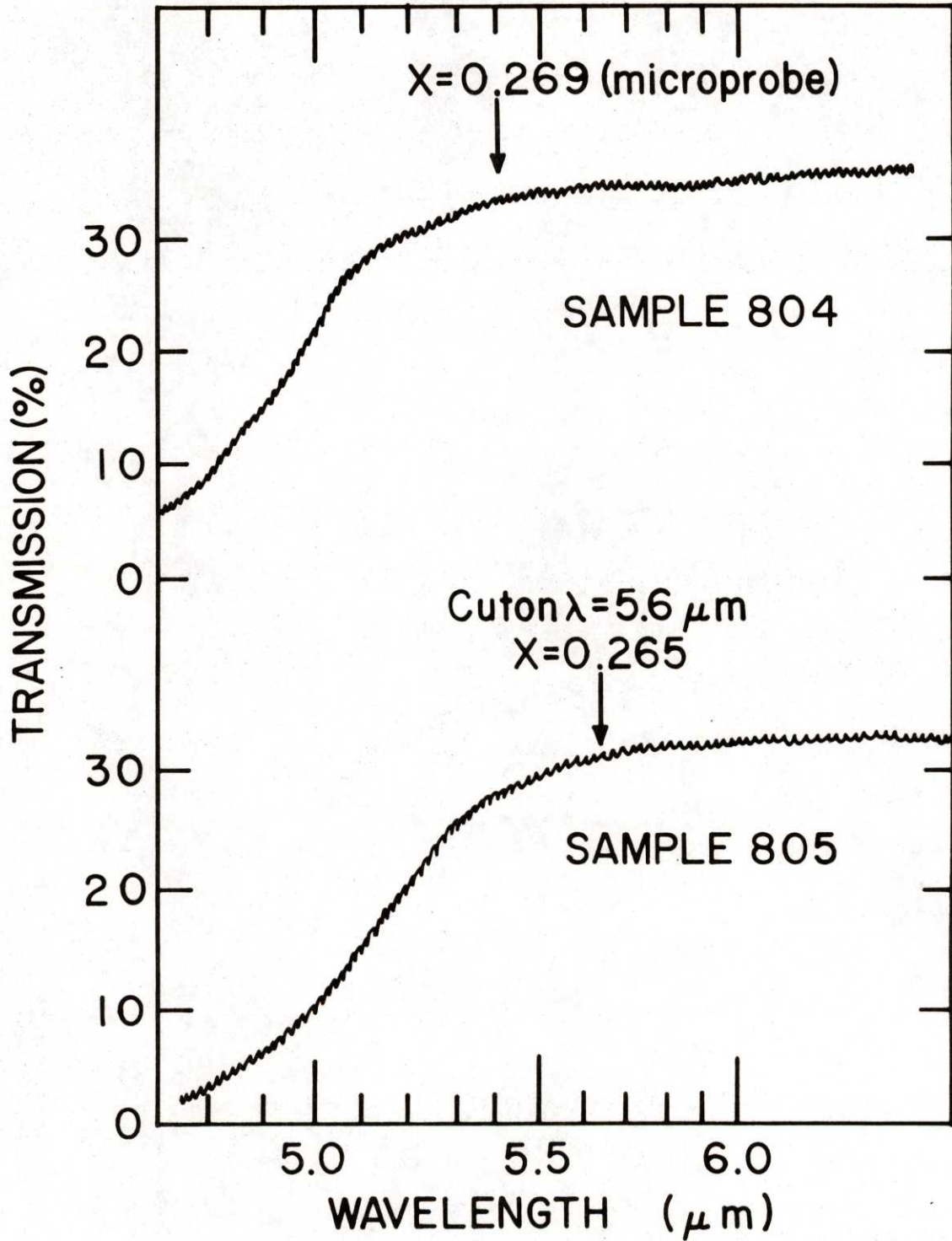


Fig. IV-2. Spectrophotometer curves for samples 804 and 805 illustrating the determination of alloy composition of sample 805.

which is indicated by the arrow in the upper curve in Fig. IV-2. The arrow marking a similar point on the lower curve indicates a cut-on wavelength of $5.6 \pm 0.3 \mu\text{m}$ for sample 805, hence from Fig. IV-1 an alloy composition of 0.265 ± 0.005 . These results differ considerably from the nominal composition 0.30 ± 0.01 . The uncertainty values in the microprobe values for x are the probable errors resulting from point-to-point variations over the sample surface; the stated uncertainty in the spectrophotometer results are due only to uncertainty in determining the cut-on wavelength, since we could not measure such variations.

One face of each slice was chemically polished and etched, and a sample approximately 6 mm wide was cut from the center portion. The sample was mounted in a sample holder using Be-Cu spring clips at each end, with a small piece of lens tissue under each clip to protect the fragile sample surface. The sample holder was attached to the cold finger of a liquid helium Dewar using two screws and also vacuum grease to improve the thermal contact. Based on measurements of the temperature of a piece of InSb held in the same arrangement in a similar Dewar provided with feed-through connections for thermocouple leads, we estimate the sample temperature to have been 24 K when the Dewar was filled with liquid helium, and 91 K using liquid nitrogen. Some early magnetoreflexivity spectra were taken with the samples mounted with vacuum grease on thin sapphire plates, with the plates held in the sample holder using grease. The spectra indicated little, if any, difference in temperature between these two arrangements, but some samples cracked indicating that the grease mounting introduced strains.

Magnetoreflexion spectra were also taken for two samples of InSb, purchased from Cominco, with reflecting faces normal to [001] and [111] crystal

axes. The electronic specifications were Cominco grade 67S, with 77 K carrier concentration of 0.7 to $1.1 \times 10^{14} \text{ cm}^{-3}$ and Hall mobility of from 6.0 to $7.2 \times 10^5 \text{ cm}^2/\text{V-sec}$.

B. Optical Apparatus

The experimental apparatus for magnetoreflexion measurements is depicted schematically in Fig. IV-3. This apparatus has been used in a number of previous investigations.⁹ It consists of an enclosed box, flushed with dry air, containing a Perkin-Elmer Model 99 double-pass grating monochromator with a globar source, a 500 Hz chopper, and mirrors to reflect and focus the light onto the sample at near normal incidence, and to collect and focus the reflected light onto the detector. Our experiments used gratings blazed at 1.5 , 3 , 6 , 12 and $22.5 \mu\text{m}$, with long wave pass interference filters appropriate to the wavelength range being used, and the light was circularly polarized using a wire-grid linear polarizer followed by a CsI Fresnel rhomb. The detector was either Ge:Cu(4K), Ge:Au(77K) or PbS(300K), depending on the wavelength range.

The sample, on the cold finger of the Dewar, was held in the center of the 2 in. diameter bore of a Bitter magnet, with the magnetic field applied normal to the reflecting surface. The optical window was either BaF_2 for wavelengths less than $10 \mu\text{m}$, or Irtran 4 for longer wavelengths. The magnetic field could be swept up to approximately 150 kG. The sense of circular polarization of the light, with respect to the magnetic field direction, was varied by sweeping the field either "positive" (towards the ceiling) or "negative".

As the magnetic field was swept, the detector signal was amplified by

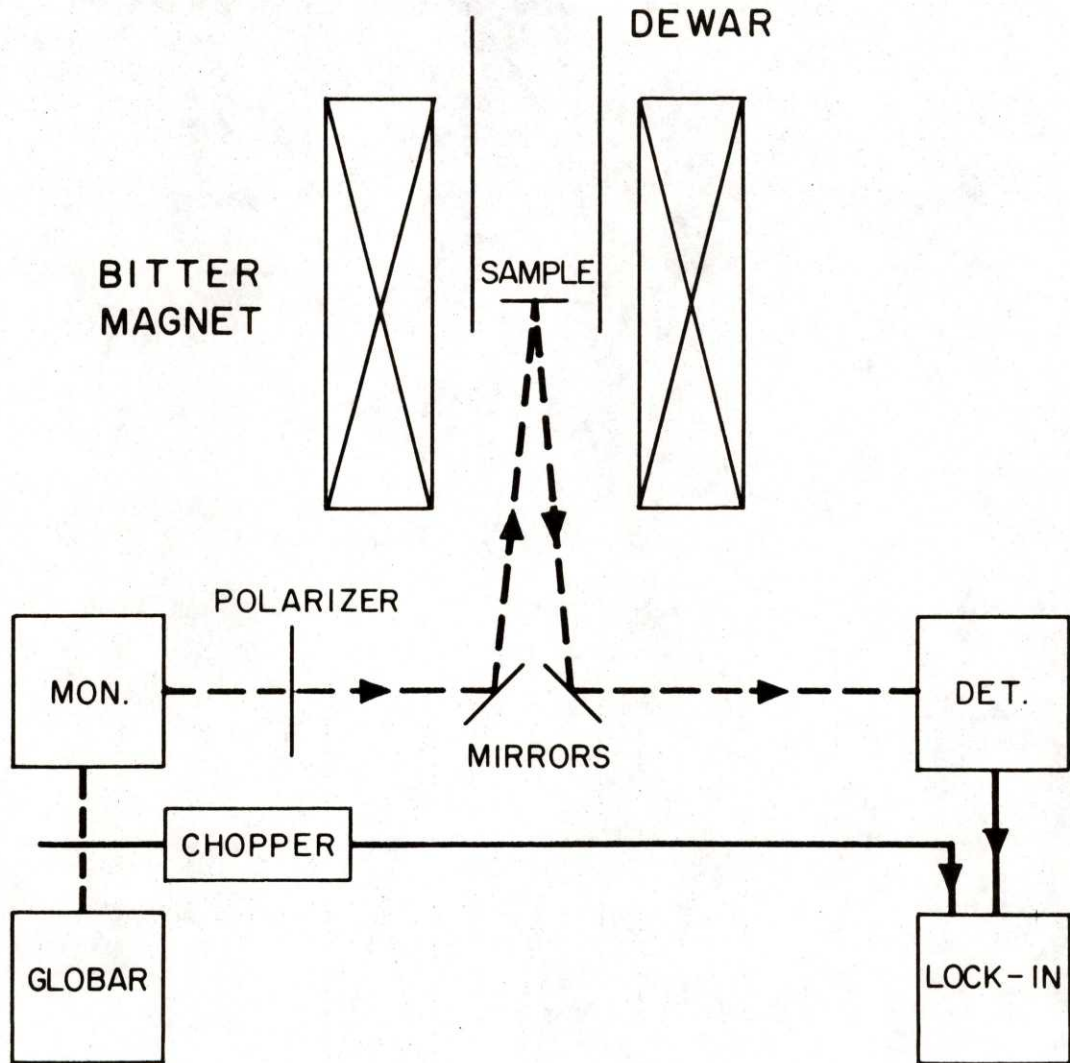


Fig. IV-3. Optical apparatus for magnetoreflexion.

a lockin amplifier (most recently a PAR Model 5101), using a reference signal from the chopper. The amplifier output was fed into a "bucking box" which expanded the signal by a variable factor and subtracted a fixed amount from this, so that signal changes of only a few percent became large changes with respect to this "bucked" signal. This signal was recorded on a two-pen chart recorder; the other pen recorded a signal proportional to the magnet current as a measure of the applied magnetic field.

The signal reflected from the sample was directly proportional to the reflectivity R given by⁸

$$R = \frac{(n-1)^2 + k^2}{(n+1)^2 + k^2} \quad (\text{IV-1})$$

where n and k are the index of refraction and extinction coefficient, respectively, determined from the equation

$$(n + ik)^2 = \epsilon_1 + i\epsilon_2 \quad (\text{IV-2})$$

where ϵ_1 and ϵ_2 are, respectively, the real and imaginary components of the dielectric constant. R is approximately proportional to ϵ_1 ; it was shown in the review article by Aggarwal⁸ that the peaks in ϵ_1 coincide (within the linewidth) of the absorption peaks in ϵ_2 . Some typical curves for $\Delta R/R$, the fractional change in reflectivity observed in the vicinity of an interband magneto-optical transition, are shown in Fig. IV-4, which was calculated using the expressions for $\epsilon_1(\omega)$ and $\epsilon_2(\omega)$ given in Ref. 8. The asymmetric line shape is the broadened form of the density of states of Landau levels in a magnetic field: $\rho(E) \approx \sum_n (E - \hbar\omega_n)^{-1/2}$. In the next Section we will compare some of our reflection spectra with these

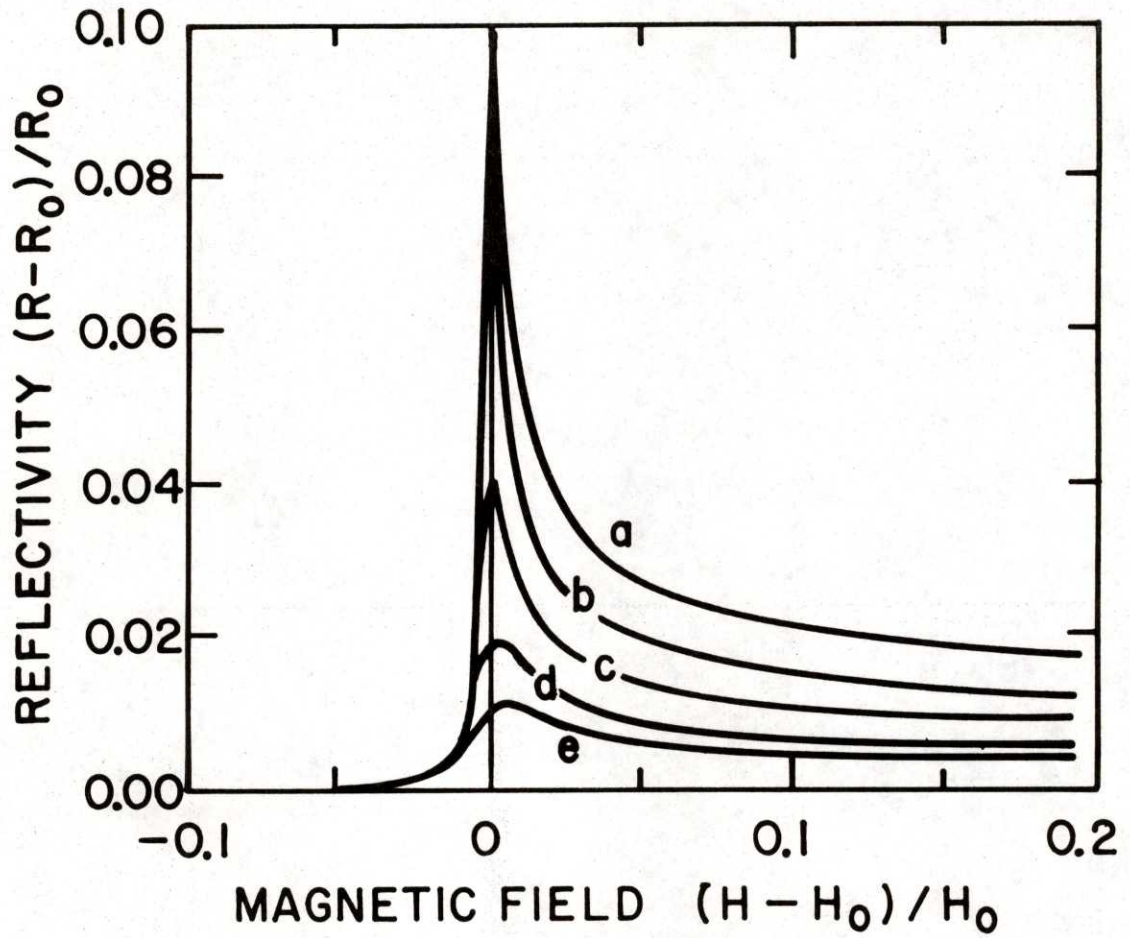


Fig. IV-4. Calculated magnetoreflexion spectra.

curves in order to estimate the scattering time τ .

C. Magnetoreflexion Spectra

Some representative experimental results are given in Figs. IV-5 through IV-11. In each case we plot a portion of the detector signal, proportional to the reflectivity R , as a function of the applied magnetic field, for both left and right circularly polarized radiation.

Figure IV-5 gives, as a reference, a spectrum for our [001] InSb sample, at a photon energy well above the band gap. A series of peaks is evident, which have been identified as some of the transitions illustrated in Fig. II-4, from the valence to the conduction band Landau levels, as calculated using the quasi Ge model outlined in Chapter II. The numbers above each peak correspond to the identification scheme given in Chapter V, where we describe the details of the identification process.

The peaks in Fig. IV-5 have the shape and approximate width of curve a in Fig. IV-4, corresponding to $\omega\tau \approx 1000$ or a relaxation time $\tau \approx 2 \times 10^{-12}$ sec. We expect these peaks to correspond closely to the peaks observed in magneto-absorption. In fact, there is a systematic shift to higher magnetic fields from the absorption peaks observed for $\vec{E}_\perp \vec{H}$ by Pidgeon and Brown,¹ corresponding to a shift of about 3 or 4 meV in energy. This is probably due to strain energy shifts in their 4 to 10 μm thick samples.

Figure IV-6 gives a similar spectrum for a sample of $\text{Hg}_{1-x}\text{Cd}_x\text{Te}$, again taken with a photon energy well above the gap and at liquid He temperature (≈ 24 K). The lines are much broader than in Fig. IV-5 for InSb, corresponding in Fig. IV-4 approximately to curve d for $\omega\tau \leq 100$ or less, so that the

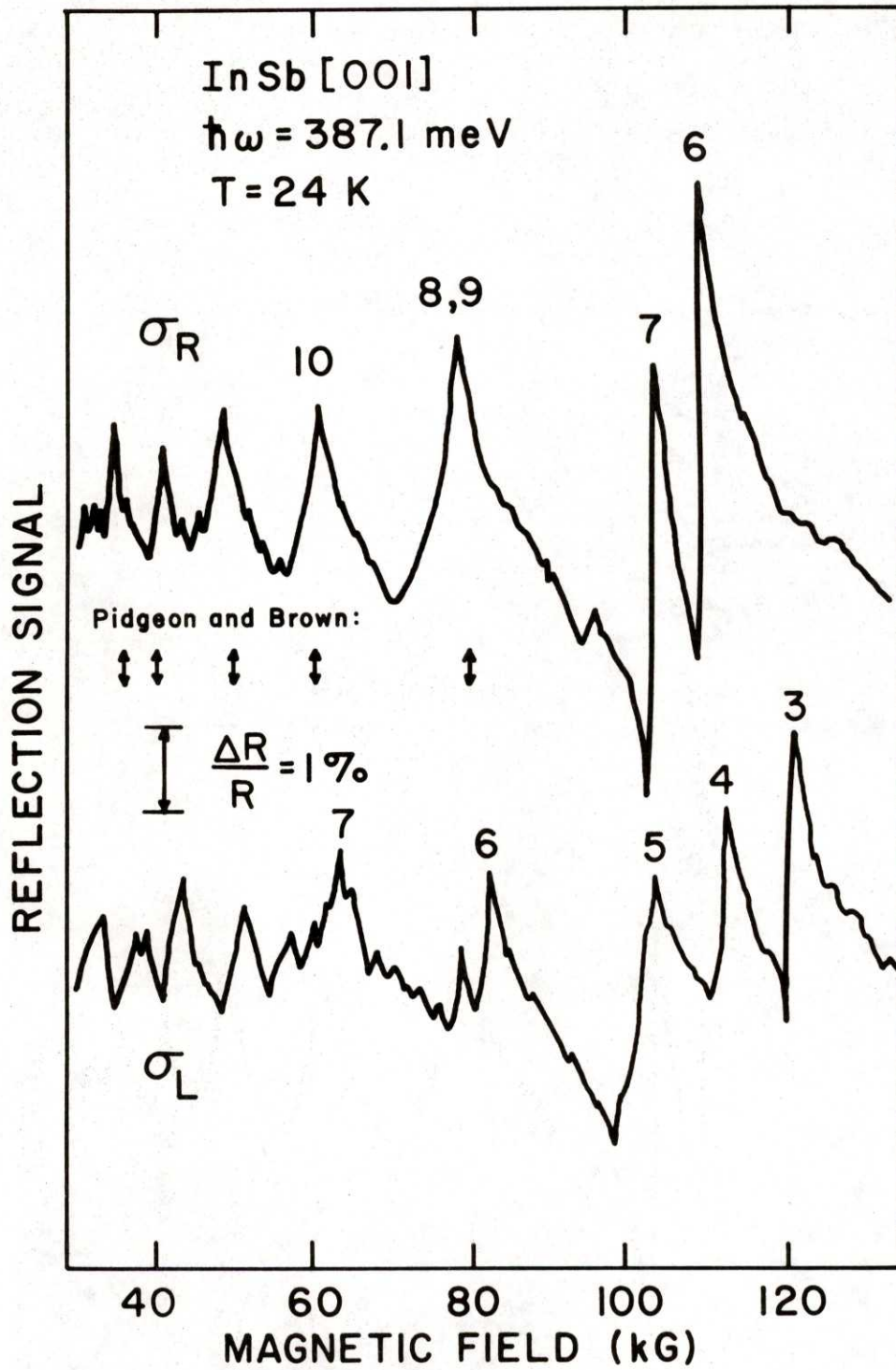


Fig. IV-5. Magnetoreflection spectra for InSb for optical polarizations σ_R and σ_L , compared to the results of Pidgeon and Brown¹ for $\vec{E} \perp \vec{H}$.

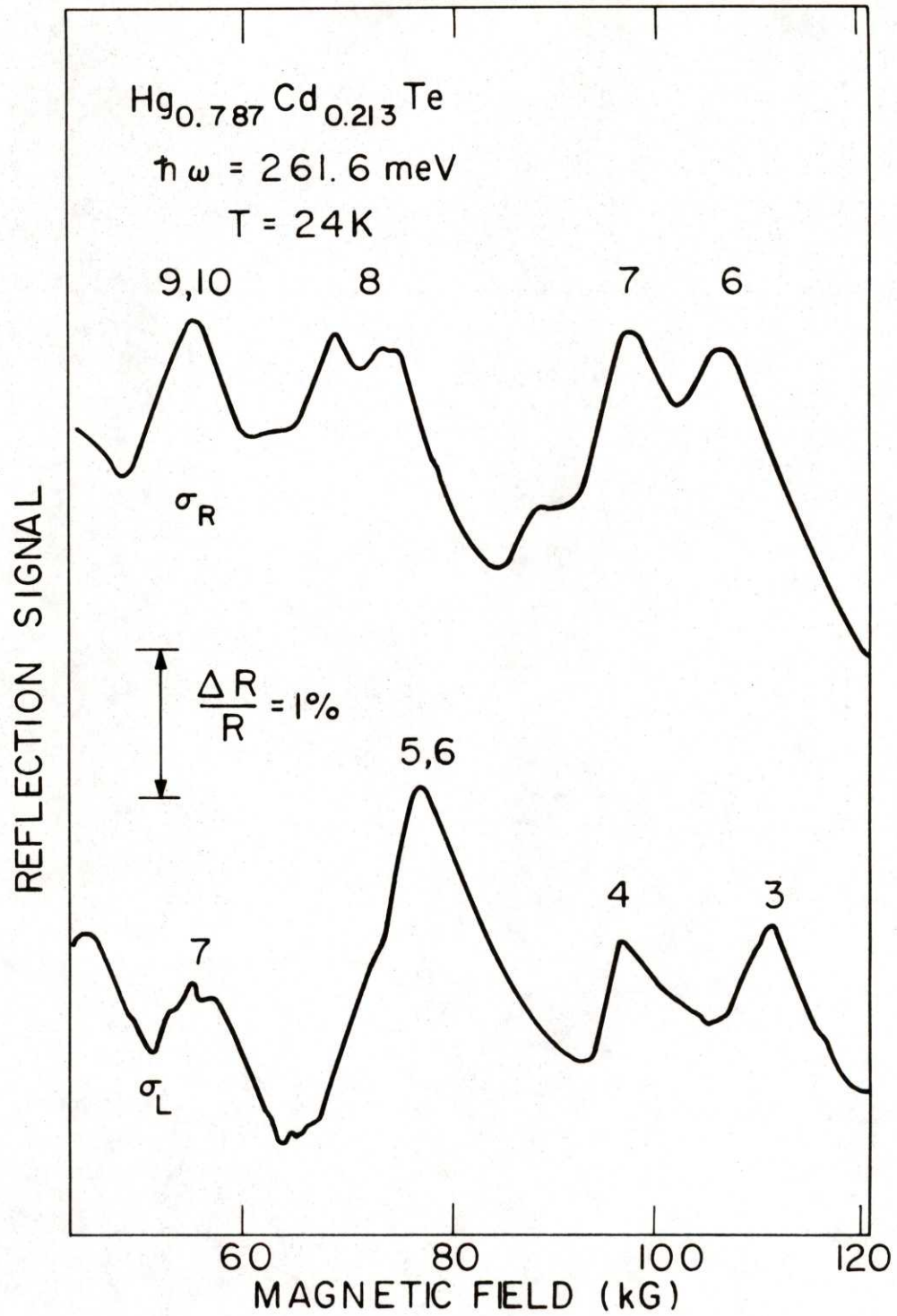


Fig. IV-6. Magnetoreflexion spectra for $\text{Hg}_{.787}\text{Cd}_{.213}\text{Te}$, $T = 24\text{K}$.

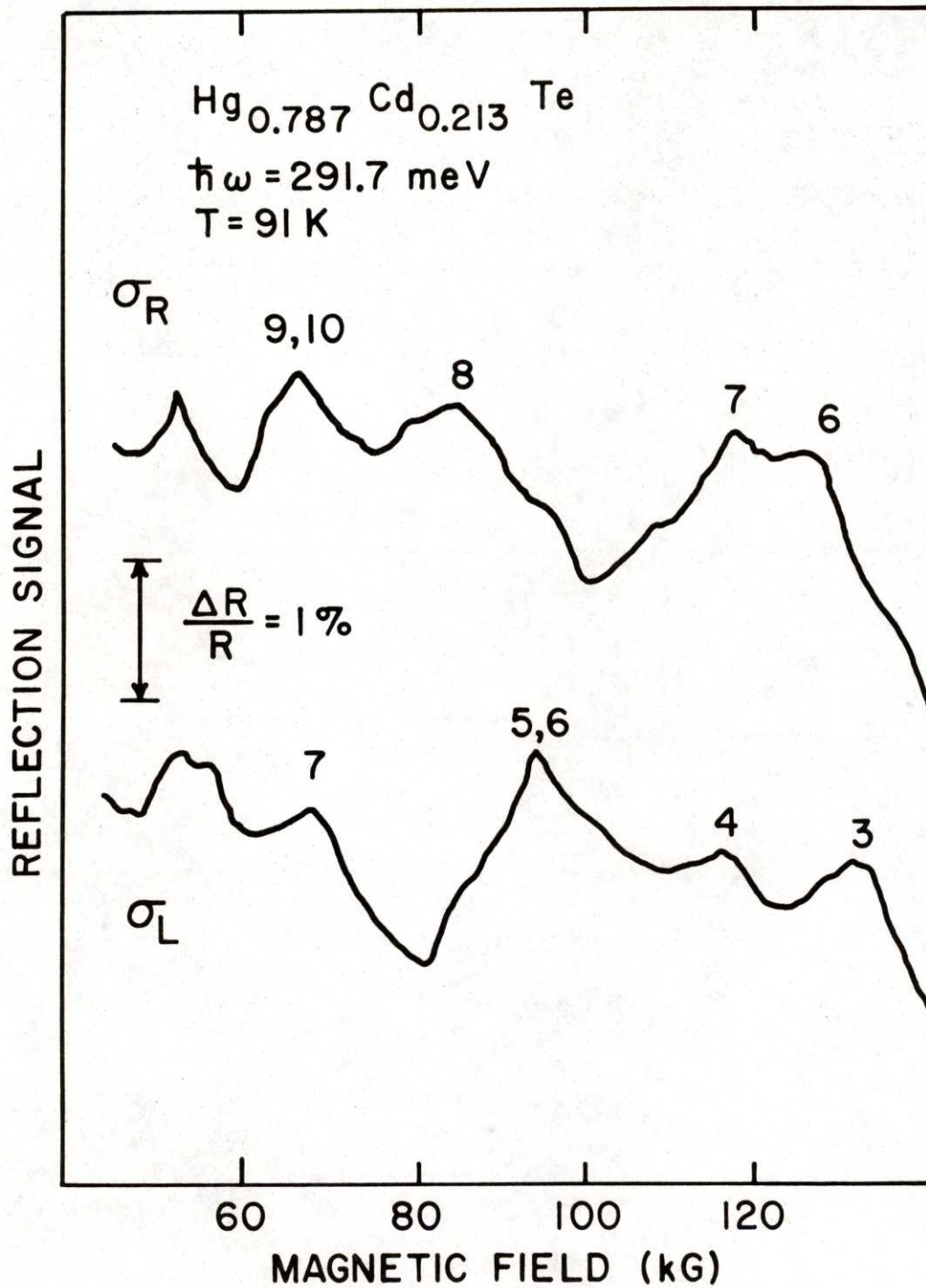


Fig. IV-7. Magnetoreflexion spectra for $\text{Hg}_{.787}\text{Cd}_{.213}\text{Te}$, $T = 91\text{K}$.

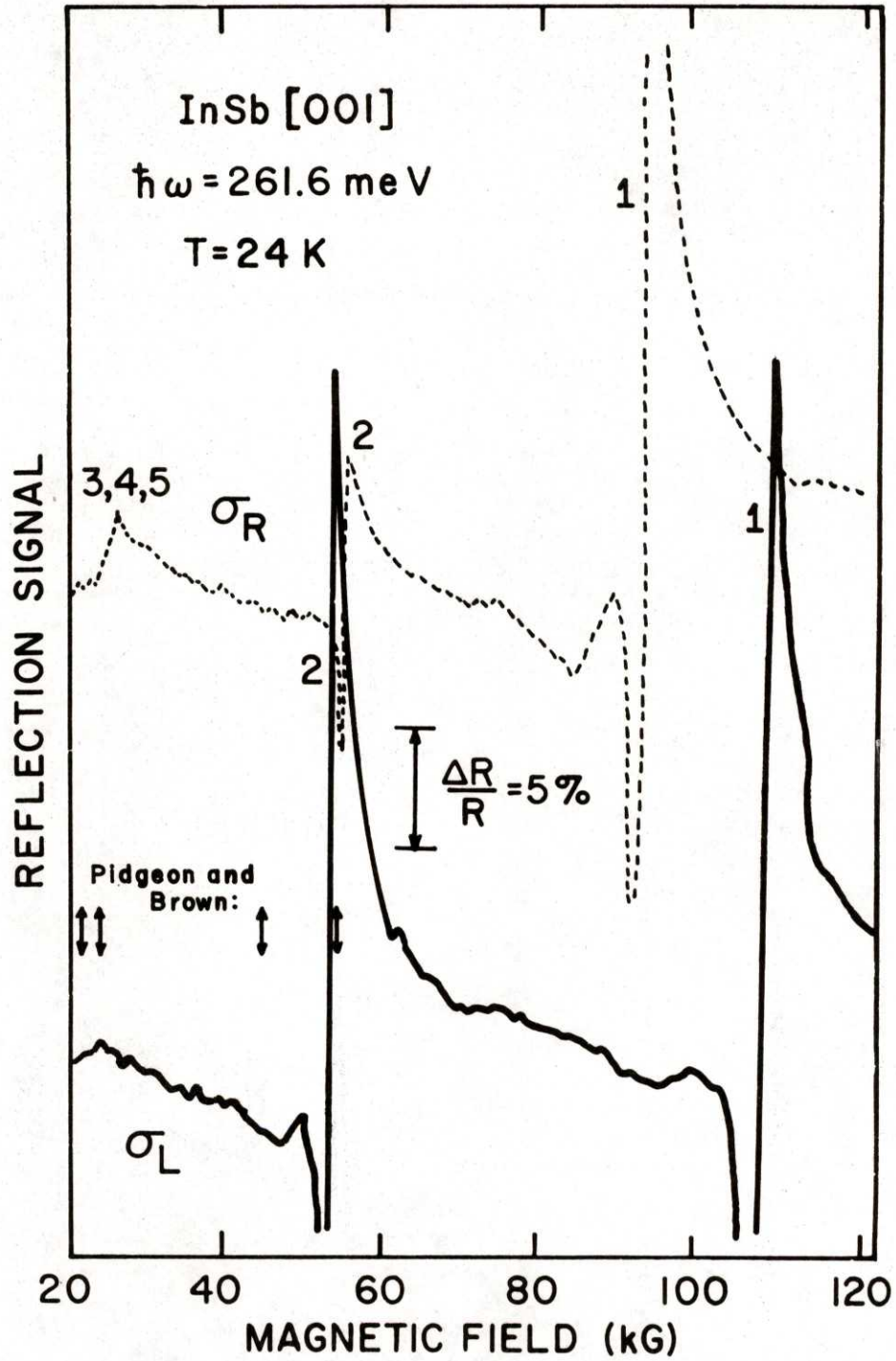


Fig. IV-8. Magnetoreflection spectra for InSb, $\vec{H} \parallel [001]$.

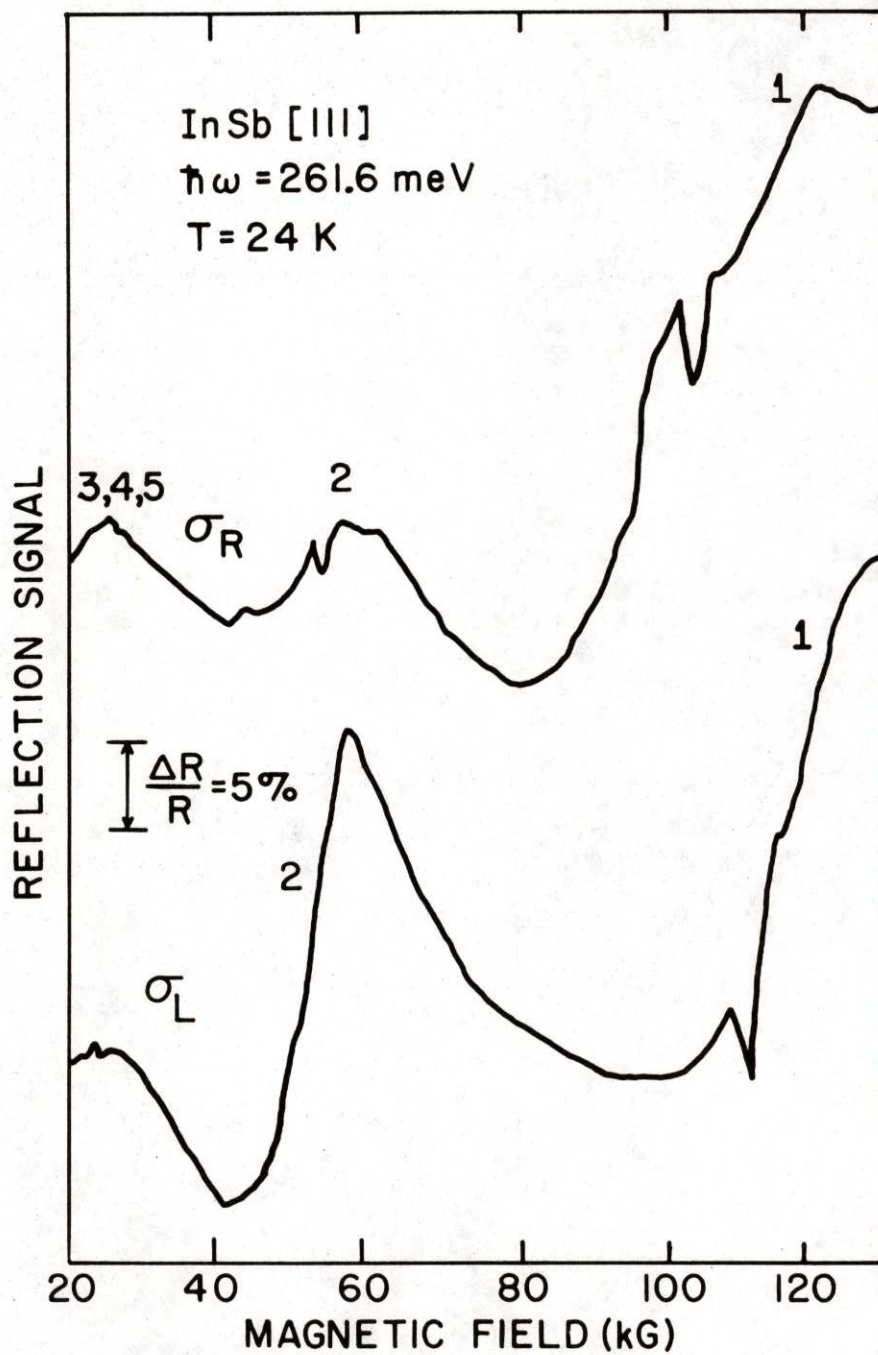


Fig. IV-9. Magnetoreflexion spectra for InSb, $\vec{H} \parallel [111]$.

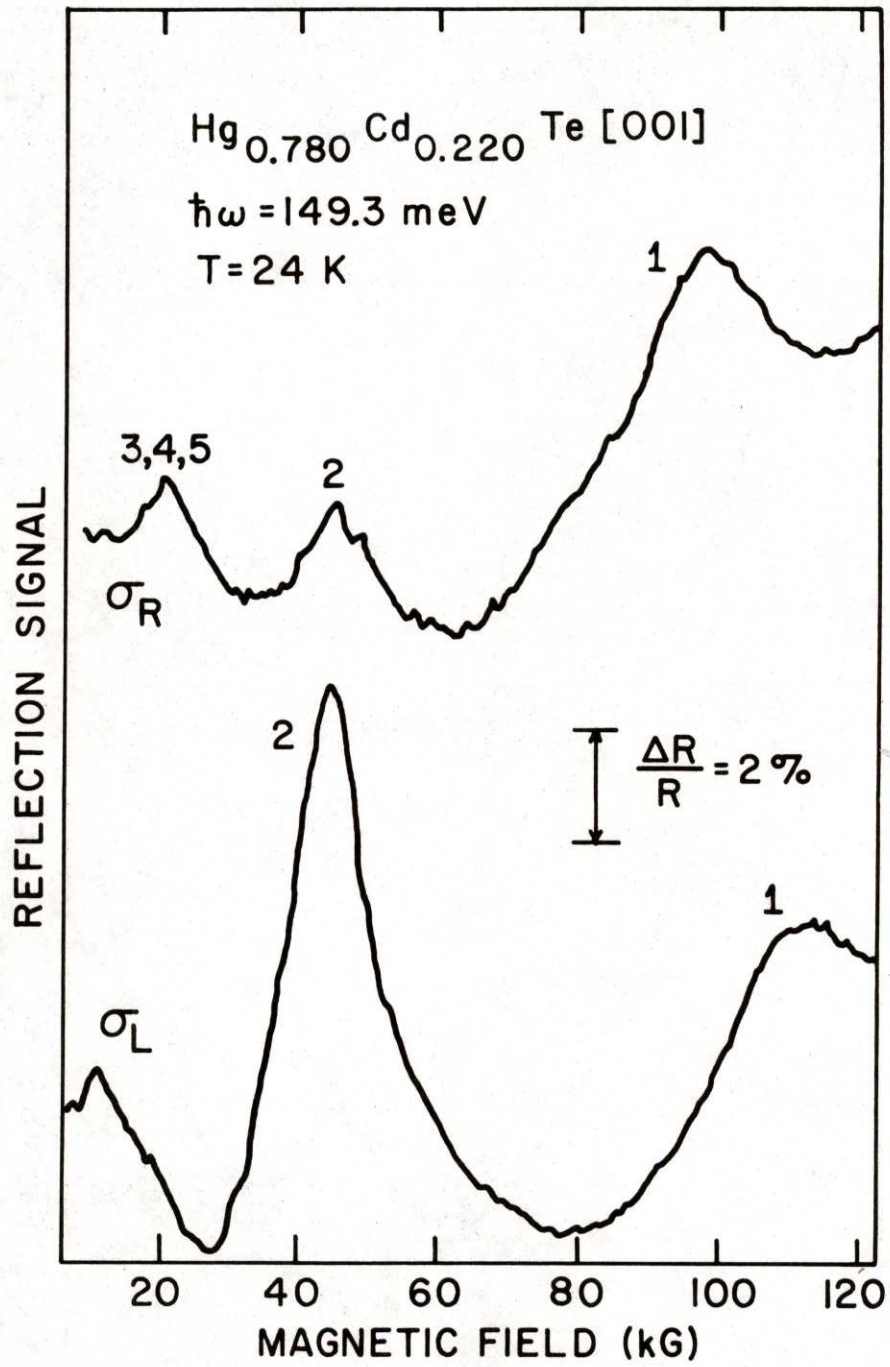


Fig. IV-10. Magnetoreflexion spectra for $\text{Hg}_{.78}\text{Cd}_{.22}\text{Te}$, $\vec{H} \parallel [001]$.

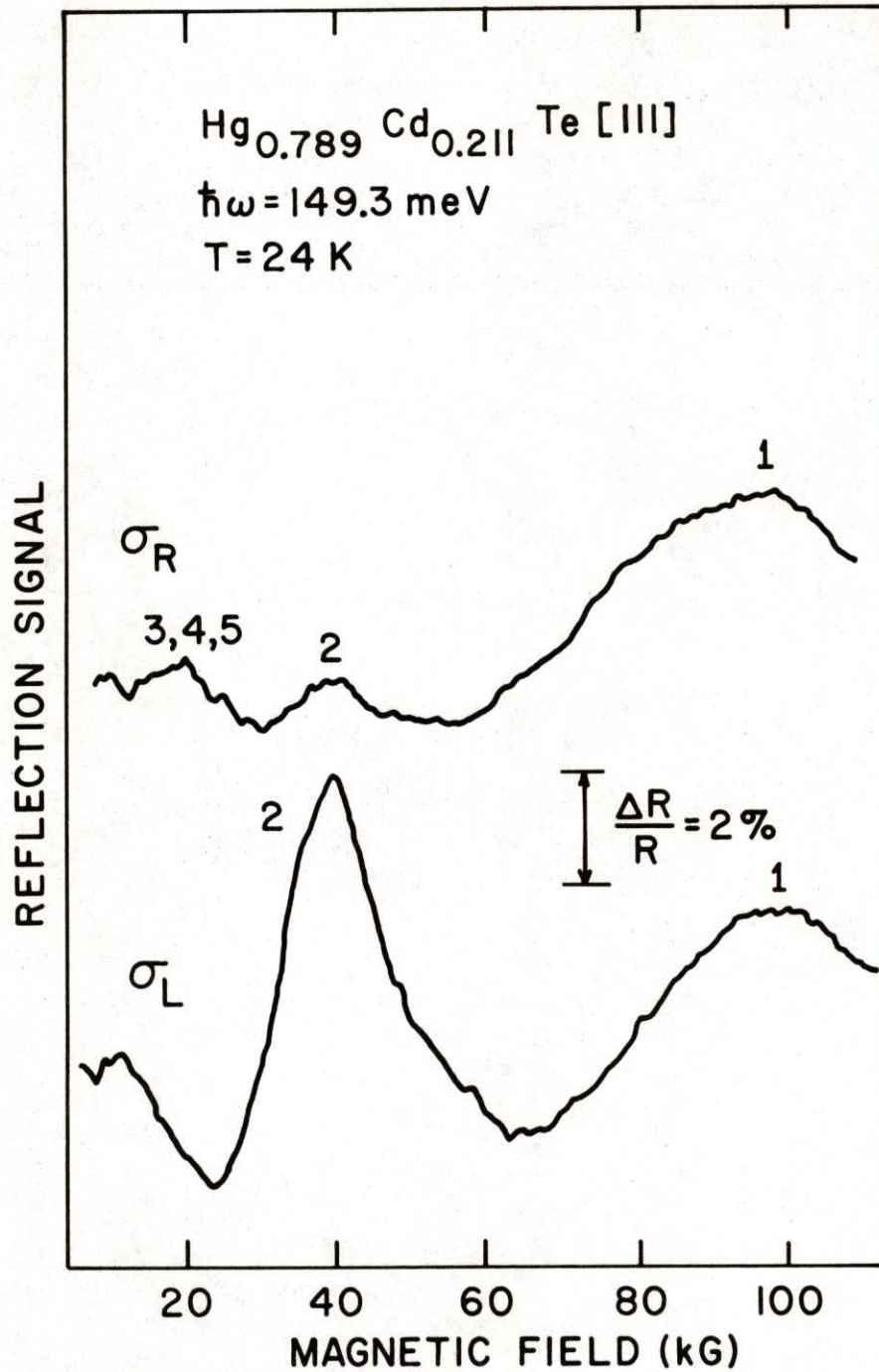


Fig. IV-11. Magnetoreflexion spectra for $\text{Hg}_{.789}\text{Cd}_{.211}\text{Te}$, $\vec{H} \parallel [111]$.

equivalent relaxation time $\tau \leq 2 \times 10^{-13}$, a factor of at least 10 shorter than for InSb.

Figure IV-7 gives a spectrum for the same $\text{Hg}_{1-x}\text{Cd}_x\text{Te}$ sample as in Fig. IV-6, but at liquid nitrogen temperature (≈ 91 K). The lines are only slightly broader and weaker. We attribute the temperature independent broadening to the inhomogeneity of the alloy composition, such as has been demonstrated graphically by Vanier et al.,¹⁰ and was indicated in the point-to-point scatter of the microprobe results for our samples. This scatter is primarily responsible for the uncertainty of these measurements of x as given in Table IV-1. Comparing Fig. IV-5 for InSb to Figs. IV-6 and IV-7, it is clear that the large linewidths limit the accuracy of our results for $\text{Hg}_{1-x}\text{Cd}_x\text{Te}$ and also limit the number of interband transitions we can resolve.

Figures IV-8 through IV-11 give some typical spectra for photon energies just above the band gap. Figure IV-8, for InSb with $\vec{H} \parallel [001]$, illustrates a typical lineshape for the low-energy transitions. We attribute the dips to the left of the peaks to competition between discrete exciton transitions and the continuum interband transitions.¹¹ Figure IV-9 gives the same spectrum for $\vec{H} \parallel [111]$. The lines are broader, possibly because of improper sample preparation, but they do exhibit the kind of extra structure observed by Pidgeon and Groves,² which they attributed to warping and inversion asymmetry effects which are most important for the [111] orientation and for these low-energy transitions.

In Figs. IV-10 and IV-11 we present spectra for two $\text{Hg}_{1-x}\text{Cd}_x\text{Te}$ samples of nearly the same alloy composition, with $\vec{H} \parallel [001]$ in Fig. IV-10 and $\vec{H} \parallel [111]$ in Fig. IV-11. We see the same exciton lineshape as in Fig. IV-8 and IV-9, but cannot resolve any structure attributable to warping and

inversion asymmetry effects. These effects may be weaker than in InSb, or the lines are too broad for such structure to be observed.

D. Fan Charts

The results of our magnetoreflexion experiments for the $\text{Hg}_{1-x}\text{Cd}_x\text{Te}$ samples are given in the fan charts in Figs. IV-12a through 12t. We plot, for each sample studied and at each temperature, the magnetic field and photon energy positions for each reflectivity peak, for both senses of circular polarization. The solid and dashed curves are those calculated, as described in Chapter V, from the best fit to the data, except for two cases, samples 798 and 804 at liquid nitrogen temperature, where the data were not sufficient to make such a fit. For these two, the curves were calculated using parameters expected to give an approximate fit to the data.

In Figs. IV-13a and 13b we given fan charts for the InSb samples studied. In Fig. IV-13a we also plot the magnetoabsorption results of Pidgeon and Brown¹ for $\vec{E} \perp \vec{H}$; as we remarked in the preceding Section, there is a slight shift to lower energies for our data. The solid and dashed lines in these Figs. were calculated using the parameters deduced by Pidgeon and Brown from their data, which were limited to magnetic fields below 100 kG. Clearly the fit could be improved, especially at higher fields and photon energies. Such a fit would require that account be taken of inversion asymmetry and warping effects, as well as cyclotron resonance results for InSb.^{12, 13}

In the next Chapter we describe the fitting procedures used to deduce the band parameters for $\text{Hg}_{1-x}\text{Cd}_x\text{Te}$ from the data presented in Figs. IV-12a through 12t.

Figs. IV-12a - 12t. Fan charts for $\text{Hg}_{1-x}\text{Cd}_x\text{Te}$ samples. The photon energy and magnetic field positions of the magnetorefectivity peaks are given for σ_L (diamonds) and σ_R (triangles). The theoretical curves for σ_L (solid lines) and σ_R (dashed lines) are labeled with the transition numbers given in Table V-1, except that most light-hole transitions are not numbered since they cross the heavy-hole lines.

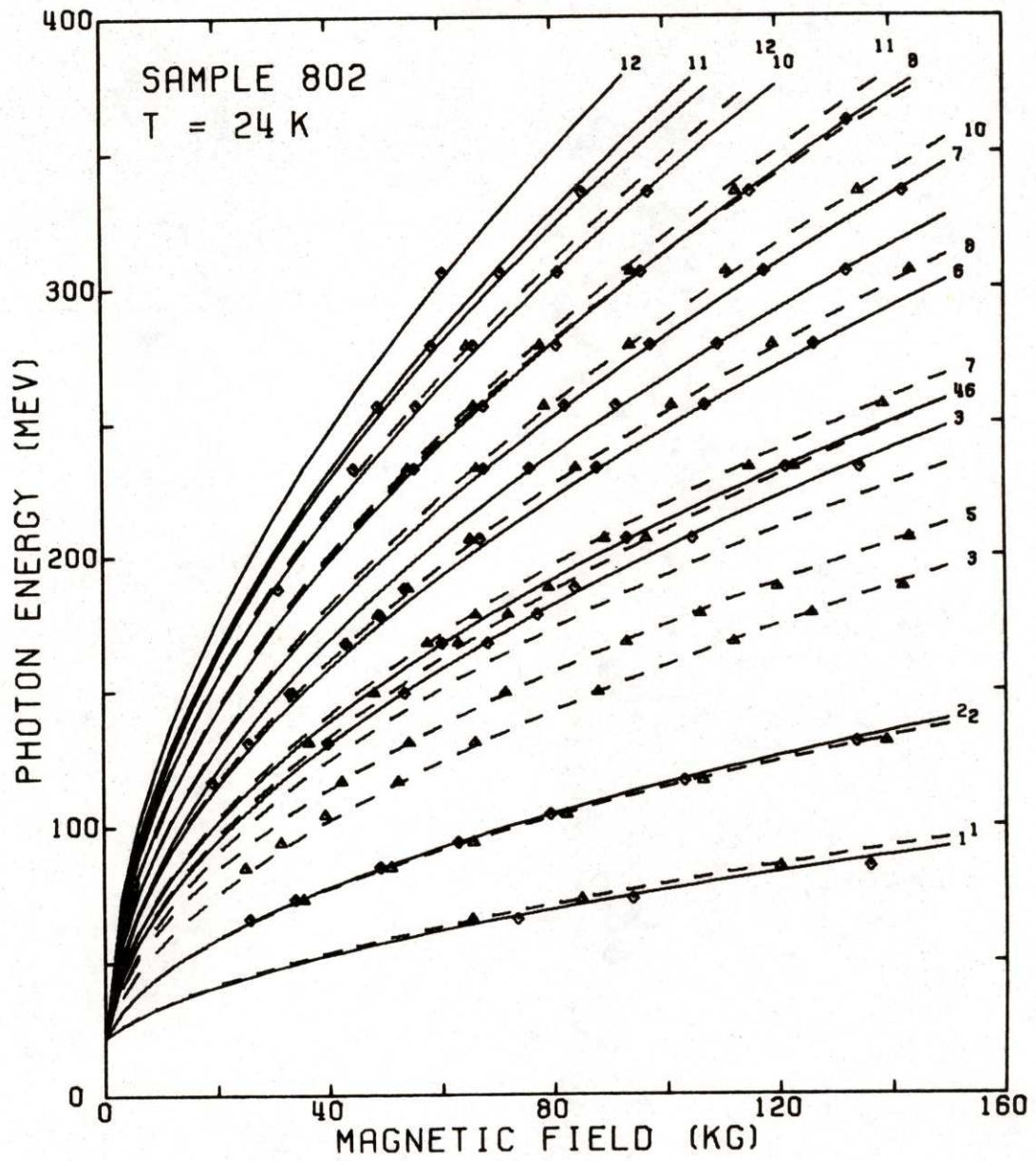


Fig. IV-12a. Fan chart for $\text{Hg}_{.825}\text{Cd}_{.175}\text{Te}$ at 24K.

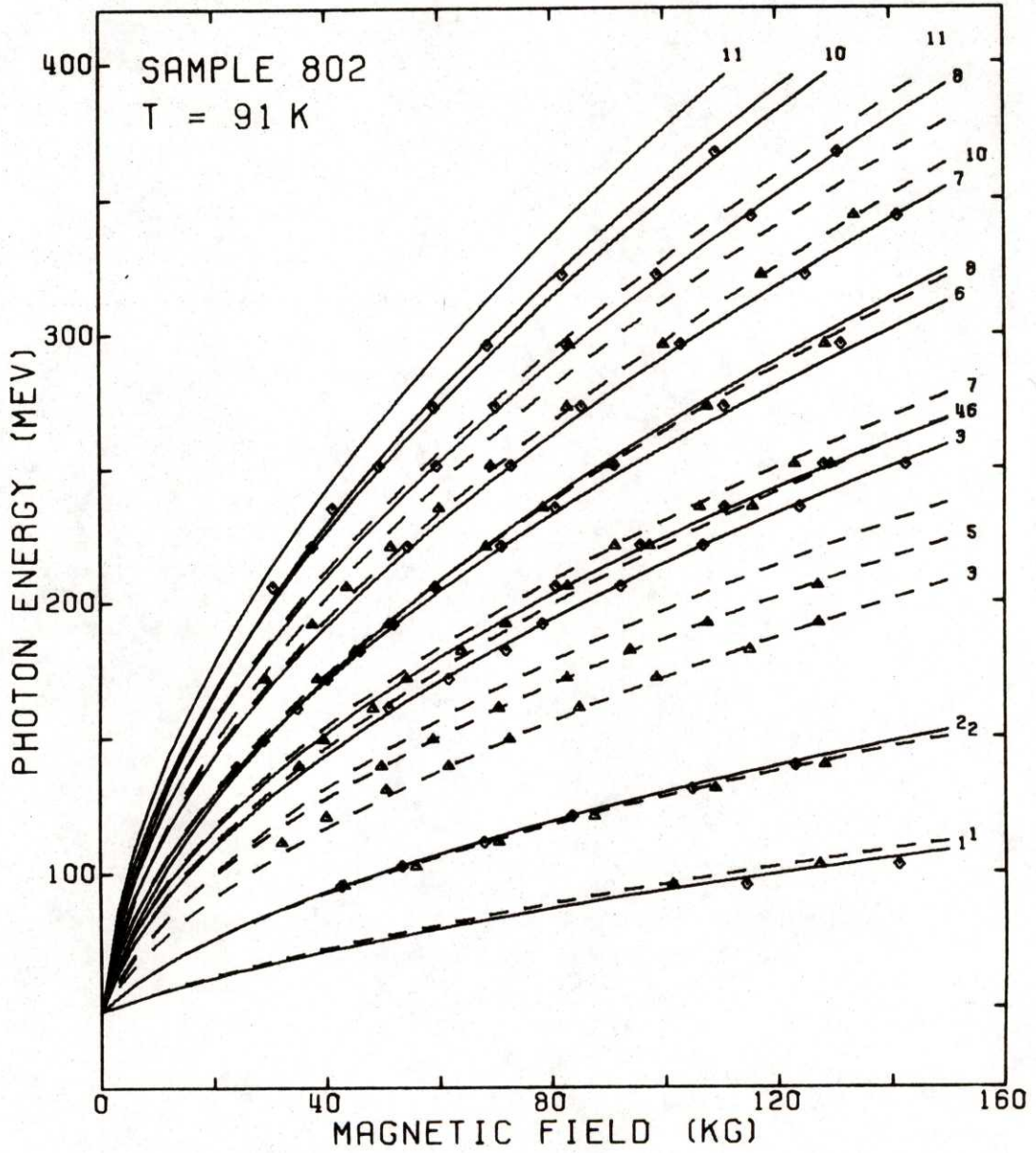


Fig. IV-12b. Fan chart for Hg._{0.825}Cd._{0.175}Te at 91K.

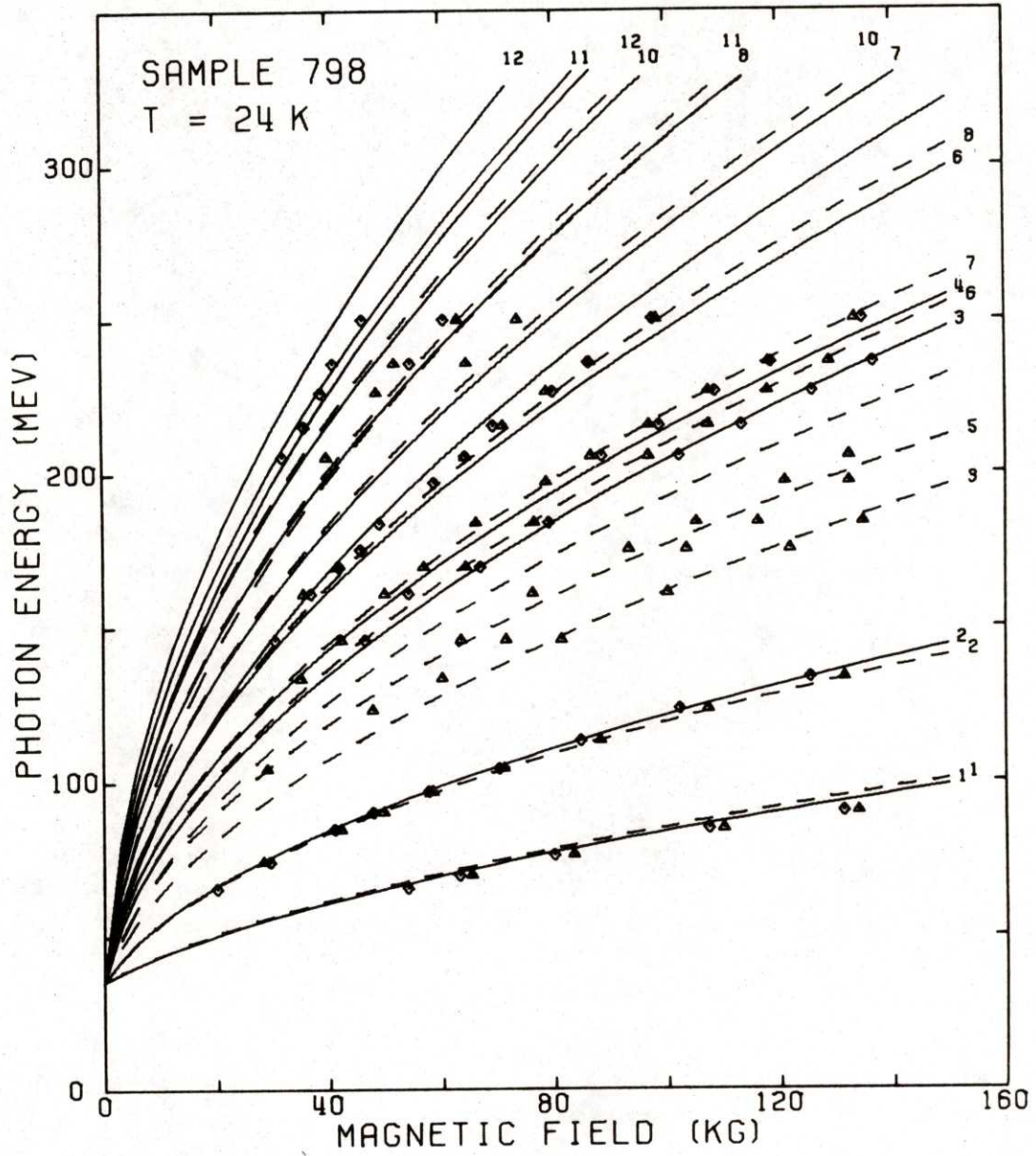


Fig. IV-12c. Fan chart for $\text{Hg}_{.818}\text{Cd}_{.182}\text{Te}$ at 24K.

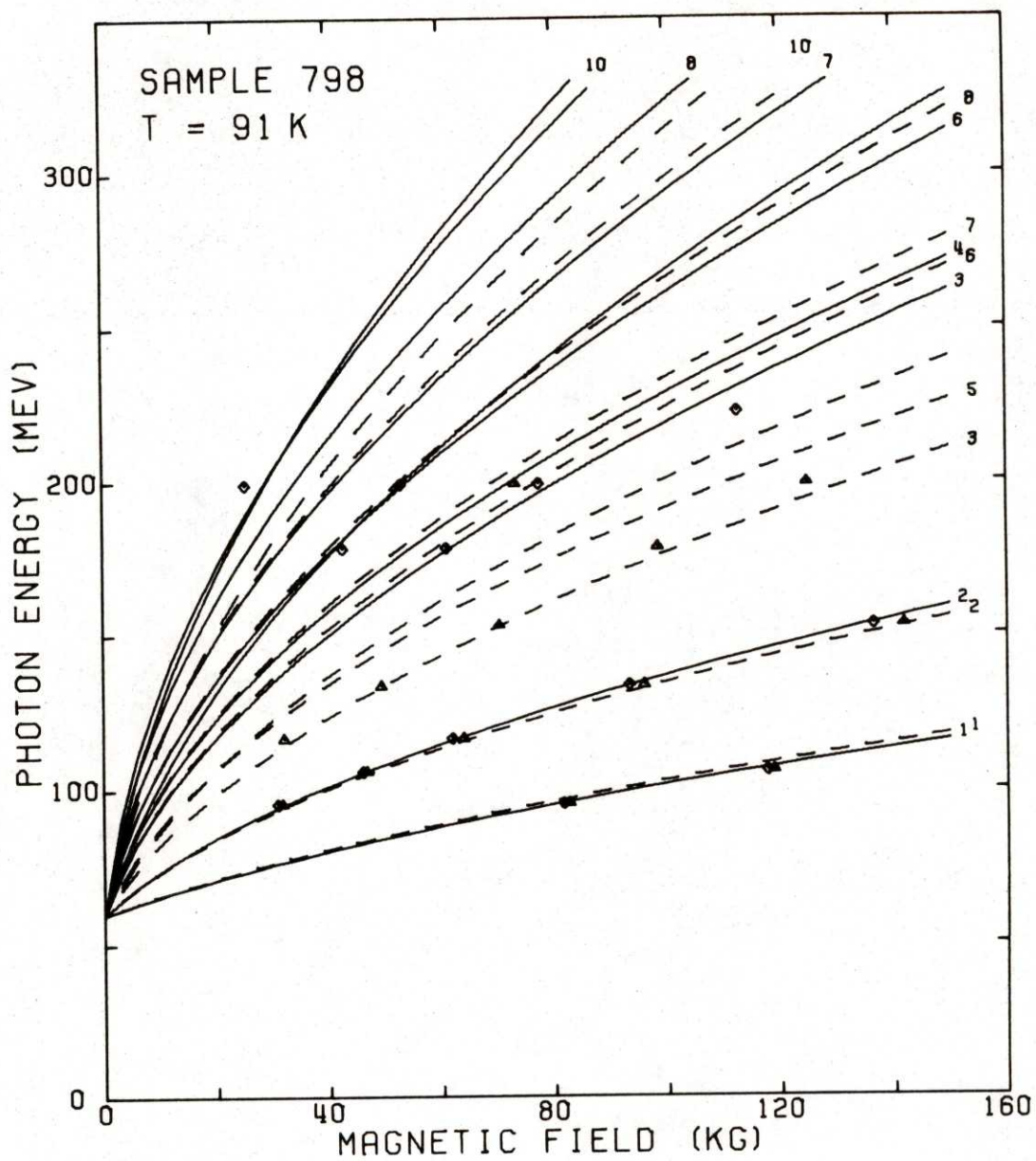


Fig. IV-12d. Fan chart for Hg_{.818}Cd_{.182}Te at 91K.

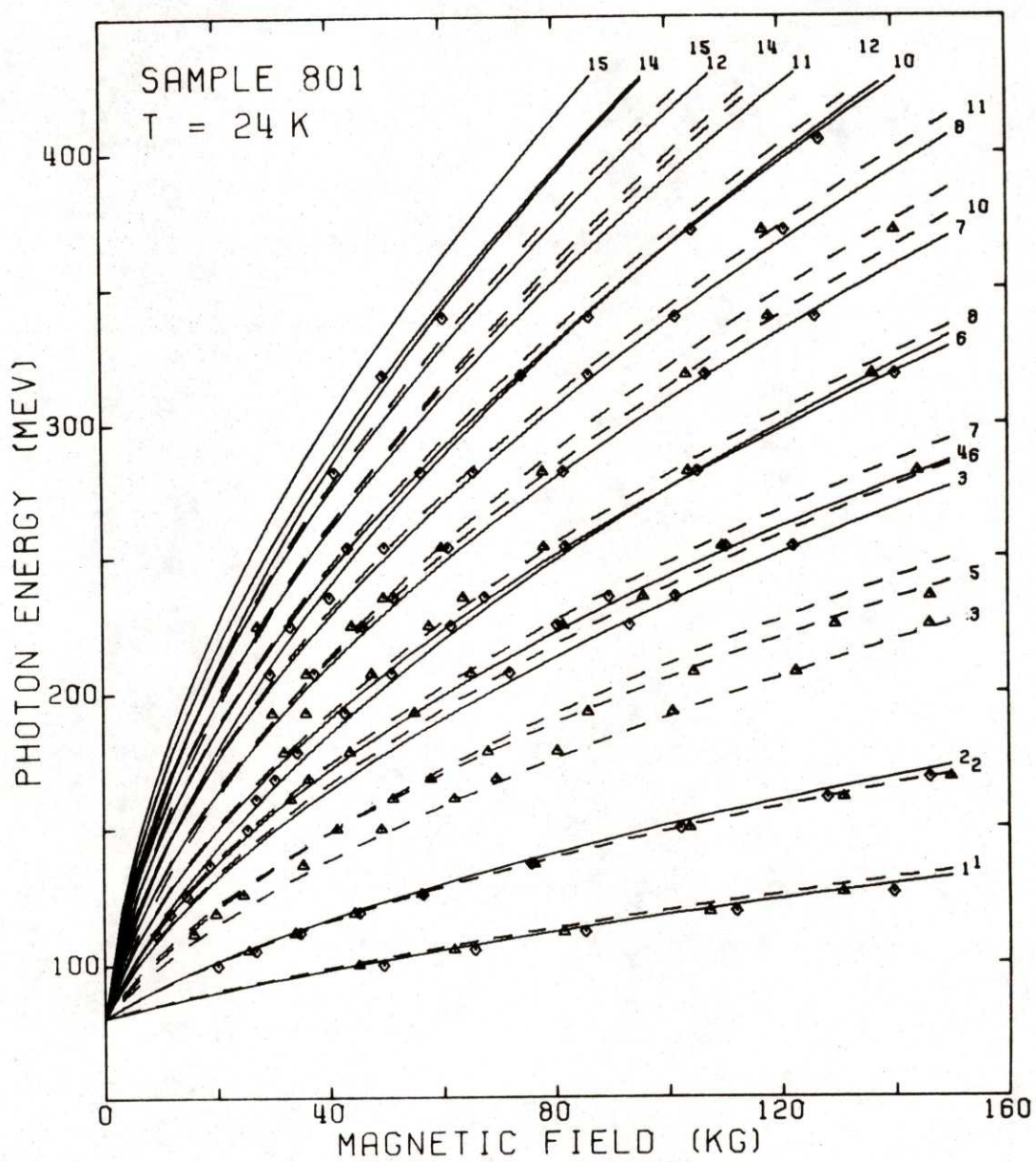


Fig. IV-12e. Fan chart for $\text{Hg}_{.804}\text{Cd}_{.196}\text{Te}$ at 24K.

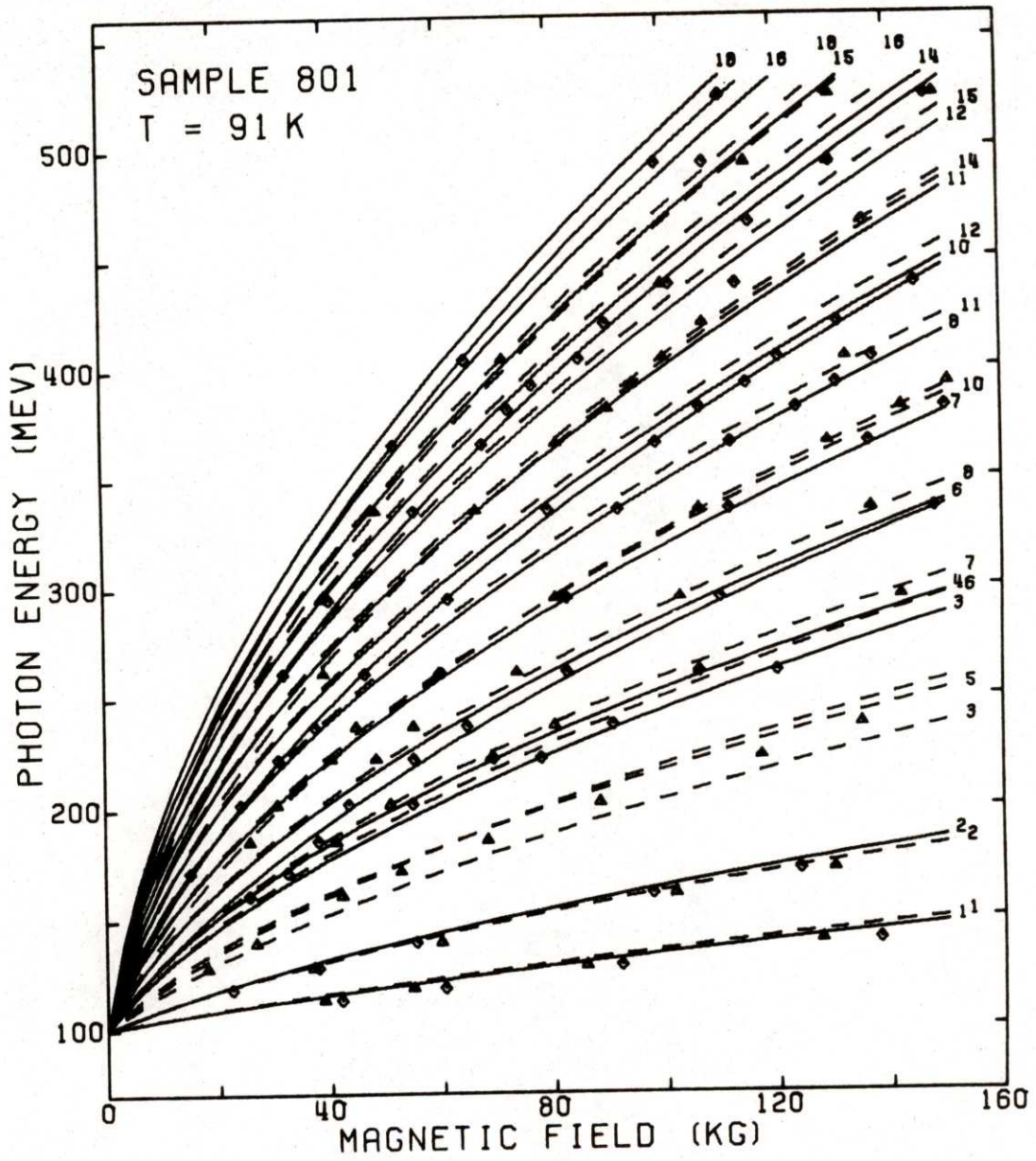


Fig. IV-12f. Fan chart for $\text{Hg}_{.804}\text{Cd}_{.196}\text{Te}$ at 91K.

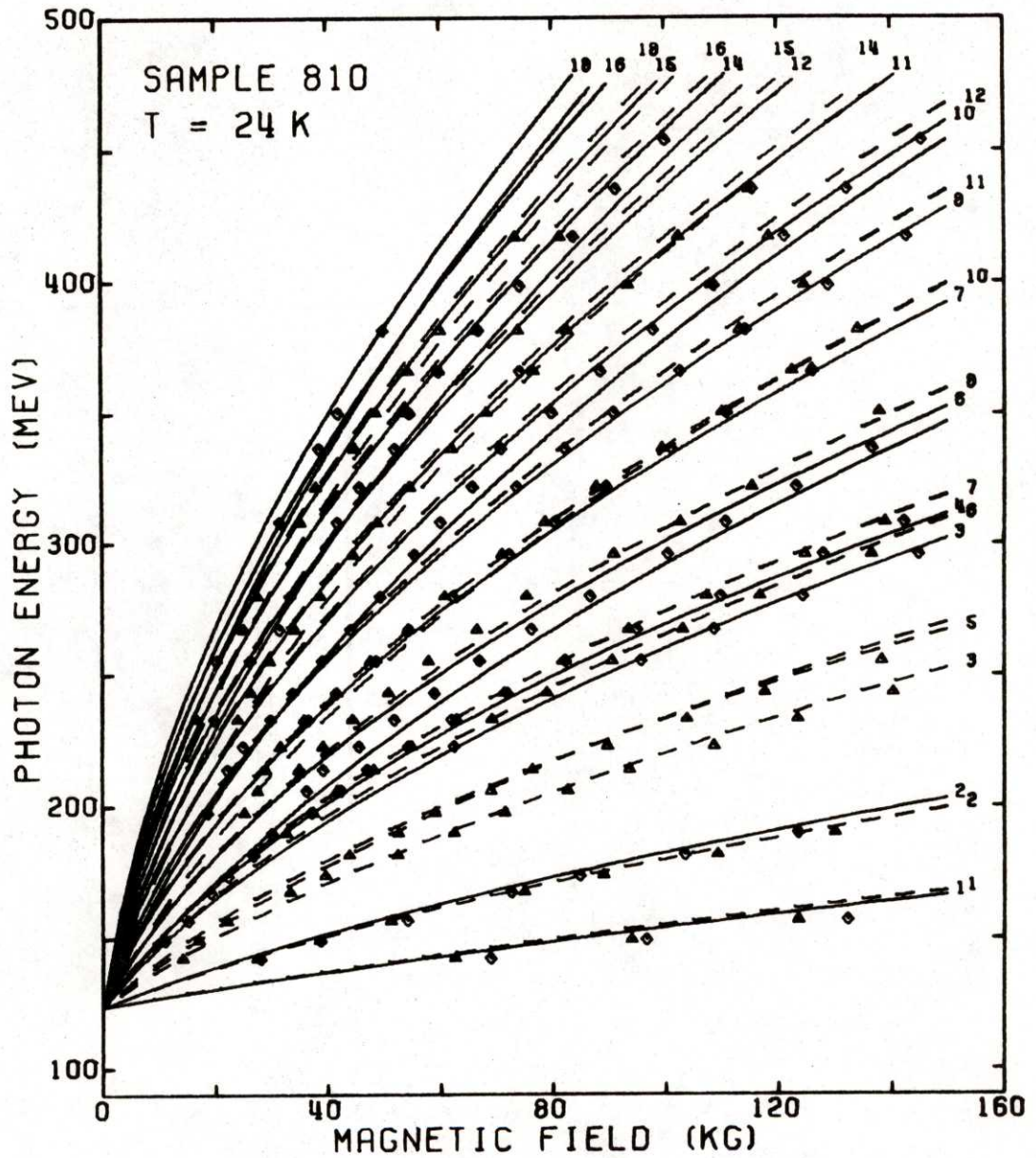


Fig. IV-12g. Fan chart for Hg.⁷⁸⁹Cd._{.211}Te at 24K.

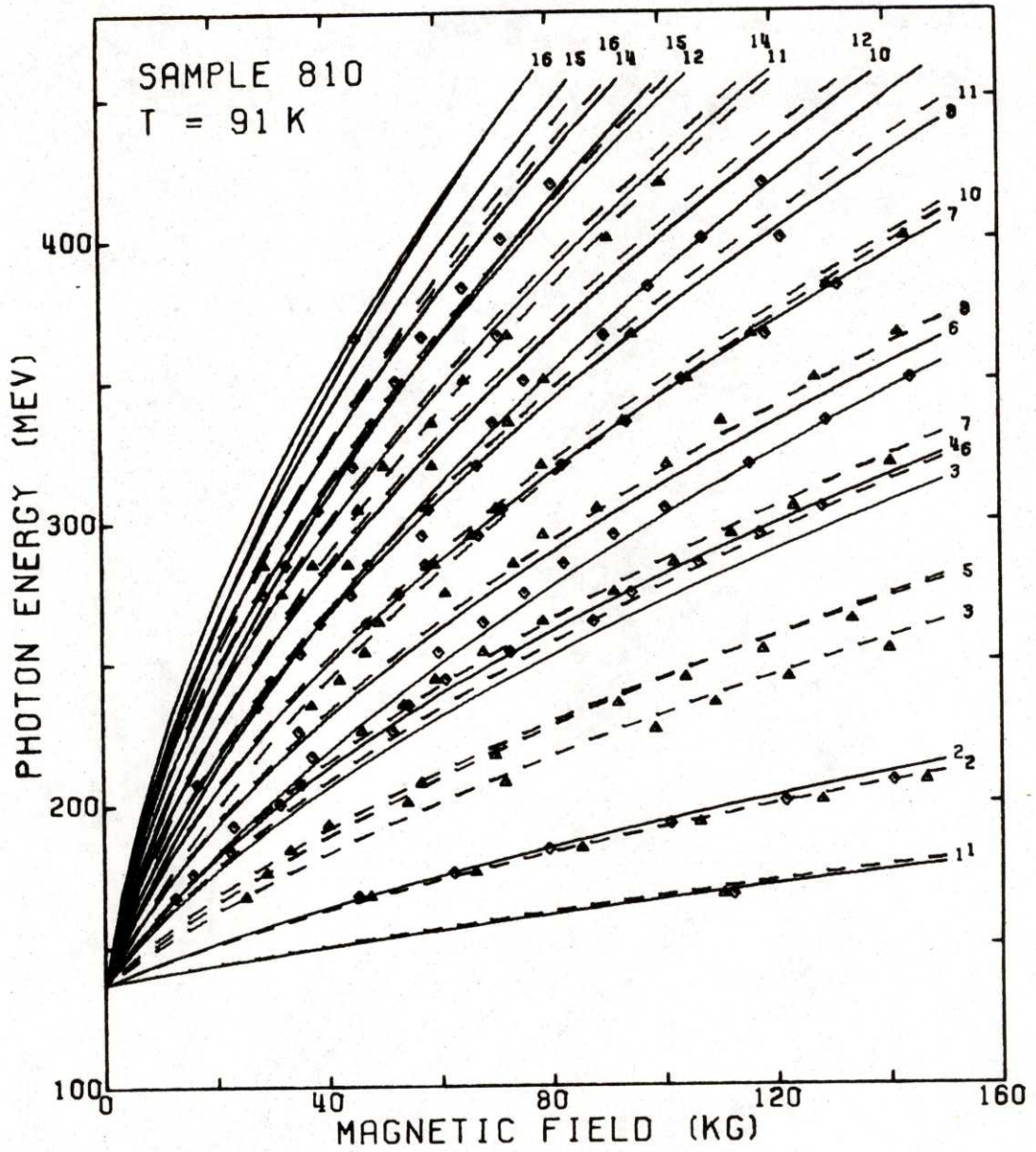


Fig. IV-12h. Fan chart for $\text{Hg}_{.789}\text{Cd}_{.211}\text{Te}$ at 91K.

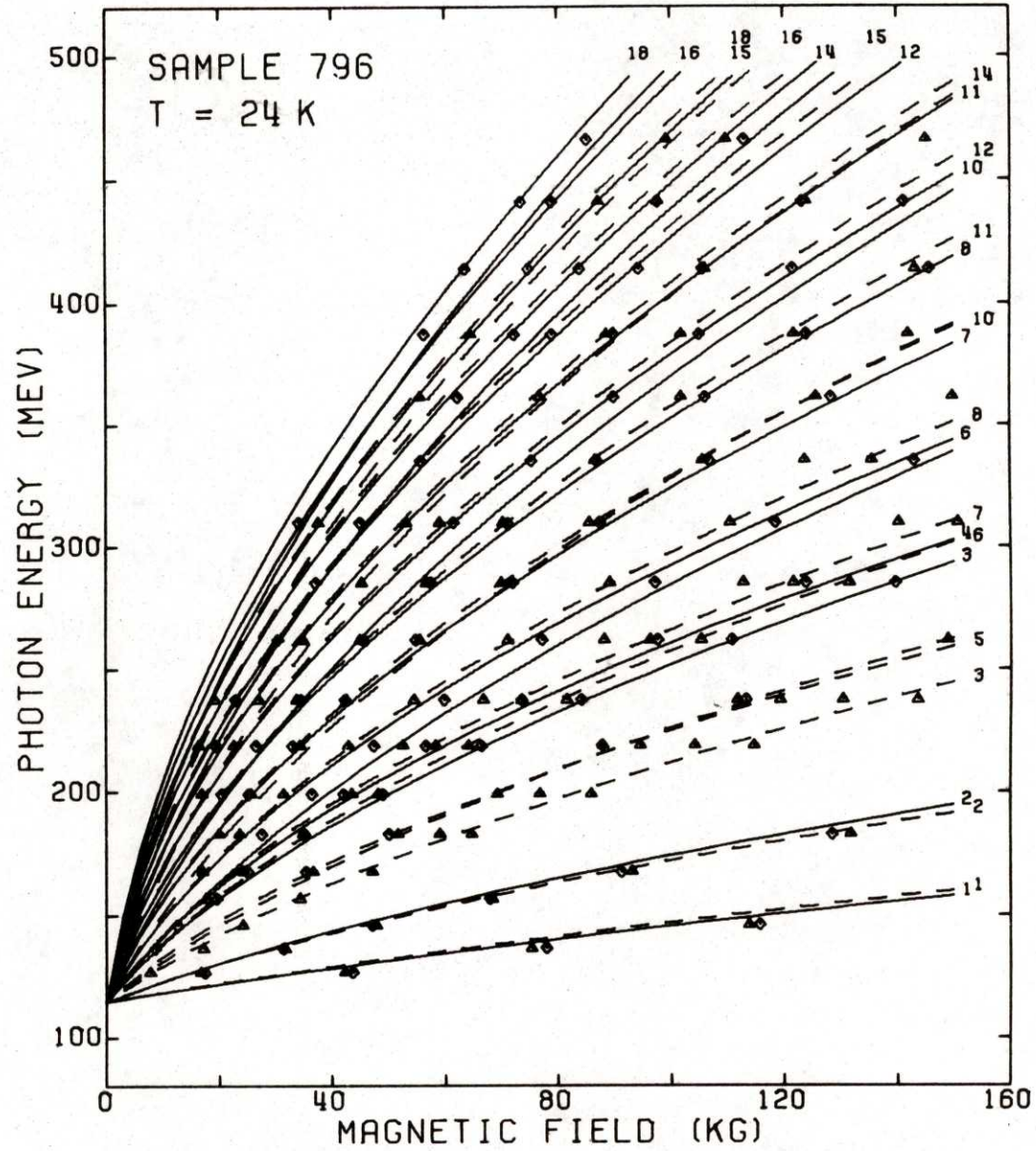


Fig. IV-12i. Fan chart for Hg_{0.787}Cd_{0.213}Te at 24K.

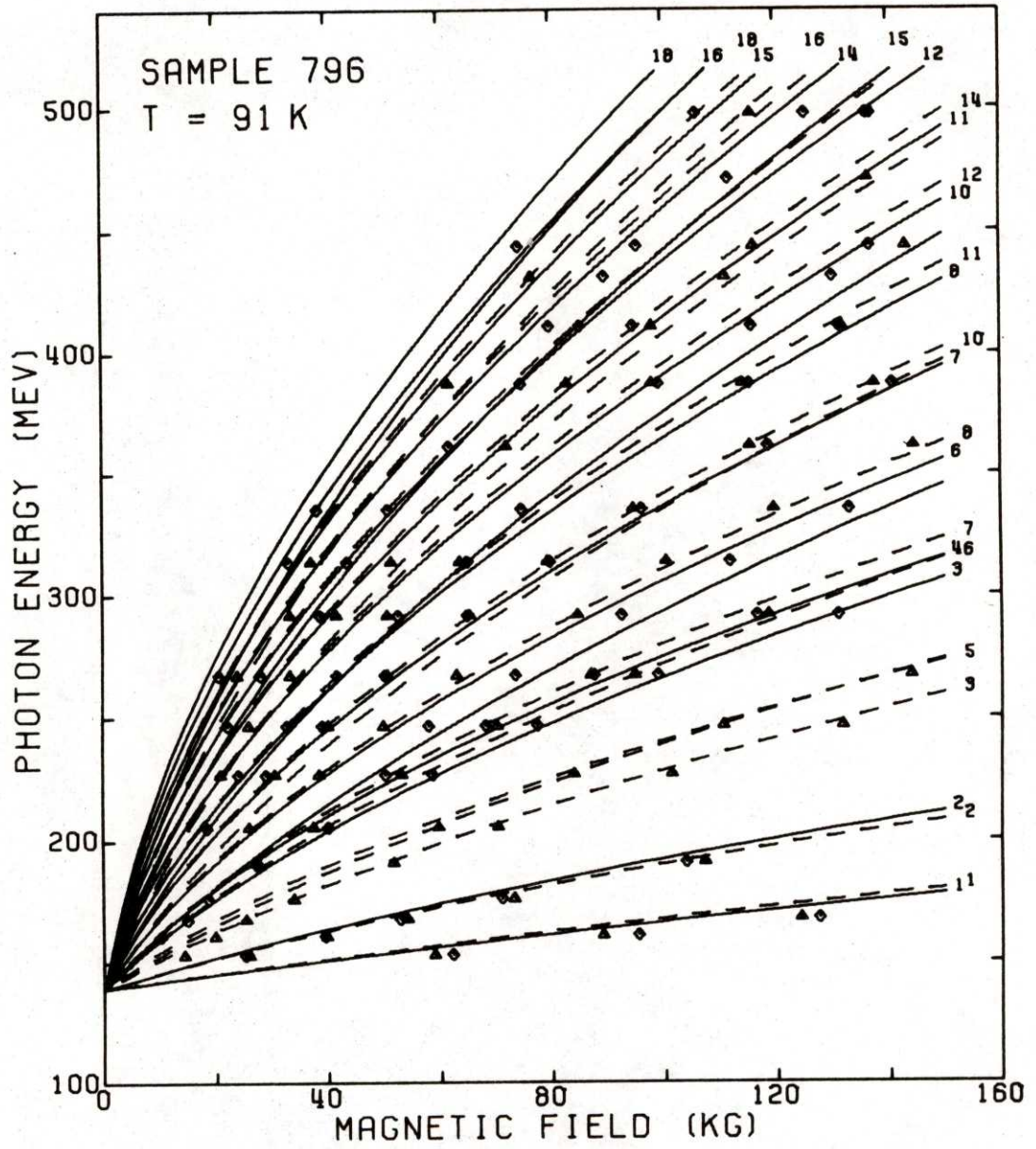


Fig. IV-12j. Fan chart for $\text{Hg}_{.787}\text{Cd}_{.213}\text{Te}$ at 91K.

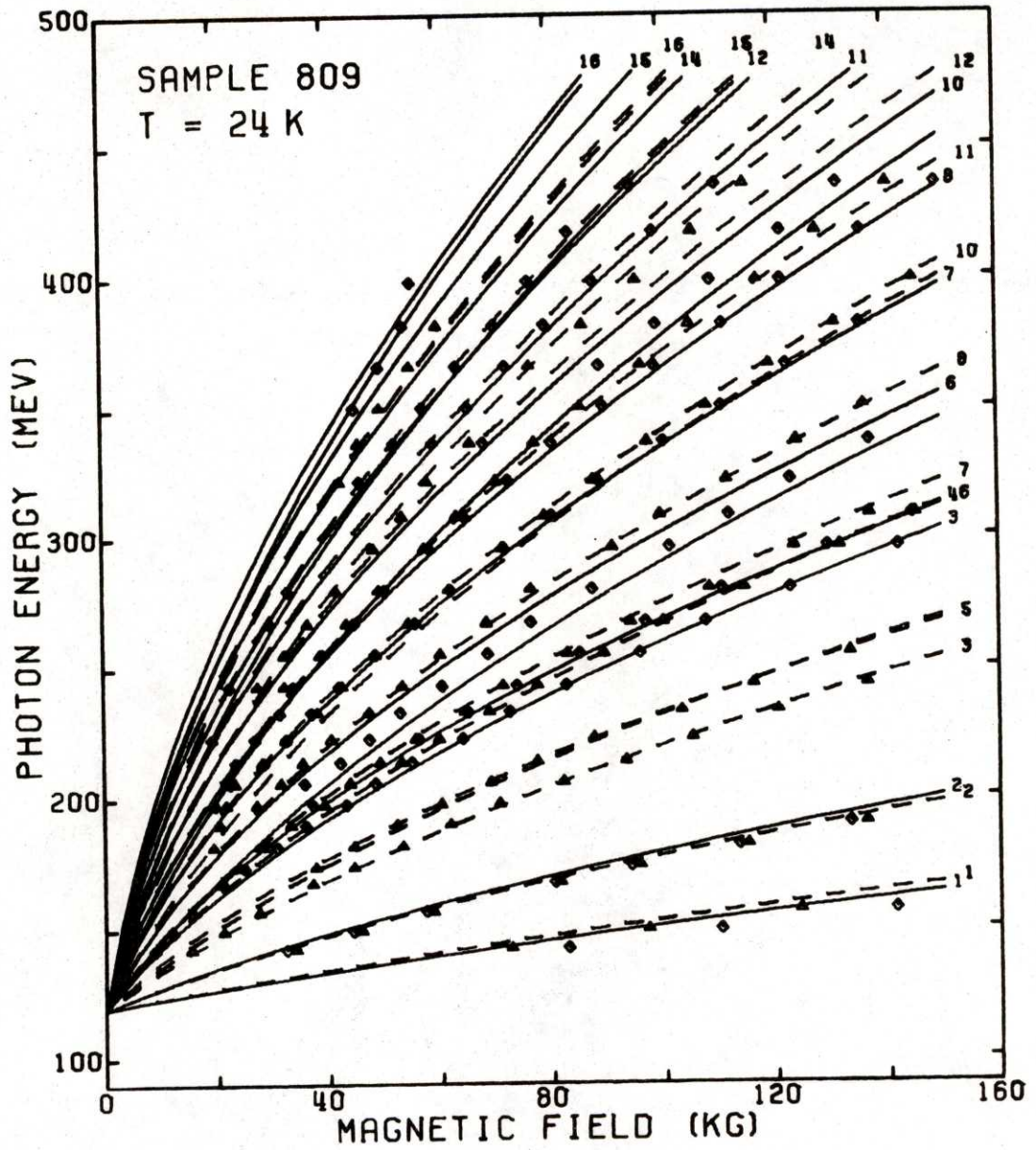


Fig. IV-12k. Fan chart for Hg_{0.78}Cd_{0.22}Te at 24K.

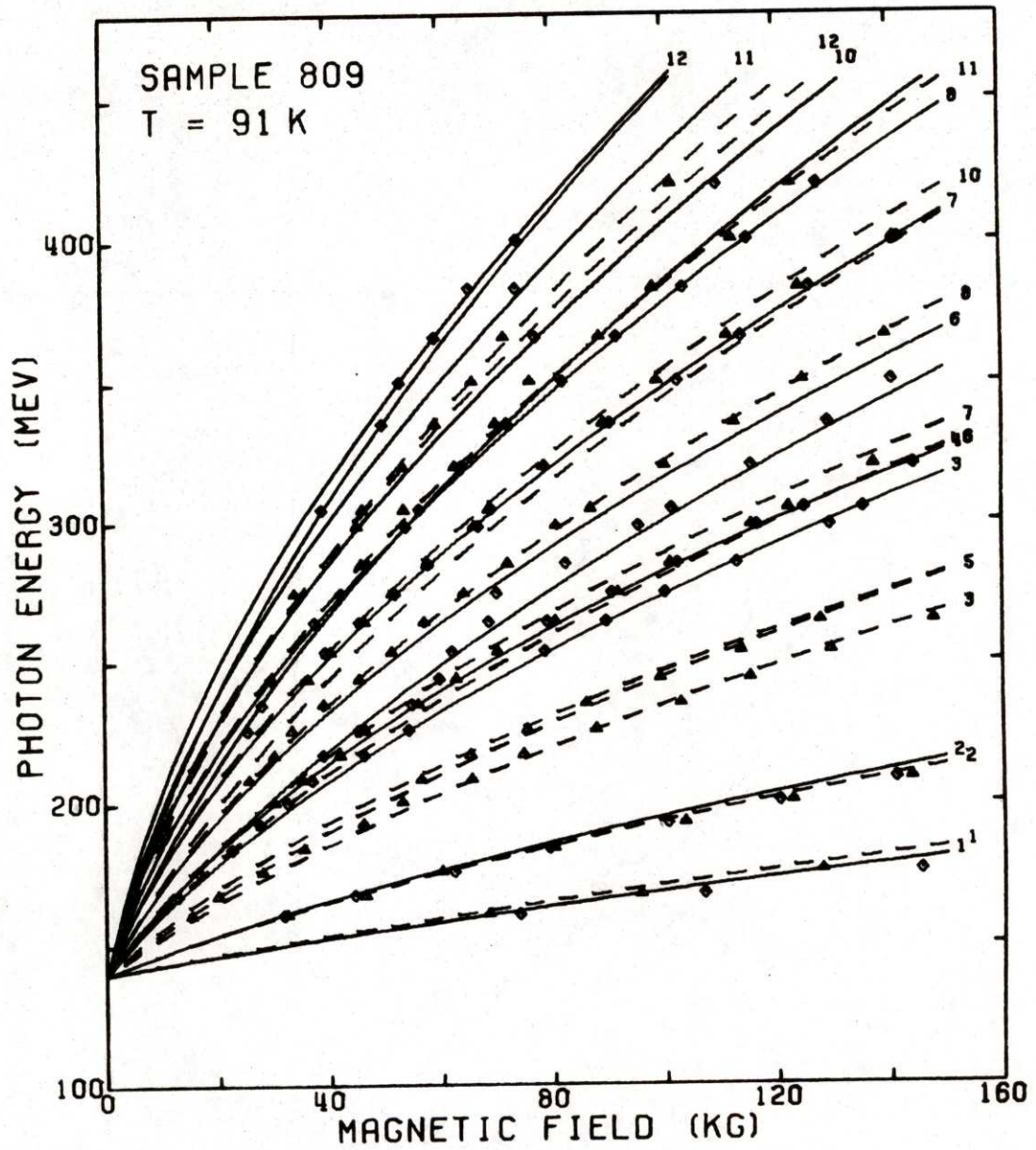


Fig. IV-121. Fan chart for Hg_{0.78}Cd_{0.22}Te at 91K.

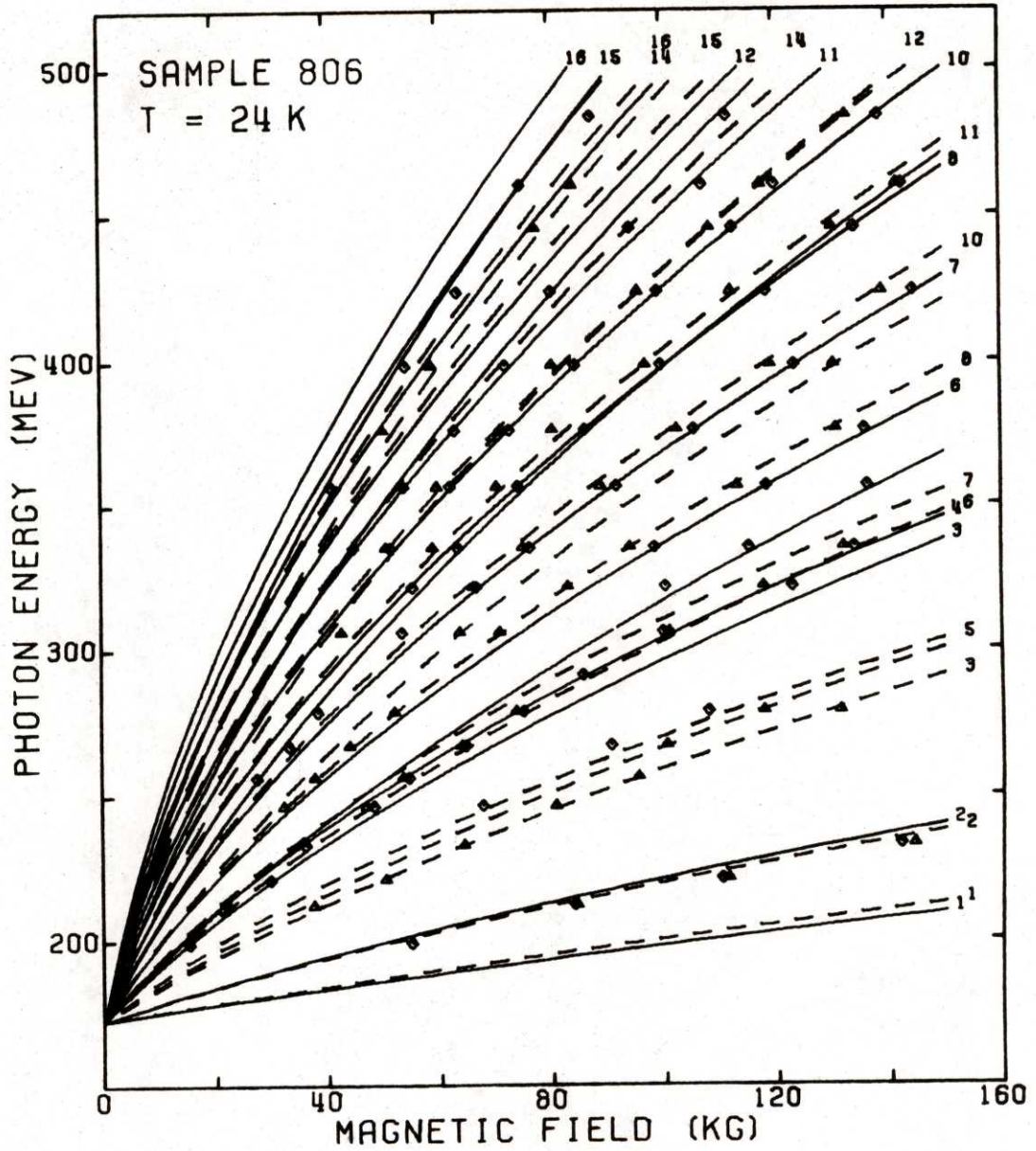


Fig. IV-12m. Fan chart for $\text{Hg}_{.753}\text{Cd}_{.247}\text{Te}$ at 24K.

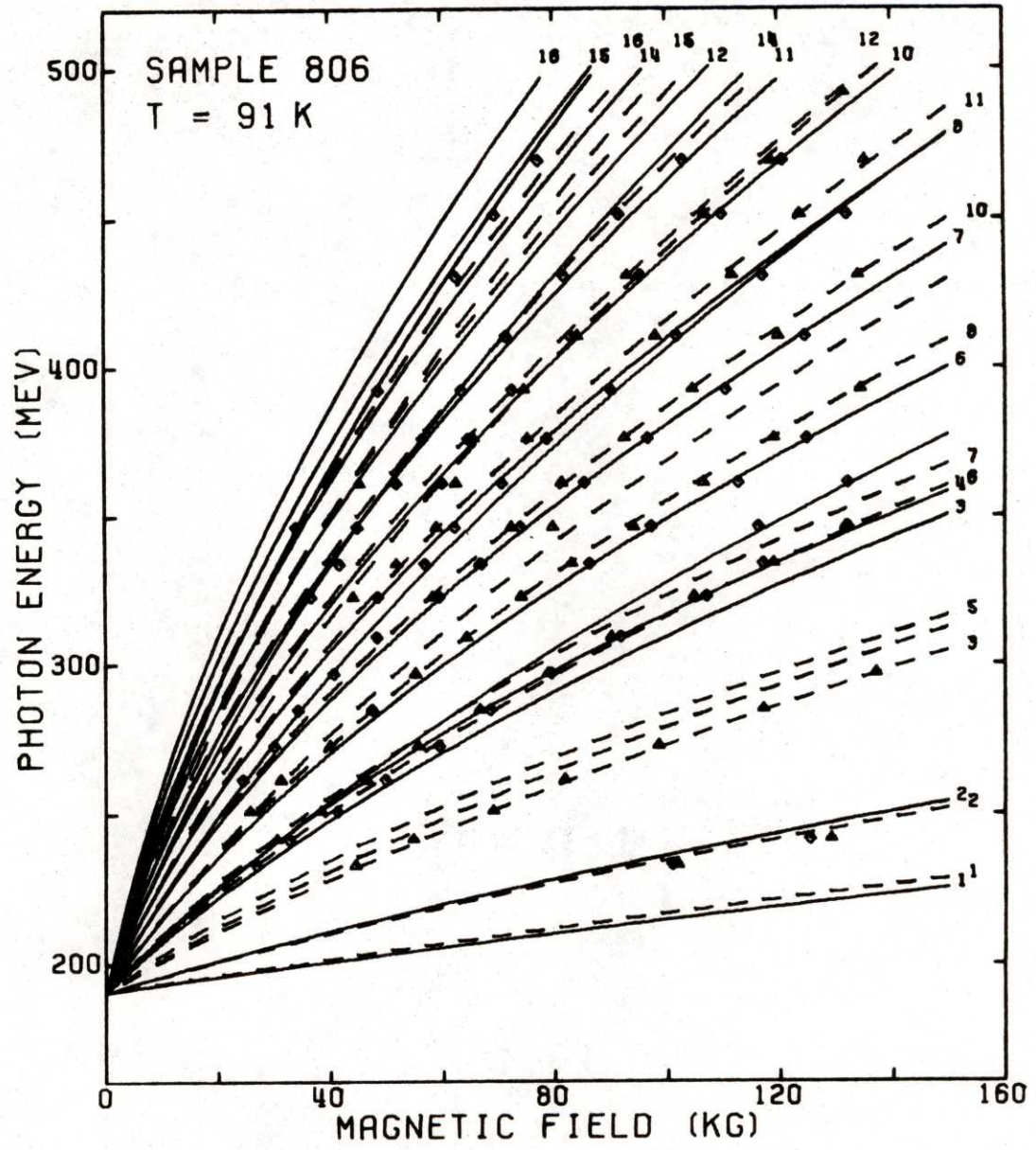


Fig. IV-12n. Fan chart for $\text{Hg}_{.753}\text{Cd}_{.247}\text{Te}$ at 91K.

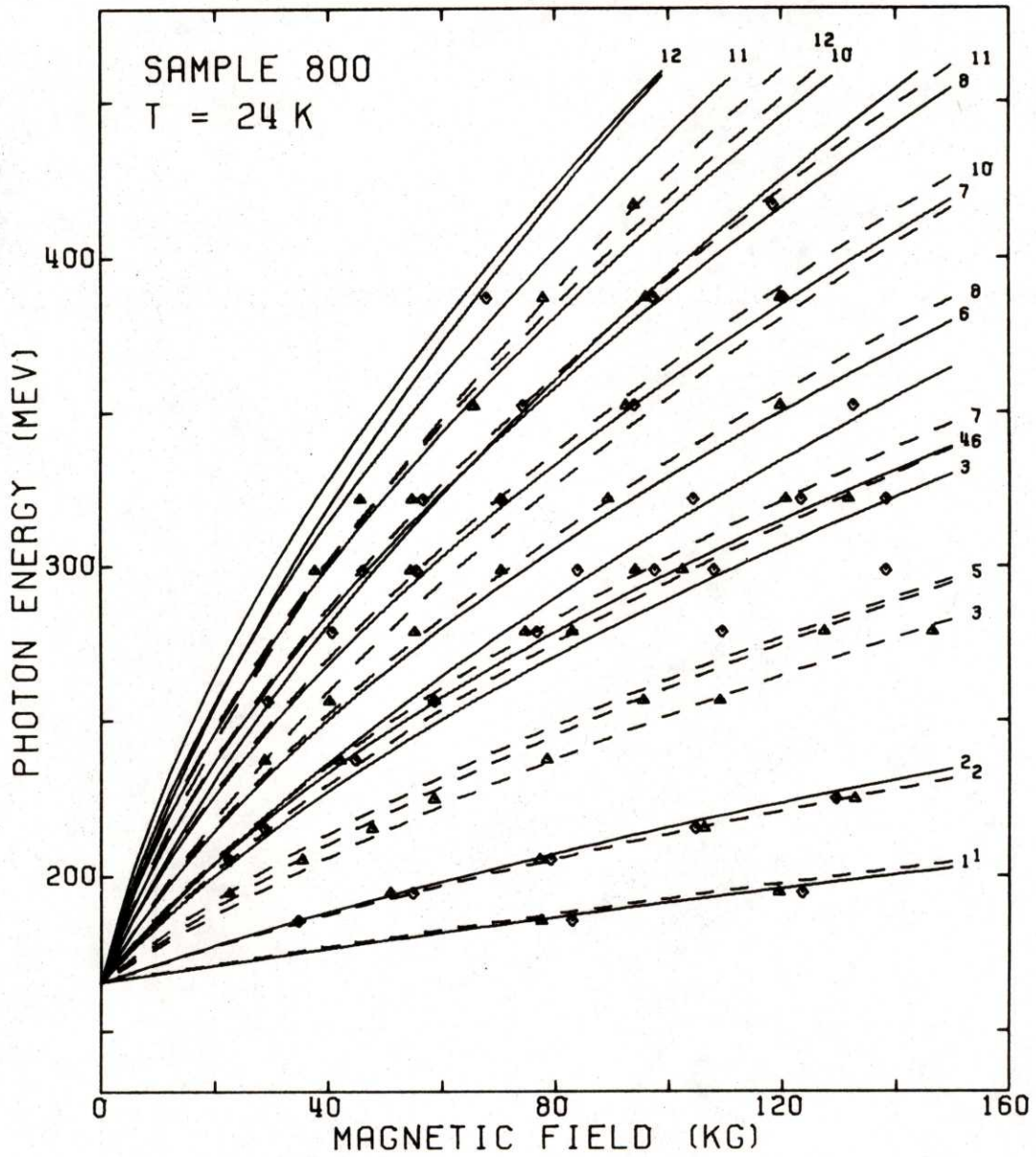


Fig. IV-12o. Fan chart for $\text{Hg}_{.752}\text{Cd}_{.248}\text{Te}$ at 24K.

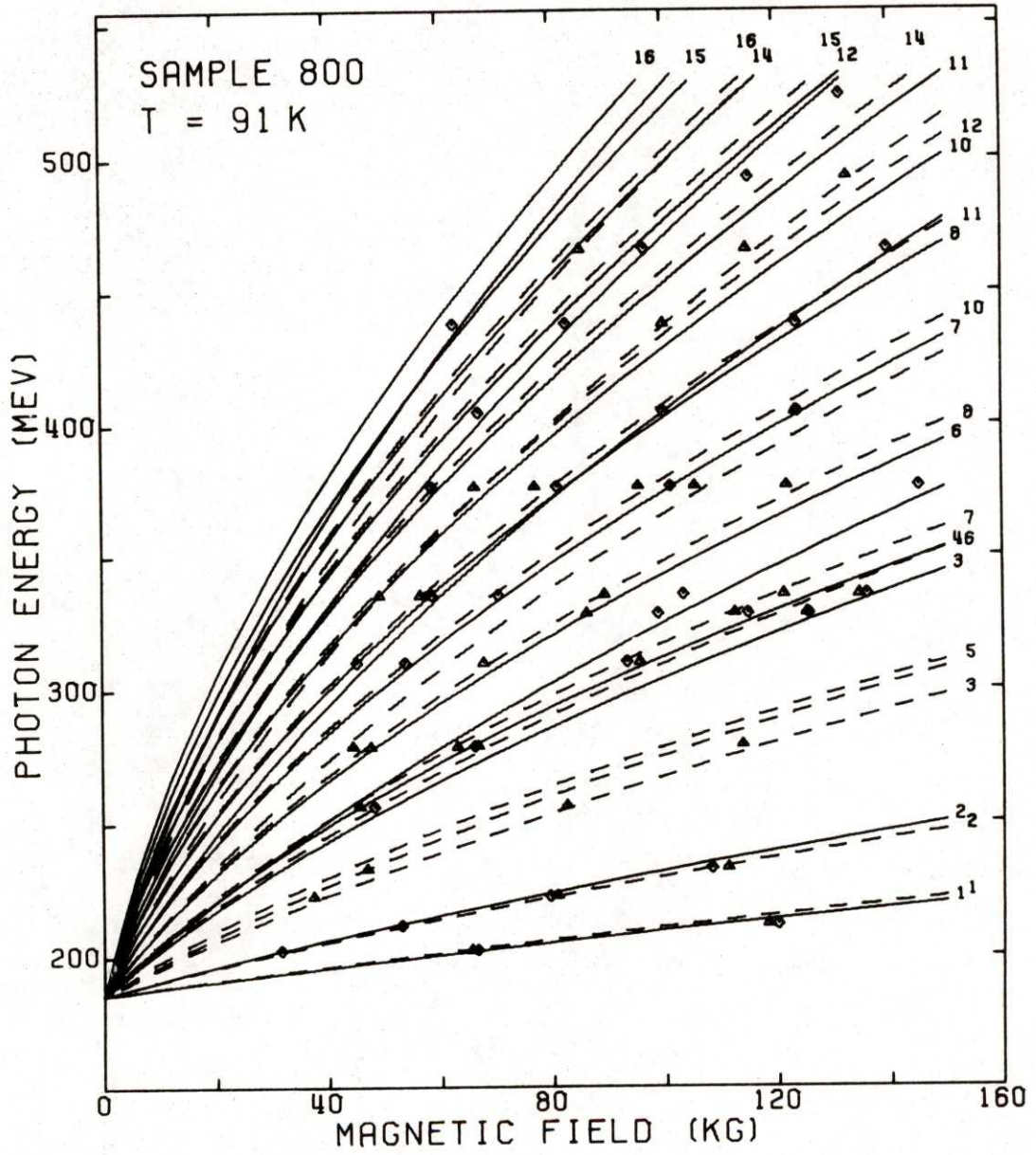


Fig. IV-12p. Fan chart for $\text{Hg}_{.752}\text{Cd}_{.248}\text{Te}$ at 91K.

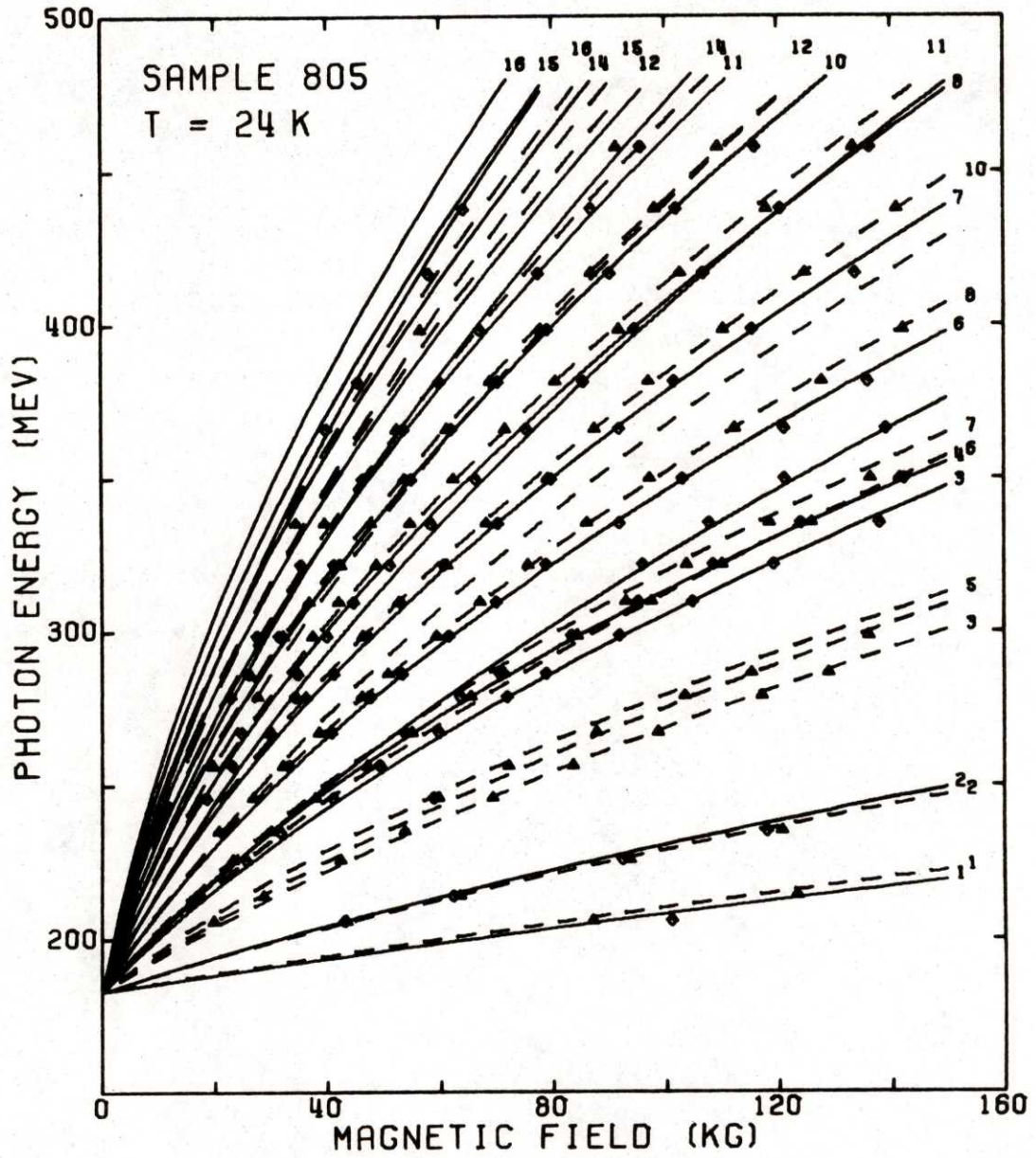


Fig. IV-12q. Fan chart for $\text{Hg}_{.735}\text{Cd}_{.265}\text{Te}$ at 24K.

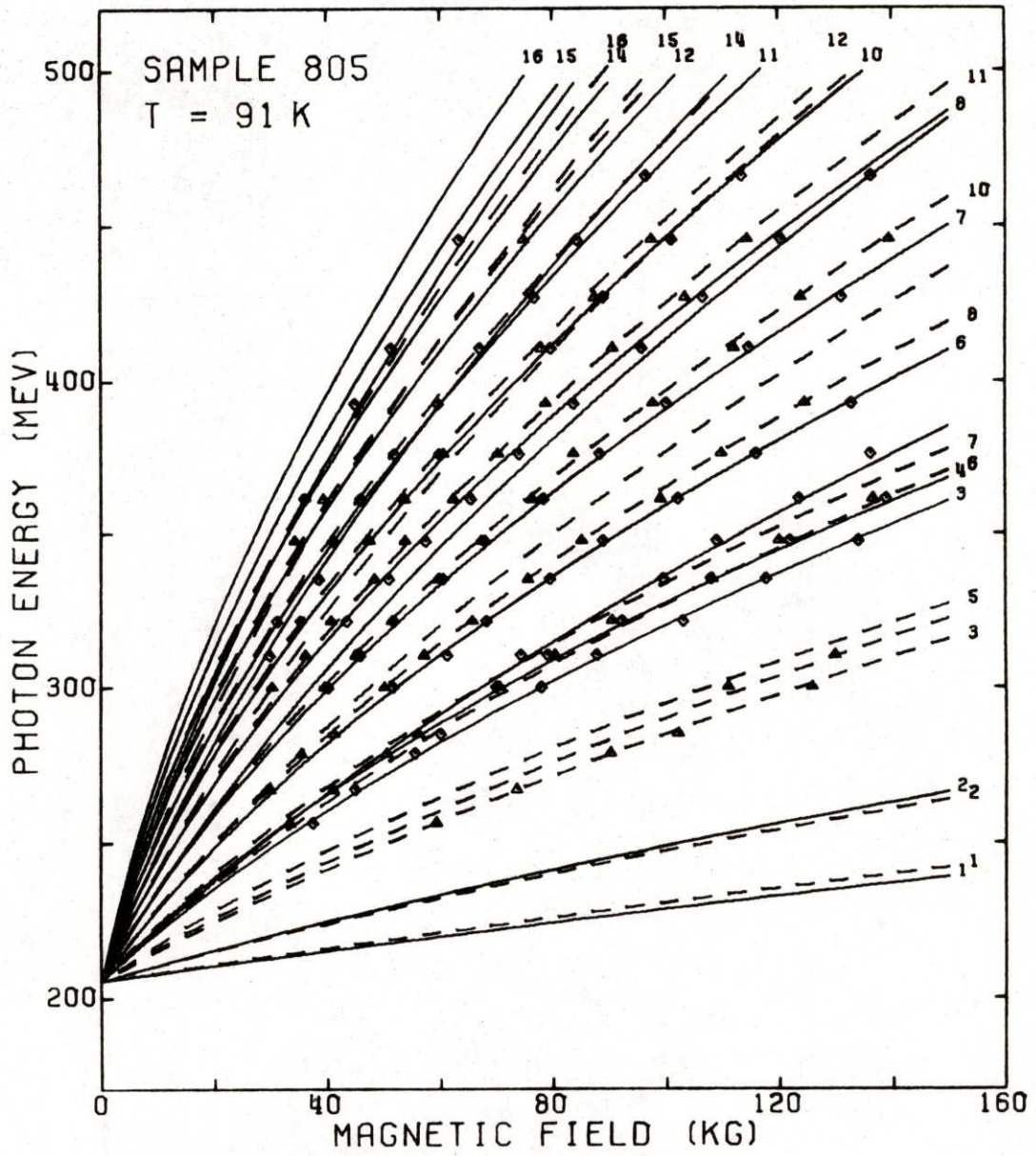


Fig. IV-12r. Fan chart for $\text{Hg}_{.735}\text{Cd}_{.265}\text{Te}$ at 91K.

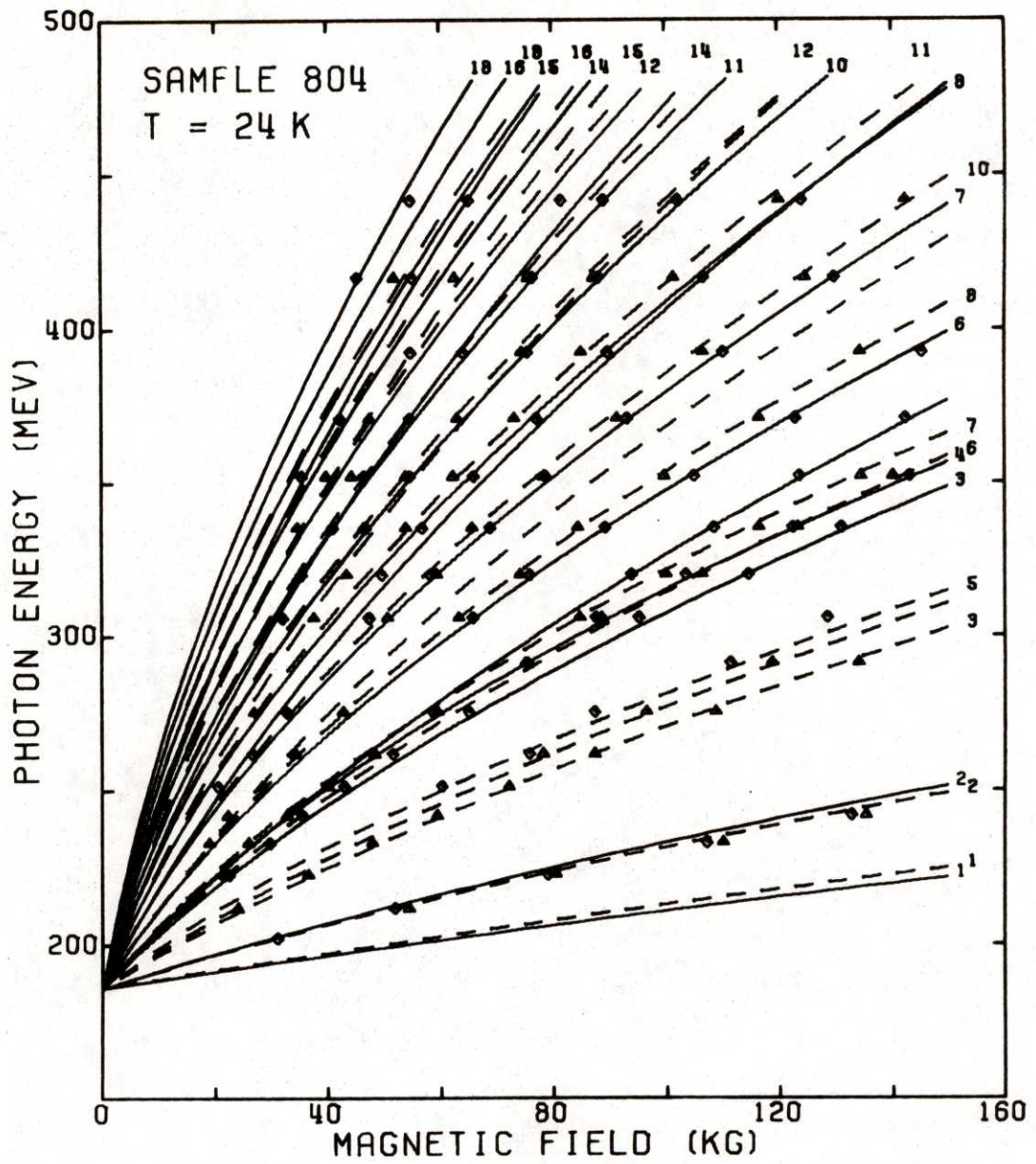


Fig. IV-12s. Fan chart for $\text{Hg}_{.731}\text{Cd}_{.269}\text{Te}$ at 24K.

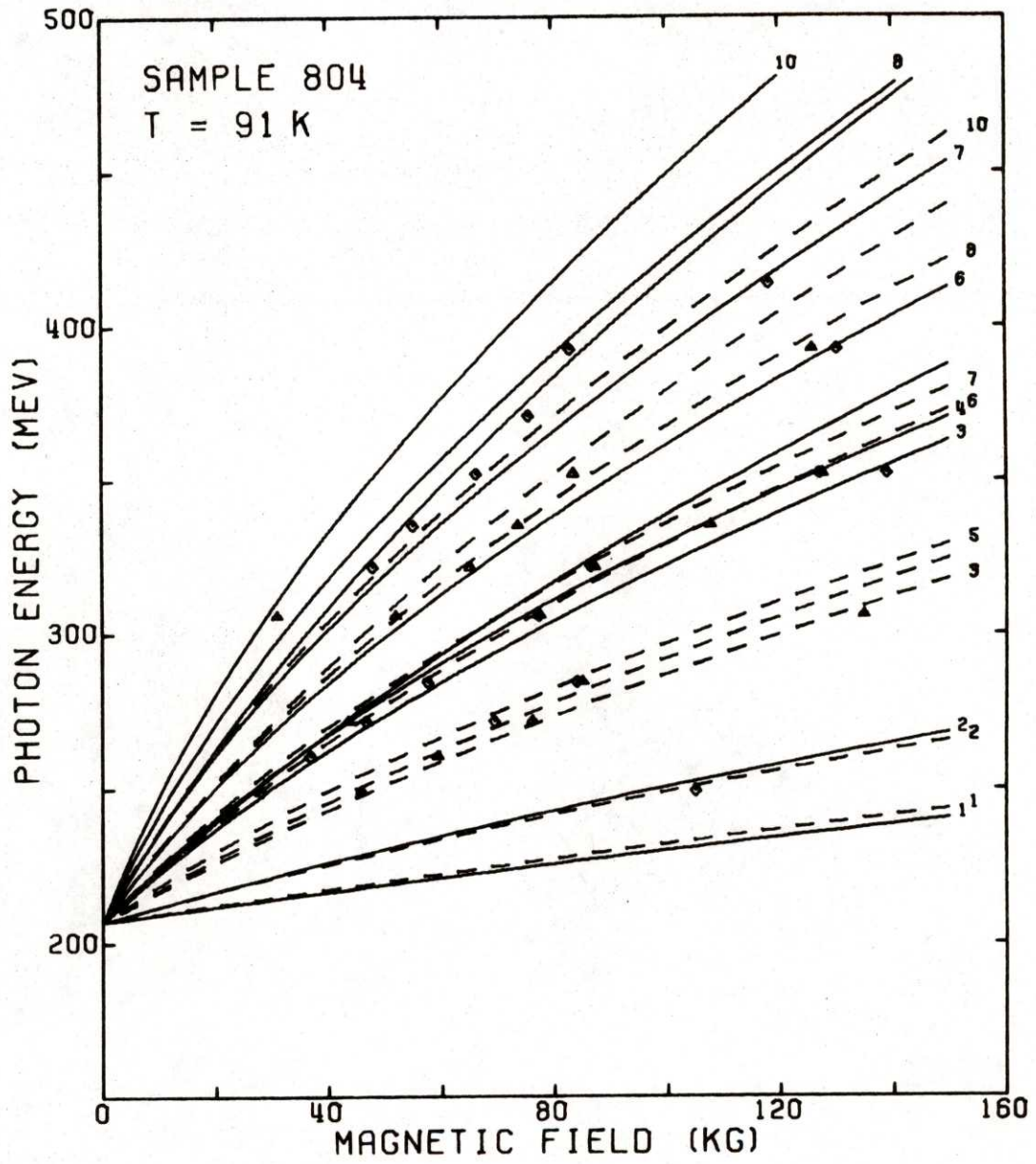


Fig. IV-12t. Fan chart for Hg_{0.731}Cd_{0.269}Te at 91K.

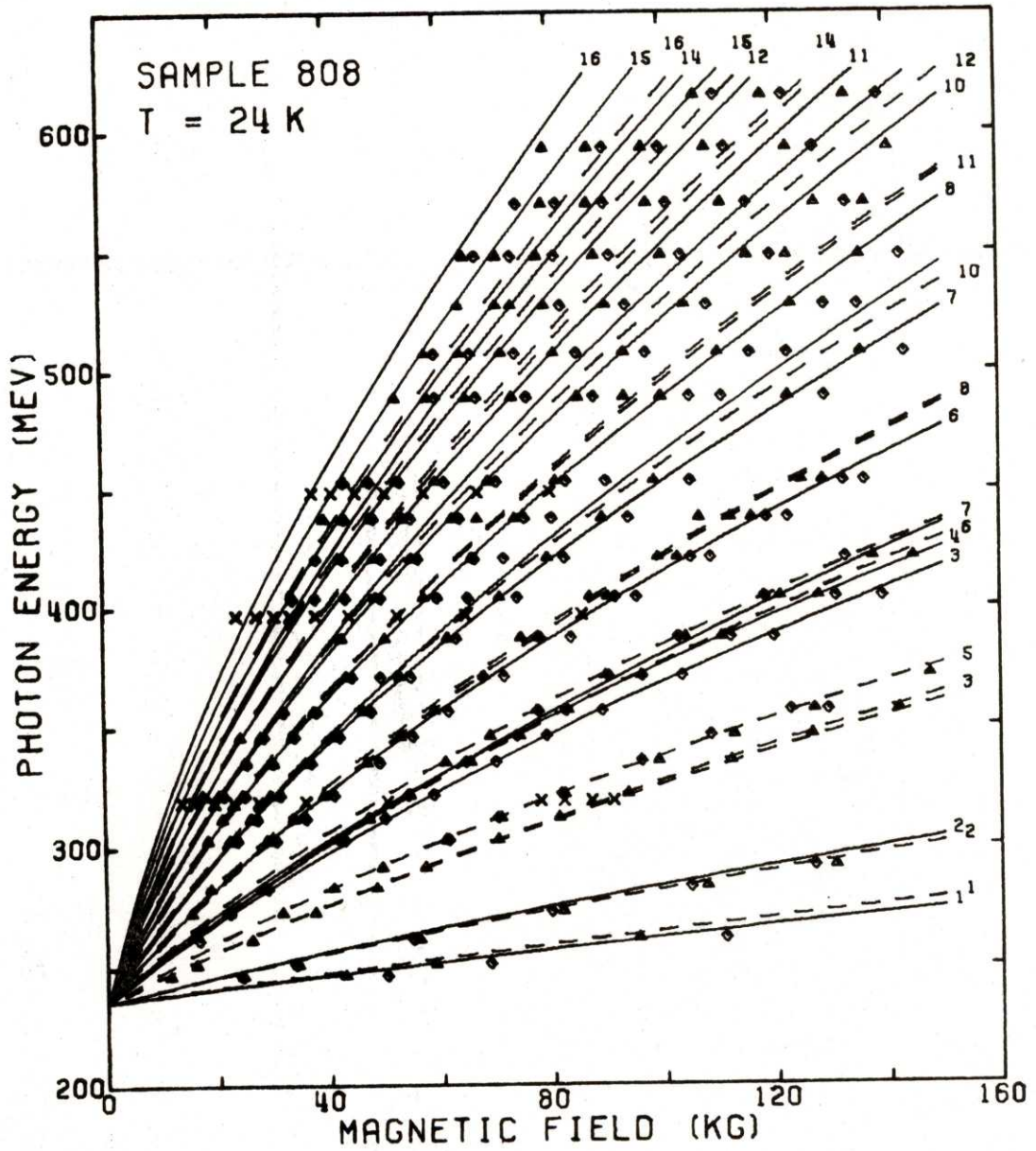


Fig. IV-13a. Fan chart for InSb, $\vec{H} \parallel [001]$. The X's are sample data from the magnetoabsorption results of Pidgeon and Brown¹ for $\vec{E}_1 \perp \vec{H}$. The points and lines are drawn as in Figs. IV-12a - 12t.

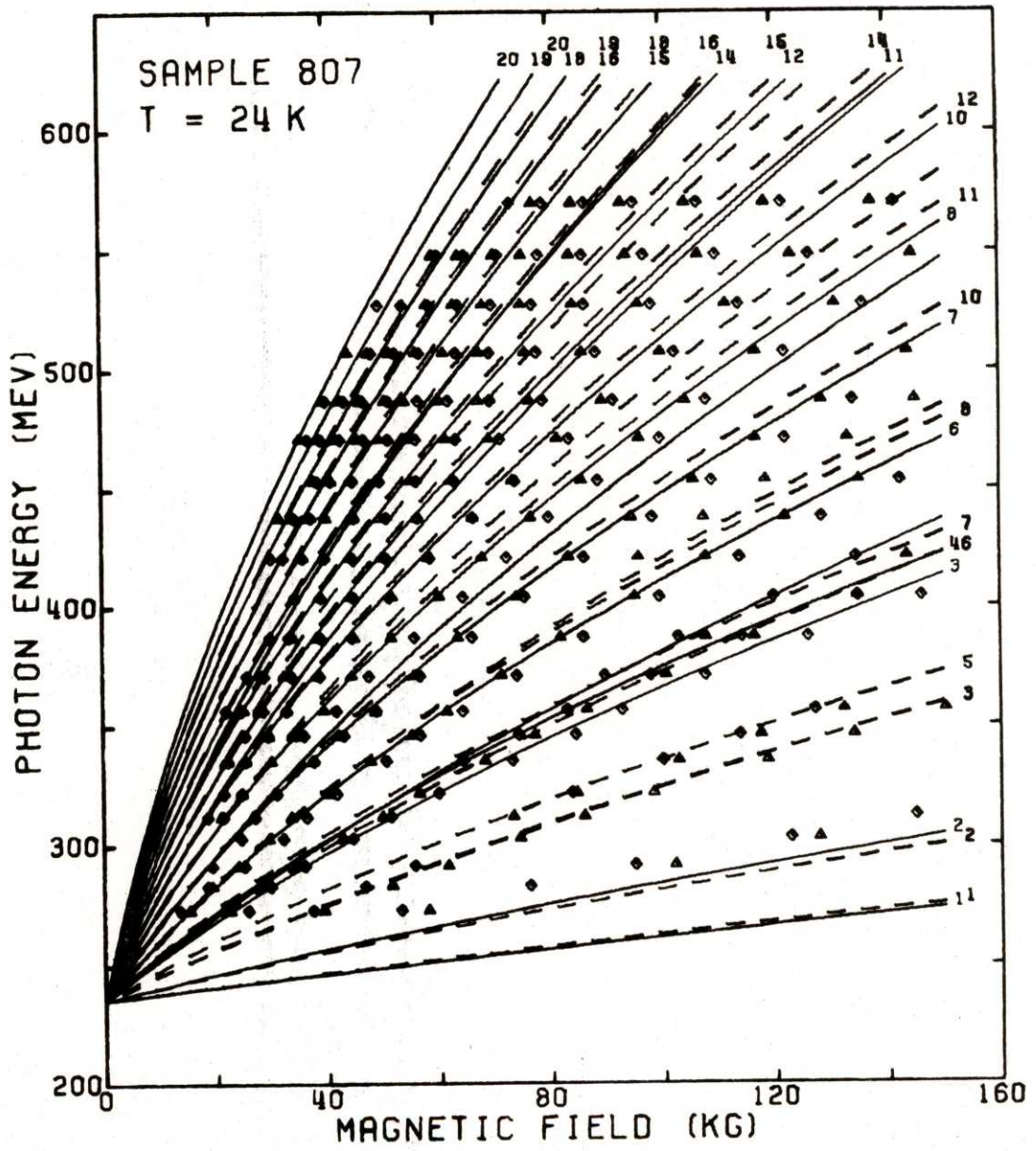


Fig. IV-13b. Fan chart for InSb, $\vec{H} \parallel [111]$.

REFERENCES

1. C.R. Pidgeon and R.N. Brown, Phys. Rev. 146, 575 (1966).
2. C.R. Pidgeon and S.H. Groves, Phys. Rev. 186, 824 (1969).
3. S.H. Groves, C.R. Pidgeon, A.W. Ewald and R.J. Wagner, J. Phys. Chem. Solids 31, 2031 (1970).
4. S.H. Groves, R.N. Brown and C.R. Pidgeon, Phys. Rev. 161, 779 (1967).
5. S.H. Groves, T.C. Harman and C.R. Pidgeon, Solid State Commun. 9, 451 (1971).
6. L.M. Roth, B. Lax and S. Zwerdling, Phys. Rev. 114, 90 (1959).
7. E. Burstein, G.S. Picus, R.F. Wallis and F. Blatt, Phys. Rev. 113, 15 (1959).
8. R.L. Aggarwal, in "Semiconductors and Semimetals", R.K. Willardson and A.C. Beer, eds. (Academic Press, New York, 1972), p. 151.
9. M. Reine, Ph.D. Thesis, Massachusetts Institute of Technology (1970);
M. Reine, R.L. Aggarwal and B. Lax, Phys. Rev. B5, 3033 (1972).
10. P.E. Vanier, F.H. Pollak and P.M. Raccah, to be published in Applied Optics.
11. K.P. Jain, Phys. Rev. 139, A544 (1965).
12. E.J. Johnson and D.H. Dickey, Phys. Rev. B1, 2676 (1970).
13. R. Ranvaud, Ph.D. Thesis, Brown University (1973).

V. BAND PARAMETERS OF $\text{Hg}_{1-x}\text{Cd}_x\text{Te}$

In this Chapter we describe the determination, from the interband magnetoreflexion results in Chapter IV, of the $\vec{k}\cdot\vec{p}$ band parameters of $\text{Hg}_{1-x}\text{Cd}_x\text{Te}$ in the small-gap semiconductor region. The parameters are those of the quasi Ge model developed in Chapter II: the energy gap E_g , which is expected to vary roughly linearly with the alloy composition x ;¹ the spin-orbit splitting Δ of the valence bands, which is expected to be about 1 eV;² the interband coupling energy E_p ; and the small higher-band parameters F , γ_1 , γ_2 , γ_3 , κ , q and N_1 , which are estimated in Appendix A. We neglect the effects of warping and inversion asymmetry considered in Chapter III for the case of intraband transitions in InSb, and by Pidgeon and Groves³ for interband transitions in InSb, since 1) these effects are expected to be even smaller for $\text{Hg}_{1-x}\text{Cd}_x\text{Te}$ (see App. A); 2) most of our samples were oriented with $\vec{H} \parallel [001]$ where such effects should be negligible; and 3) even for our $\vec{H} \parallel [111]$ samples where these effects are maximum, we observed no structure attributable to them. Our calculations in the quasi Ge model are made using $k_H = 0$, since this corresponds to the peak intensity for interband transitions. For intra-valence-band transitions, especially for the heavy holes, $k_H \neq 0$ effects can be important.

In Sec. A below we describe the computer techniques developed to calculate and plot the theoretical transitions, identify the experimental peaks with particular transitions, and perform a least-squares fit for the parameters. In Sec. B we use the energy differences between a pair of transitions involving the same conduction band Landau level, to determine approximate values for the higher-band parameters γ_1 , γ_2 , γ_3 , and κ .

Estimating $q \approx N_1 \approx 0$, and $\Delta \approx 1$ eV, in Sec. C we carry out a two-parameter fit to each set of data in order to determine a best value for F and then to obtain E_g and E_p as a function of temperature and of alloy composition. In Sec. D we discuss our results and compare them with previous results.

A. Parameter Fitting Techniques

The process of identifying each transition plotted in the fan charts in Figs. IV-12a through 12t, and finding the band parameters for a best fit between theory and experiment, involved several steps making use of the M.I.T. time-sharing computer system (TSO). First, approximate parameters were chosen for each set of data. Second, these were used to calculate the expected interband transition energies as a function of magnetic field, by diagonalizing the Hamiltonians in Table II-5, and these energies were plotted on-line on photocopies of the data. The transition intensities calculated from Eqs. (II-18) were used to estimate which transitions were most likely to be observed. The plots which gave a reasonable fit to the data were used to identify most data points with one or, at most, two particular interband transitions. These were stored in an on-line disc dataset and used as input to the least-squares fitting routines described below. These routines provided new parameter sets with which to make new plots and complete the line identifications. The computer programs used are listed in Appendix C.

The data points were fit to the transitions listed in Table V-1, which were calculated to be significantly stronger than the other transitions allowed by the selection rules in Eqs. (II-19), using the matrix elements in Eqs. (II-18)

TABLE V-1. Interband transitions identified for $\text{Hg}_{1-x}\text{Cd}_x\text{Te}$.

	σ_L	σ_R
1	$a^+(-1) \rightarrow a^c(0)$	$a^-(-1) \rightarrow a^c(0)$
2	$b^+(-1) \rightarrow b^c(0)$	$b^-(-1) \rightarrow b^c(0)$
3	$a^-(1) \rightarrow a^c(2)$	$a^-(2) \rightarrow a^c(1)$
4	$b^-(1) \rightarrow b^c(2)$	$a^+(1) \rightarrow a^c(0)$
5	$b^+(0) \rightarrow b^c(1)$	$b^-(2) \rightarrow b^c(1)$
6	$a^-(2) \rightarrow a^c(3), b^-(2) \rightarrow b^c(3)$	$a^-(3) \rightarrow a^c(2)$
7	$a^-(3) \rightarrow a^c(4), b^-(3) \rightarrow b^c(4)$	$b^-(3) \rightarrow b^c(2)$
8	$a^-(4) \rightarrow a^c(5), b^-(4) \rightarrow b^c(5)$	$a^-(4) \rightarrow a^c(3), b^-(4) \rightarrow b^c(3)$
9	$b^+(1) \rightarrow b^c(2)$	$a^+(2) \rightarrow a^c(1)$
10	$a^-(5) \rightarrow a^c(6), b^-(5) \rightarrow b^c(6)$	$a^-(5) \rightarrow a^c(4), b^-(5) \rightarrow b^c(4)$
11	$a^-(6) \rightarrow a^c(7), b^-(6) \rightarrow b^c(7)$	$a^-(6) \rightarrow a^c(5), b^-(6) \rightarrow b^c(5)$
12	$a^-(7) \rightarrow a^c(8), b^-(7) \rightarrow b^c(8)$	$a^-(7) \rightarrow a^c(6), b^-(7) \rightarrow b^c(6)$
13	$b^+(2) \rightarrow b^c(3)$	$a^+(3) \rightarrow a^c(2)$
14	$a^-(8) \rightarrow a^c(9), b^-(8) \rightarrow b^c(9)$	$a^-(8) \rightarrow a^c(7), b^-(8) \rightarrow b^c(7)$
15	$a^-(9) \rightarrow a^c(10), b^-(9) \rightarrow b^c(10)$	$a^-(9) \rightarrow a^c(8), b^-(9) \rightarrow b^c(8)$
16	$a^-(10) \rightarrow a^c(11), b^-(10) \rightarrow b^c(11)$	$a^-(10) \rightarrow a^c(9), b^-(10) \rightarrow b^c(9)$
17	$b^+(3) \rightarrow b^c(4)$	$a^+(4) \rightarrow a^c(3)$
18	$a^-(11) \rightarrow a^c(12), b^-(11) \rightarrow b^c(12)$	$a^-(11) \rightarrow a^c(10), b^-(11) \rightarrow b^c(10)$

involving the solutions in Eqs. (II-11) to the Schrödinger equations, Eqs. (II-10). The calculated curves in Figs. IV-12a through 12t, and the reflectivity peaks in Figs. IV-5 through 11 are labeled with the transition numbers listed in Table V-1.

The least-squares fit calculation was based on a method described by Reine.⁵ Given a set of N energy and magnetic field pairs (E_i, H_i) corresponding to each observed reflectivity peak, and a function $E(H_i)$ for calculating a theoretical transition energy for a given magnetic field H_i , we wish to minimize the root mean square deviation

$$\delta = \left\{ \frac{1}{N} \sum_{i=1}^N [E(H_i) - E_i]^2 \right\}^{1/2} \quad (\text{V-1})$$

where the function $E(H)$ depends on a set of parameters a_j , $j=1, \dots, M$. Reine showed that to minimize δ to first order in the corrections δa_j to the parameters

$$a_j \rightarrow a_j + \delta a_j \quad (\text{V-2})$$

one must solve the $M \times M$ system of equations

$$\sum_{k=1}^M \sum_{i=1}^N \frac{\partial E(H_i)}{\partial a_j} \frac{\partial E(H_i)}{\partial a_k} \delta a_k = \sum_{i=1}^N \frac{\partial E(H_i)}{\partial a_j} [E_i - E(H_i)] \quad (\text{V-3})$$

Successive corrections are made to the parameters a_j until satisfactory convergence to a minimum is obtained.

Reine⁵ calculated the derivatives $\partial E(H_i)/\partial a_j$ in Eq. (V-3) using approximate expressions for the transition energies to first order in H . This

was sufficiently accurate for large gap materials such as GaAs and GaSb. Since the transition energies in small gap materials are strongly nonparabolic, i.e. depend on higher-order terms in H , we used exact expressions for these derivatives, obtained by differentiating the fourth-order determinantal equation for the energy eigenvalues with respect to the parameters a_j . The details of this calculation are given in Appendix B.

The parameters of the quasi Ge model Hamiltonian in Table II-5, including the diagonal parts of the terms proportional to q in Table III-1, are the energy gap E_g , the spin-orbit splitting Δ , the interband coupling energy E_p , the higher-band effective mass parameters F , γ_1 , γ_2 , and γ_3 , and the g-factor contributions N_1 , κ , and q . In the absence of a direct experimental determination of the spin-orbit splitting, we use the estimated value $\Delta \approx 1 \text{ eV}$.² In Appendix A we show that q and N_1 are expected to be small for $\text{Hg}_{1-x}\text{Cd}_x\text{Te}$, so we set these to zero.

Thus we have a possibility of determining seven parameters: E_g , E_p , F , γ_1 , γ_2 , γ_3 , and κ . However we found that the data were not sensitive enough to fit all these parameters simultaneously. It is shown in Appendix A that the Luttinger parameters γ_1 , γ_2 , γ_3 and κ depend primarily on two Kane parameters B_K and C_K . Therefore we attempted to fit the five parameters E_g , E_p , F , B_K and C_K ; however this still was not possible. In the next Section we show that we can determine approximate average values for the parameters B_K and C_K , hence the Luttinger parameters, by examining the energy difference between transitions from two different heavy-hole levels to the same conduction-band level, for several sets of data. With these parameters fixed for all sets of data, we have been able to make an approximate determination of the best value for F . We were then able to make two-parameter fits for each set of data,

for the energy gap E_g and the interband coupling energy E_p .

B. Determination of γ_1 , γ_2 , γ_3 and κ

The transitions listed in Table V-1 include two, $\sigma_L(3)$ and $\sigma_R(6)$, from the heavy-hole levels $a^-(1)$ and $a^-(3)$, to the conduction-band level $a^c(2)$.

We use the energy difference between these two to determine the Luttinger parameters γ_1 , γ_2 , γ_3 , and κ .

The expressions in Eqs. (II-14) give

$$E[\sigma_R(6)] - E[\sigma_L(3)] \equiv 4\beta H \gamma_H \quad (V-4)$$

where, to lowest order in H

$$\gamma_H \approx \frac{1}{65} \left[71\gamma_1 - 34(\gamma' + 3\gamma'') - 6\kappa - \frac{3}{2}(9-2f)q \right] \quad (V-5)$$

which is of the same order of magnitude as the high-quantum-number inverse heavy-hole effective mass m/m_- in Eq. (II-16):

$$\frac{m}{m_-} \approx \gamma_1 - \frac{1}{2}(\gamma' + 3\gamma'') \quad (V-6)$$

where both results are valid only if $E_p/E_g \gg \gamma_1$, γ' , γ'' and κ . The above result for γ_H is much less sensitive to the small parameter q than a similar energy difference

$$E[\sigma_L(2)] - E[\sigma_R(2)] \approx \frac{4}{7}\beta H [-\gamma_1 + 2(\gamma' + 3\gamma'') - 6\kappa - \frac{3}{2}(9-2f)q] \quad (V-7)$$

For $q \approx 0$ Eq. (V-5) can be rewritten

$$\gamma_H(\theta, \phi) = \gamma_H([100]) - \frac{81}{65}(\gamma_3 - \gamma_2)f(\theta, \phi) \quad (V-8)$$

We could only measure the energy differences in Eq. (V-4) for those samples for which we could resolve the $[\sigma_L(3), \sigma_L(4)]$ and $[\sigma_R(6), \sigma_R(7)]$ doublets. Representative spectra for these transitions are shown in Fig. IV-6. The doublets are clearly resolved, but for other samples the $[\sigma_R(6), \sigma_R(7)]$ doublet was only barely resolved. For each sample where the doublets were resolved, we plotted the magnetic field and photon energy positions of the $\sigma_L(3)$ and $\sigma_R(6)$ peaks as shown in Fig. V-1 for the same sample whose spectrum is given in Fig. IV-6. From this plot the energy differences, and hence γ_H , were determined; the average γ_H found for each sample are given in Table V-2. The first part of the Table gives γ_H for just the [001] oriented samples, giving an average over all these samples of

$$\gamma_H([001]) \approx 2.9 \pm 0.2 \quad (V-9)$$

where 0.2 is the probable error. Then the second part of Table V-2 give $\gamma_H(\theta, \phi)$ for the other samples. Equations (V-8) and (V-9) were used to give the value for $(\gamma_3 - \gamma_2)$ to yield an average value

$$(\gamma_3 - \gamma_2) \approx 0.8 \pm 0.3 \quad (V-10)$$

These results, along with Eq. (V-5) and the expressions in Appendix A for $\gamma_1, \gamma_2, \gamma_3$ and κ in terms of the two Kane parameters B_K and C_K (with $A_K \approx B_K \approx 0$) give

$$\begin{aligned} B_K &\approx -1.2 \pm 0.5 \\ C_K &\approx -2.1 \pm 0.2 \end{aligned} \quad (V-11)$$

which then give

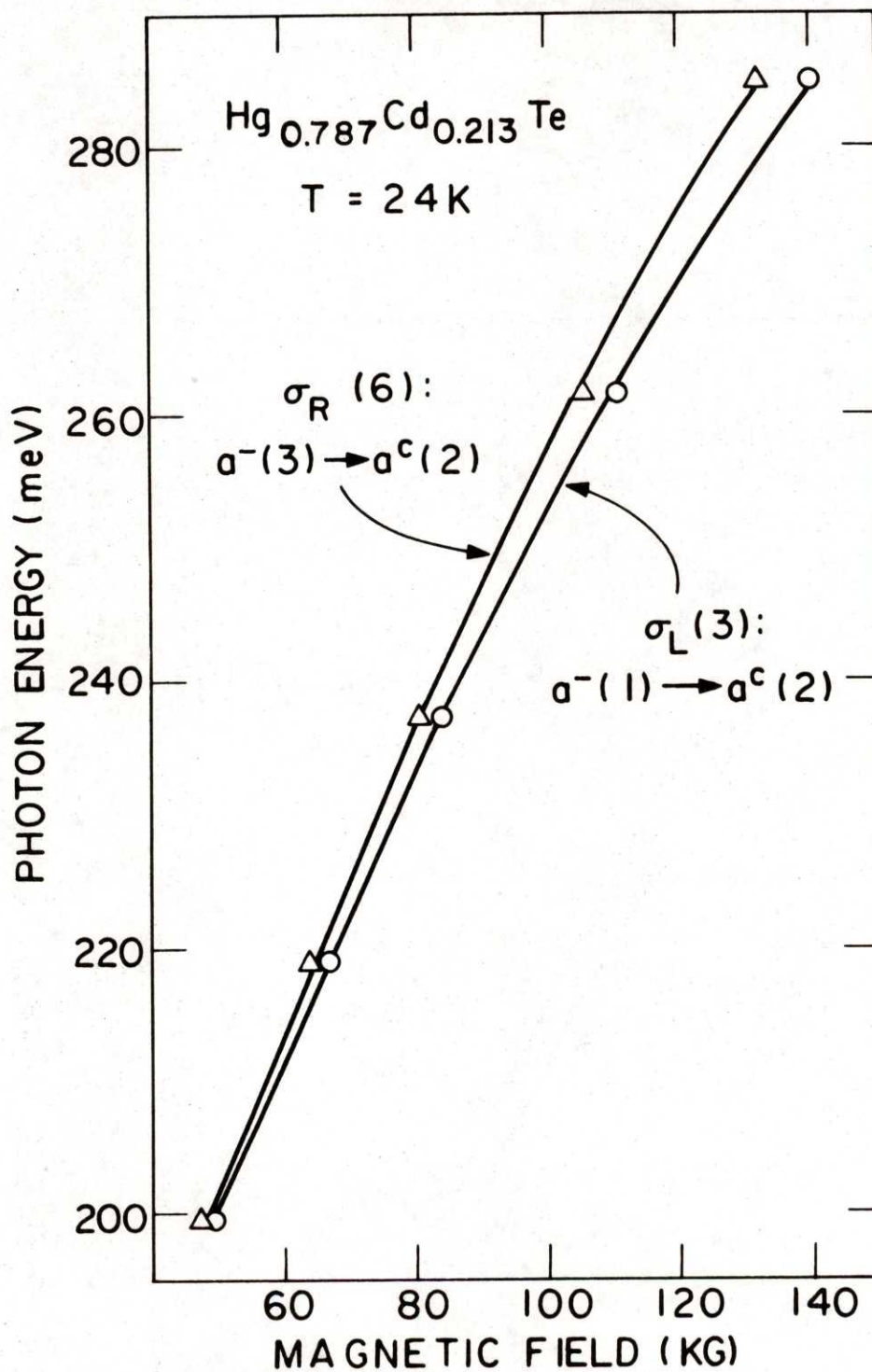


Fig. V-1. Determination of $E[a^-(1)] - E[a^-(3)]$ from the transitions $\sigma_R(6)$ and $\sigma_L(3)$ for sample 796.

TABLE V-2. Results for the heavy-hole mass parameter γ_H for samples with $\vec{H} \parallel [001]$, and for other orientations θ, ϕ .

SAMPLE	$\gamma_H(1001)$
802	3.46 ± 0.09
804	2.42 ± 0.09
805	3.05 ± 0.10
809	2.77 ± 0.04

SAMPLE	$f(\theta, \phi)$	$\gamma_H(\theta, \phi)$	$\gamma_3 - \gamma_2$
796	0.202	1.82 ± 0.04	1.12 ± 0.21
798	0.000	2.13 ± 0.08	0.64 ± 0.17
810	0.000	2.04 ± 0.08	0.71 ± 0.17

$$\begin{aligned}
 \gamma_1 &\approx 2.5 \pm 0.4 \\
 \gamma_2 &\approx -0.3 \pm 0.2 \\
 \gamma_3 &\approx 0.5 \pm 0.1 \\
 \kappa &\approx -1.2 \pm 0.1
 \end{aligned}
 \tag{V-12}$$

C. Determination of E_g , E_p and F

Using the valence band parameters from the previous Section for all our sets of data, we next attempted to fit the three parameters remaining, F , E_g and E_p , simultaneously for each. Again the fits were not successful: the deviation δ was insensitive to small variations in F , so that convergence was slow and a minimum was found in only a few cases. In these cases the value of F for the minimum ranged from about -0.4 to -1.0, so we next made two-parameter fits for just E_g and E_p for all sets of data, using fixed values $F = -0.1, -0.4, -0.7, -1.0,$ and -1.3 to span this region of F . For each value of F we plot in Fig. V-2 the average $\bar{\delta}$, over all sets of data, of the r.m.s. deviation δ [Eq. (V-1)] and also the average of the absolute energy differences $|\overline{\Delta E_p}|$ between the 24 K and 91 K results for E_p . Using the minimum of both of these as criteria for a best fit, we find from Fig. V-2 the best choice of F is

$$F \approx -0.7 \pm 0.3 \tag{V-13}$$

The results for E_p and E_g , using the value $F = -0.7$, are given in Table V-3 for the samples at liquid He temperature, and in Table V-4 for

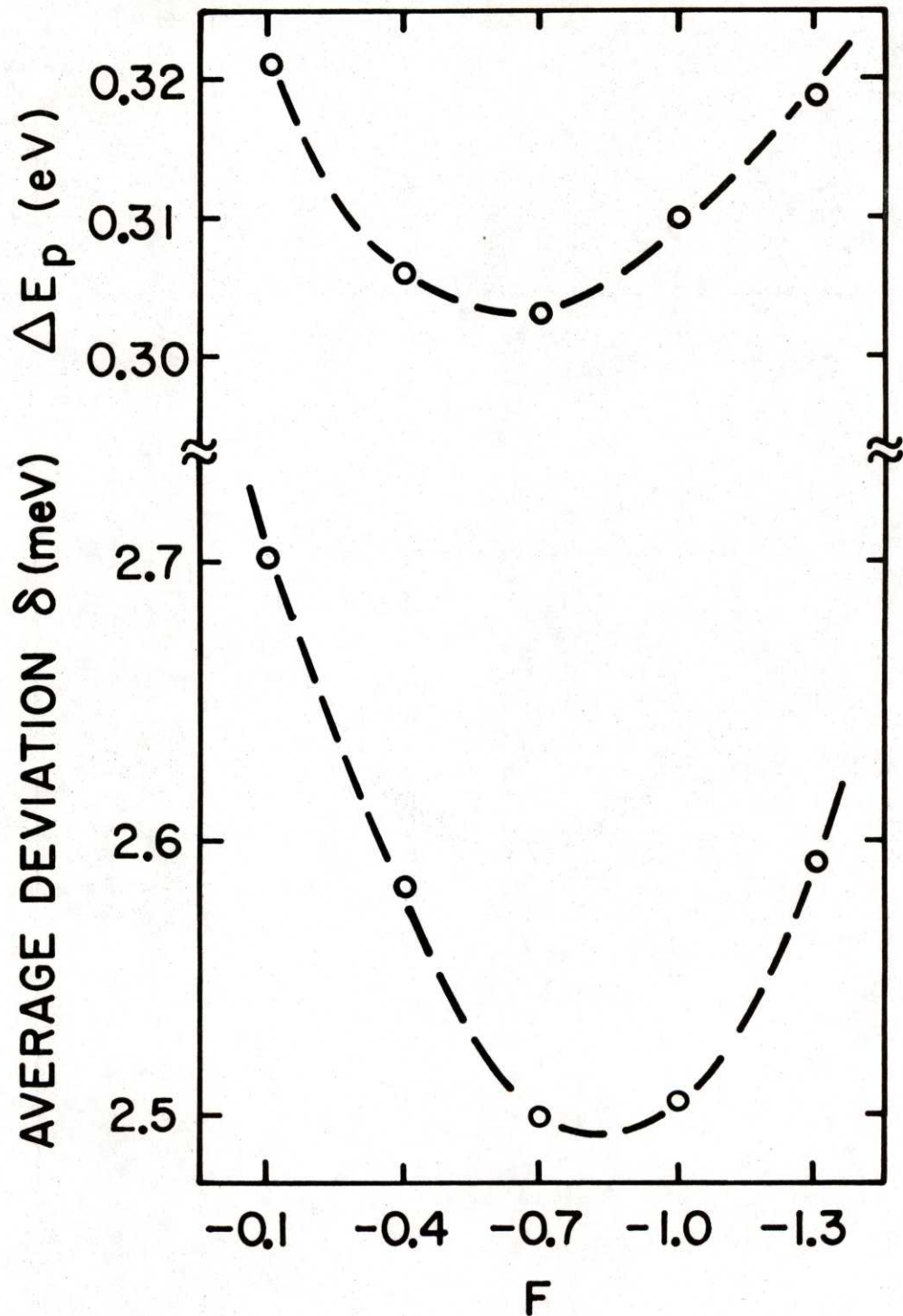


Fig. V-2. Determination of $F = -0.7 \pm 0.3$ from the lowest average r.m.s. deviation of the two-parameter fits for E_g and E_p , and the lowest average difference $|E_p(91K) - E_p(24K)| \equiv \Delta E_p$.

TABLE V-3. Results for $\text{Hg}_{1-x}\text{Cd}_x\text{Te}$ samples at $T = 24\text{K}$.

SAMPLE	x	E_g (meV)	E_p (eV)	m_c ($\times 10^{-2}m$)	$-g_c$	$m_+([100])$ ($\times 10^{-2}m$)
802	.175 ± .013	22.2 ± .4	18.6 ± .2	.177 ± .005	547 ± 16	.177 ± .005
798	.182 ± .015	35.8 ± .2	17.9 ± .1	.295 ± .001	320 ± 2	.297 ± .001
801	.196 ± .013	80.6 ± .3	18.0 ± .2	.65 ± .01	136 ± 2	.66 ± .01
810	.211 ± .005	123.9 ± .4	17.8 ± .3	.99 ± .01	83 ± 1	1.02 ± .01
796	.213 ± .004	114.9 ± .6	17.4 ± .3	.95 ± .02	88 ± 2	.97 ± .02
809	.220 ± .005	119.8 ± .2	17.9 ± .2	.96 ± .01	87 ± 1	.98 ± .01
806	.247 ± .005	172.9 ± .3	17.8 ± .2	1.369 ± .02	56 ± 1	1.41 ± .01
800	.248 ± .014	166.0 ± .3	17.7 ± .3	1.32 ± .01	59 ± 1	1.36 ± .02
805	.265 ± .005	183.2 ± .4	18.1 ± .3	1.42 ± .02	54 ± 1	1.46 ± .03
804	.269 ± .017	186.2 ± .1	18.0 ± .2	1.45 ± .01	52 ± 1	1.49 ± .02

TABLE V-4. Results for $\text{Hg}_{1-x}\text{Cd}_x\text{Te}$ samples at $T = 91\text{K}$.

SAMPLE	x	E_g (meV)	E_p (eV)	m_c ($\times 10^{-2}m$)	$-g_c$	$m_+(1001)$ ($\times 10^{-2}m$)
802	.175 \pm .013	49.5 \pm .5	17.8 \pm .2	.408 \pm .008	227 \pm 5	.413 \pm .009
801	.196 \pm .013	100.8 \pm .6	17.8 \pm .1	.817 \pm .003	104.7 \pm .1	.834 \pm .001
810	.211 \pm .005	137.2 \pm .3	18.3 \pm .2	1.064 \pm .001	76.3 \pm .4	1.092 \pm .006
796	.213 \pm .004	139.2 \pm .5	16.9 \pm .3	1.17 \pm .02	69.2 \pm 1.5	1.20 \pm .02
809	.220 \pm .005	140.0 \pm .3	18.0 \pm .2	1.10 \pm .01	73.1 \pm 1.2	1.13 \pm .02
806	.247 \pm .005	190.6 \pm .2	17.8 \pm .3	1.50 \pm .01	56.3 \pm .6	1.55 \pm .02
800	.248 \pm .014	185.5 \pm .1	17.8 \pm .2	1.46 \pm .01	51.9 \pm .8	1.51 \pm .02
805	.265 \pm .005	205.6 \pm .2	17.7 \pm .3	1.62 \pm .01	45.5 \pm 1.2	1.67 \pm .03

the samples at liquid N_2 temperature. The stated error limits are the variations due to the limits in Eq. (V-13) on F . The results for E_p give an average value

$$E_p = 17.9 \pm 0.2 \text{ eV} \quad (\text{V-14})$$

D. Discussion

Using the results in Sec. B for γ_1 , γ_2 , γ_3 and κ and Eq. (V-6), we find the heavy-hole effective mass

$$\begin{aligned} m_-([001])/m &\simeq 0.40 \begin{matrix} +0.08 \\ -0.06 \end{matrix} \\ m_-([110])/m &\simeq 0.45 \begin{matrix} +0.10 \\ -0.07 \end{matrix} \\ m_-([111])/m &\simeq 0.53 \begin{matrix} +0.13 \\ -0.09 \end{matrix} \end{aligned} \quad (\text{V-15})$$

These results are in excellent agreement with the recent results of Uchida and Tanaka⁶ $m_-([001])/m \simeq 0.38$, $m_-([110])/m \simeq 0.47$ and $m_-([111])/m \simeq 0.50$ from their far-infrared magneto-optical studies of HgTe, with their precision similar to ours. Guldner and his co-workers have used values for m_-/m ranging from 0.4 ± 0.1 ,⁷ in rough agreement with ours, to a value 0.25,^{8,9} to fit magnetoabsorption results for $Hg_{1-x}Cd_xTe$ and HgTe. Groves et al.¹⁰ estimated $m_-([001])/m = 0.28 \pm 0.1$, for $Hg_{0.84}Cd_{0.16}Te$. Earlier results and estimates have ranged from 0.3 to 0.71.¹¹ The estimate of Lawaetz¹² of $m_-/m \gtrsim 1.0$ does not seem to be realistic.

Our result $(\gamma_3 - \gamma_2) = 0.8 \pm 0.3$ is identical to that of Uchida and Tanaka,⁶ and is not inconsistent with that of Suzuki et al.,¹³ 0.5 ± 0.4 . Lawaetz estimated 0.6 for both HgTe and CdTe.¹² This result, and those for m_-/m ,

emphasize the importance of anisotropy: the use of an "average" value $\bar{\gamma} = \gamma_2 \approx \gamma_3$ ⁷⁻⁹ cannot be justified.

Our result $F = -0.7 \pm 0.3$ is consistent with the estimate of -1.2 in Appendix A. This parameter has not been used in any previous studies of HgTe, CdTe or $\text{Hg}_{1-x}\text{Cd}_x\text{Te}$. Our values for B_K and C_K [Eqs. (V-11)] are about the same as one set of parameters used by Groves et al.¹⁴ for HgTe, based on earlier results for InSb (see Appendix A) and Ge. Lawaetz¹² estimated values about half of ours. The parameters chosen by Guldner et al.⁷⁻⁹ result in values of C_K comparable to ours (-2.1 and -2.4) but much larger values of B_K (-2.8, -3.2, and -3.4) and non-zero values for D_K (0.4 and ± 0.1). Again, we do not regard these parameter choices as realistic.

Our results for E_p are plotted in Fig. V-3. The average value $E_p = 17.9 \pm 0.2$ eV is comparable to a number of previous results for $\text{Hg}_{1-x}\text{Cd}_x\text{Te}$ ^{10, 15} and HgTe ¹⁴ and to the results of band calculations (17.2 and 18.0 eV) for the wave functions in $\text{Hg}_{0.854}\text{Cd}_{0.146}\text{Te}$,¹⁶ as well as the estimate of Lawaetz¹² for HgTe. However, other results have ranged from 16 eV for HgTe ^{9, 10, 13} to about 27 eV for $\text{Hg}_{0.788}\text{Cd}_{0.212}\text{Te}$.¹⁷ Guldner et al.⁷ used $E_p = 19.0 \pm 0.1$ eV to fit their magnetoabsorption results for semiconducting $\text{Hg}_{1-x}\text{Cd}_x\text{Te}$ alloys ($E_g > 0$), with a systematic shift, for $E_g \leq 0$, towards 18.0 eV at $x=0$. We find no evidence for such a systematic shift away from 18 eV. The different results for E_p may be partially a result of different choices for the valence band parameters, but more likely a result of differences in the interpretation of the experiments: Uchida and Tanaka⁶ found such a difference between their results and those of Tuchendler et al.⁹ from far-infrared magnetoabsorption in HgTe.

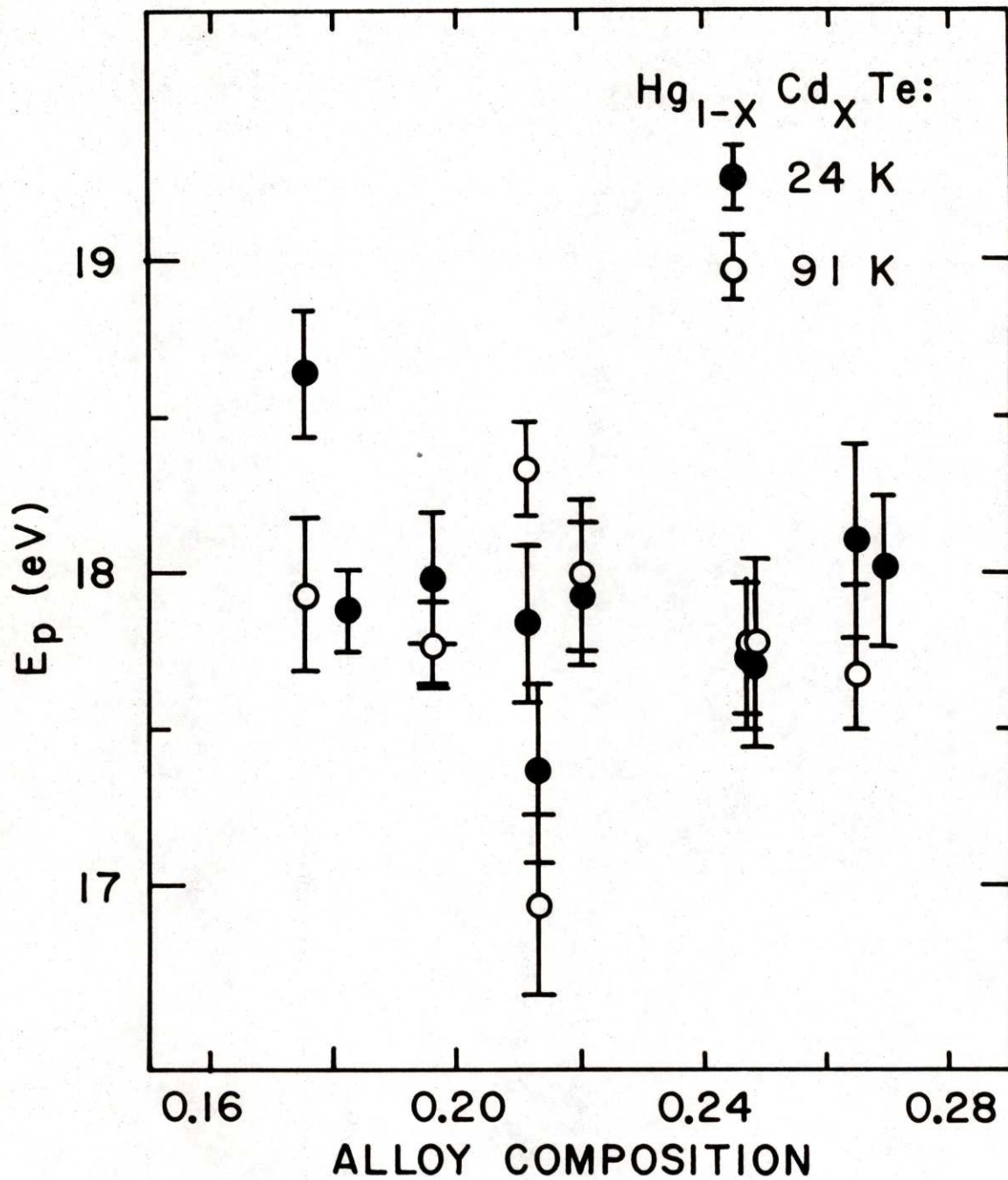


Fig. V-3. E_p vs. alloy composition x for the $\text{Hg}_{1-x}\text{Cd}_x\text{Te}$ samples.

In Fig. V-4 we plot our results for E_g as a function of x . The filled circles are for $T = 24$ K and the open circles for $T = 91$ K. Figure V-4 also gives previous results, from the interband magnetoreflexion experiments of Groves et al.¹⁰ at 25K and 90K for $x = 0.161 \pm 0.003$, and of Strauss et al.¹⁸ for $x = 0.17$ at liquid helium temperature, and from fits to the intra-conduction-band experiments of McCombe et al.^{15, 19} for $x = 0.193$ and 0.203 , of Kinch and Buss²⁰ and Antcliffe²¹ for $x = 0.204$, and of Kahlert and Bauer¹⁷ for $x = 0.212$, all at liquid helium temperatures. We also include curves which fit the results of a recent calculation by Chadi and Cohen² for the $\text{Hg}_{1-x}\text{Cd}_x\text{Te}$ band structure at $T=0$, including approximately the temperature dependence of Schmit and Stelzer¹:

$$E_g(\text{meV}) = -310 + 1880x + (1 - 2x) 0.5 T(\text{K}) \quad (\text{V-16})$$

Guldner et al.⁷ did not give their results for E_g as a function of x .

In Fig. V-4 our results, and those of the interband measurements at $x = 0.16$ and 0.17 , form a continuous curve which agrees fairly well with Eq. (V-16). There is considerable deviation from the equation of Schmit and Stelzer¹ which was developed for temperatures above 77K.

In Figs. V-5 and V-6 we present our results for the conduction band band-edge effective mass m_c and g -factor g_c as a function of x , for the samples at liquid He temperature. As in Fig. V-4, there is considerable deviation from our results by those of the intra-conduction-band experiments^{15, 19-21} which were obtained by fitting their results to the model of Bowers and Yafet,²² which omits all the higher-band parameters. Using our parameters, and values of E_g consistent with our results in Fig. V-4, gives calculated curves which deviate significantly, by as much as 4 meV or 30 cm^{-1} ,

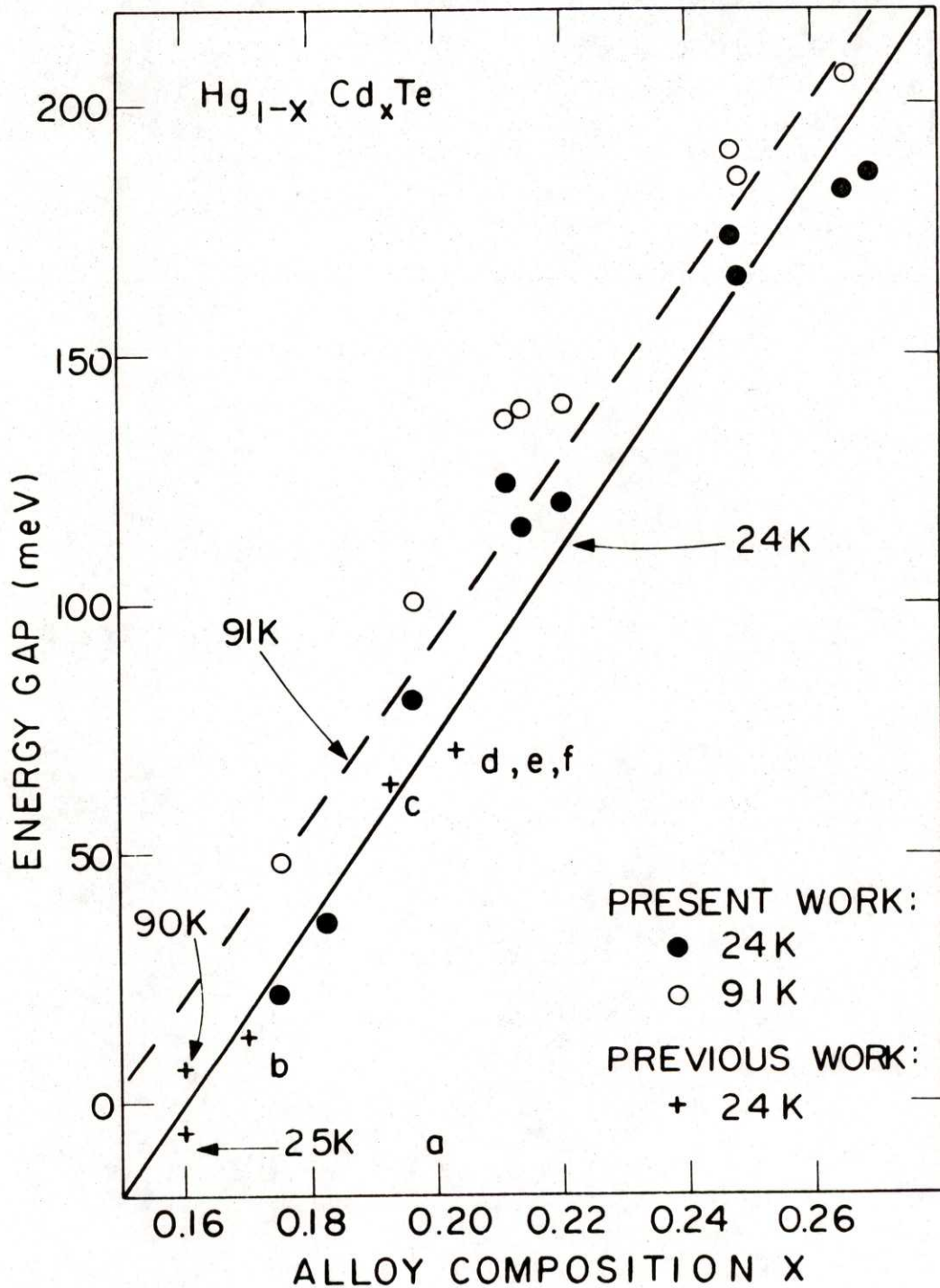


Fig. V-4. E_g vs. x for $\text{Hg}_{1-x}\text{Cd}_x\text{Te}$ samples. The previous results are from interband magnetoreflexion experiments: a - Ref. 10, b - Ref. 18; and from intraband experiments: c - Ref. 19, d - Ref. 20, e - Ref. 15, and f - Ref. 21. Except for a the points have been adjusted to $T = 24\text{K}$.

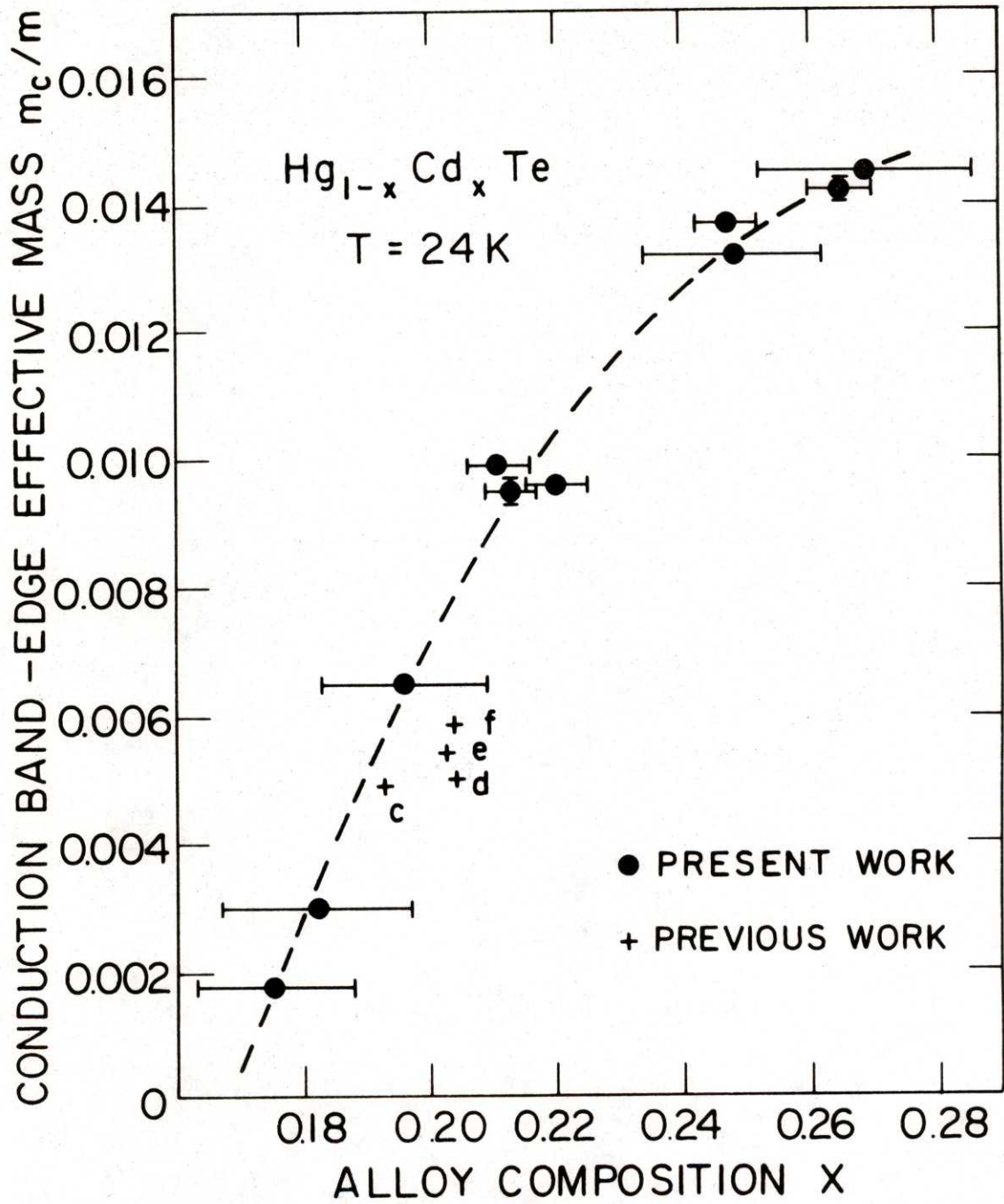


Fig. V-5. Conduction band-edge effective mass for the $\text{Hg}_{1-x}\text{Cd}_x\text{Te}$ samples at $T = 24\text{K}$. The previous results are labeled as in Fig. V-4.

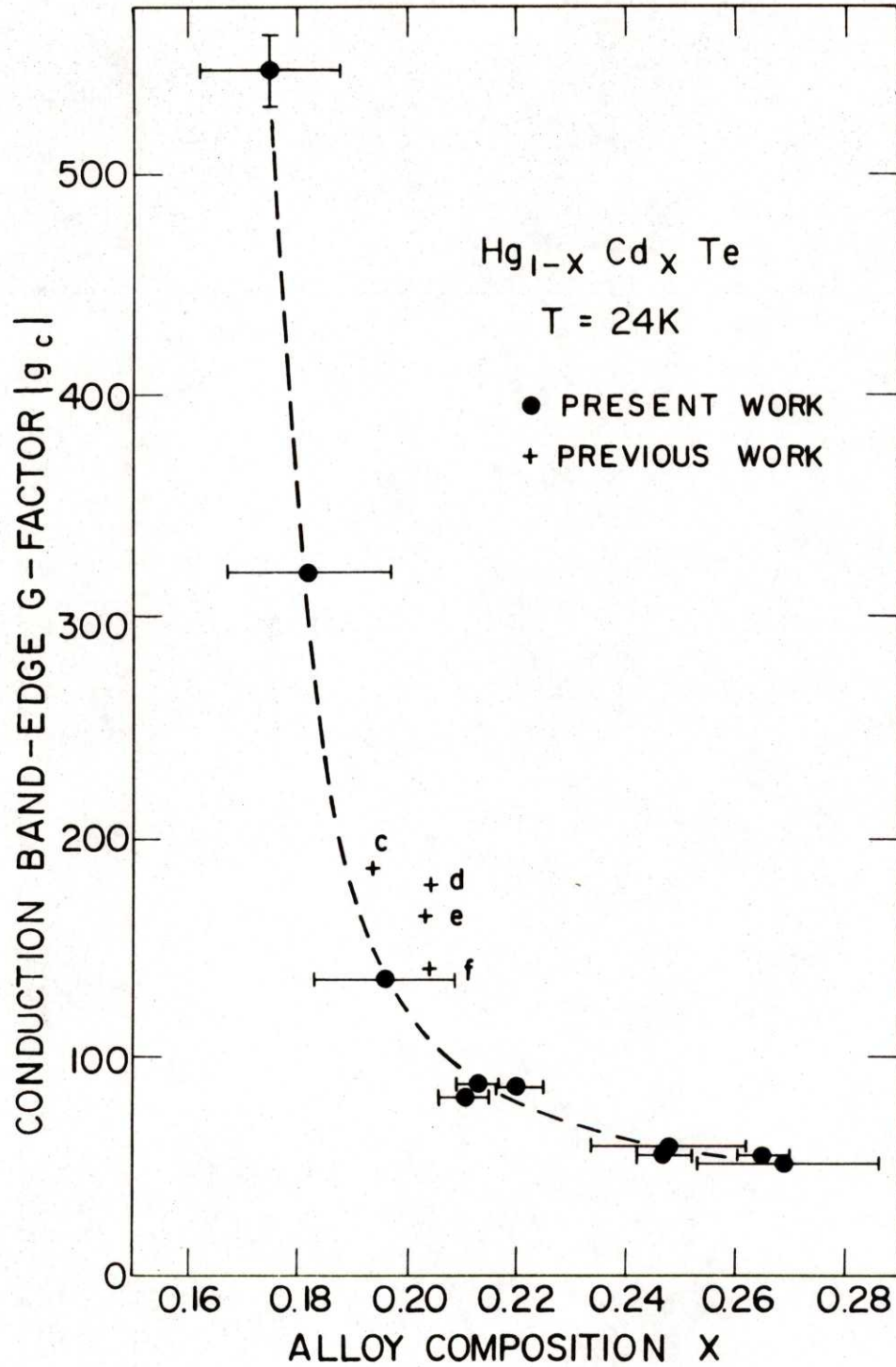


Fig. V-6. Conduction band-edge g -factor for the $\text{Hg}_{1-x}\text{Cd}_x\text{Te}$ samples at $T = 24\text{K}$. The previous results are labeled as in Fig. V-4.

from the experimental results of McCombe et al.^{15, 19} Again, as for InSb,^{23, 24} there is a discrepancy between the parameters derived from interband and intraband experiments; and as for InSb the intraband effective masses are smaller and the g-factors larger. This is a general problem which needs further study beyond the scope of this investigation. For example, the effects of population ($k_H = 0$) on both interband and intraband lineshapes must be carefully evaluated, since they can produce shifts in absorption peaks and can introduce extra transitions, especially for intra-valence-band experiments.

The agreement between our results in Eqs. (V-14) and those of Uchida and Tanaka⁶ gives confidence in these values for the heavy-hole effective masses and, more generally, in the valence band parameters in Eqs. (V-12). Similarly our results for $E_g(x)$ in Fig. V-4 establish Eq. (V-16) as a good approximation for the energy gap of $\text{Hg}_{1-x}\text{Cd}_x\text{Te}$ as a function of x and temperature. Thus, apart from the discrepancy between interband and intraband results, we have presented a comprehensive and systematic model for the electronics structure of $\text{Hg}_{1-x}\text{Cd}_x\text{Te}$ alloys in the small-gap semiconductor region.

REFERENCES

1. J.L. Schmit and E.L. Stelzer, *J. Appl. Phys.* 40, 4865 (1969).
2. D.H. Chadi and M.L. Cohen, *Phys. Rev.* B7, 692 (1973).
3. C.R. Pidgeon and S.H. Groves, *Phys. Rev.* 186, 824 (1969).
4. Y. Ohmura, *J. Phys. Soc. Japan* 25, 740 (1969).
5. M. Reine, Ph.D. Thesis, Massachusetts Institute of Technology (1970).
6. S. Uchida and S. Tanaka, *J. Phys. Soc. Japan* 40, 118 (1976).
7. Y. Guldner, C. Rigaux, A. Mycielski and Y. Couder, *Proc. 13th International Conf. on the Physics of Semiconductors*, F.G. Fumi, ed. (Tipographia Marves, Rome, 1976), p. 1175.
8. Y. Guldner, C. Rigaux, M. Grynberg and A. Mycielski, *Phys. Rev.* B8, 3875 (1973).
9. J. Tuchendler, M. Grynberg, Y. Couder, H. Thome and R. Le Toullec, *Phys. Rev.* B8, 3884 (1973).
10. S.H. Groves, T.C. Harman and C.R. Pidgeon, *Solid State Commun.* 9, 451 (1971).
11. See Table I in J.L. Schmit, *J. Appl. Phys.* 41, 2876 (1970).
12. P. Lawaetz, *Phys. Rev.* B4, 3460 (1971).
13. K. Suzuki, N. Miura, S. Uchida and S. Tanaka, *Phys. Stat. Sol. (b)* 76, 787 (1976).
14. S.H. Groves, R.N. Brown and C.R. Pidgeon, *Phys. Rev.* 161, 779 (1967).
15. B.D. McCombe, R.J. Wagner and G.A. Prinz, *Solid State Commun.* 8, 1687 (1970).
16. S. Katsuki and M. Kunimune, *J. Phys. Soc. Japan* 31, 415 (1971).
17. H. Kahlert and G. Bauer, *Phys. Rev. Letters* 30, 1211 (1973).

18. A.J. Strauss, T.C. Harman, J.G. Mavroides, D.H. Dickey and M.S. Dresselhaus, Report of the International Conference on the Physics of Semiconductors, A.C. Strickland, ed. (The Institute of Physics and The Physical Society, London, 1962), p. 703.
19. B.D. McCombe, S.G. Bishop and R. Kaplan, Phys. Rev. Letters 18, 748 (1967).
20. M.A. Kinch and D.D. Buss, J. Phys. Chem. Solids Suppl. 32, 461 (1971).
21. G.A. Antcliffe, Phys. Rev. B2, 345 (1970).
22. R. Bowers and Y. Yafet, Phys. Rev. 115, 1165 (1959).
23. E.J. Johnson and D.H. Dickey, Phys. Rev. B1, 2676 (1970).
24. R. Ranvaud, Ph.D. Thesis, Massachusetts Institute of Technology (1973).

VI. CONCLUSION

In the first part of this investigation we have shown that, with one exception, the cyclotron harmonic transitions observed in the small-gap semiconductor InSb are induced by the warping and inversion asymmetry effects which are neglected in the quasi Ge model for this material. We suggest that careful measurements be made of the intensity of these transitions, including the $2\omega_c$, $\vec{E}_\perp \vec{H} \parallel [001]$ transition which may be due to impurity effects, as a function of carrier concentration, crystal orientation and optical polarization. Such measurements, when compared to calculated intensities using the model we have presented, could allow a determination of the six warping and inversion asymmetry parameters including the two new parameters we have defined.

In the latter part of this investigation we have analyzed our magneto-reflection results for $\text{Hg}_{1-x}\text{Cd}_x\text{Te}$ using the quasi Ge model which neglects such warping and inversion asymmetry effects, and have determined the parameters of this model for alloy compositions x in the small-gap semiconductor region. Within the accuracy of our results, which is limited primarily by the sample inhomogeneity, we find that all the parameters except the energy gap are independent of x and of the sample temperature. Since the higher-band energies are approximately the same in HgTe and CdTe (see App. A), it is not surprising that the higher-band parameters are insensitive to x . It would be useful to extend our experiments to a larger range of x in order to check these conclusions.

Another useful extension of our studies of $\text{Hg}_{1-x}\text{Cd}_x\text{Te}$ would be intra-band experiments on the same (n-type) samples. Our calculations indicate

that cyclotron and combined resonance, and perhaps harmonics and phonon-assisted transitions, could be observed using the same optical apparatus with, in some cases, the use of higher magnetic fields or detectors operating at longer wavelengths. In view of the general discrepancy between parameters deduced from inter- and intra-band measurements in the zincblende semiconductors, such experiments might provide a crucial test of the validity of the quasi Ge model for these materials. Such a combination of intraband and interband experiments, using the same apparatus, is possible only for materials like our $\text{Hg}_{1-x}\text{Cd}_x\text{Te}$ samples, with extremely small energy gaps and effective masses.

APPENDIX A. ESTIMATES OF PARAMETERS

We estimate the parameters of Table II-2 by expressing them in terms of \vec{p} matrix elements among the band-edge states belonging to the single-group representations of the T_d group. We begin with the parameters defined by Kane,¹ in terms of the conduction and valence band states S, X, Y and Z and higher band states Γ'_i :

$$P \equiv -i \frac{\hbar}{m} \langle S | p_x | X \rangle \quad (\text{A-1})$$

$$A_K \equiv \frac{1}{m} \sum_{\Gamma'_1} \frac{\langle X | p_x | \Gamma'_1 \rangle \langle \Gamma'_1 | p_x | X \rangle}{E_0 - E(\Gamma'_1)}$$

$$B_K \equiv \frac{1}{m} \sum_{\Gamma'_3} \frac{\langle X | p_x | \Gamma'_3 \rangle \langle \Gamma'_3 | p_x | X \rangle}{E_0 - E(\Gamma'_3)}$$

$$C_K \equiv \frac{1}{m} \sum_{\Gamma'_4} \frac{\langle X | p_y | \Gamma'_4 \rangle \langle \Gamma'_4 | p_y | X \rangle}{E_0 - E(\Gamma'_4)}$$

$$D_K \equiv \frac{1}{m} \sum_{\Gamma'_5} \frac{\langle X | p_y | \Gamma'_5 \rangle \langle \Gamma'_5 | p_y | X \rangle}{E_0 - E(\Gamma'_5)}$$

(A-2)

$$F \equiv \frac{1}{m} \sum_{\Gamma_4'} \frac{|\langle S | p_x | \Gamma_4' \rangle|^2}{E_0 - E(\Gamma_4')}$$

$$G \equiv \frac{1}{m} \sum_{\Gamma_4'} \frac{\langle S | p_x | \Gamma_4' \rangle \langle \Gamma_4' | p_y | Z \rangle}{E_0 - E(\Gamma_4')}$$
(A-3)

where E_0 is approximately the band edge energy of the conduction and valence bands which are not included in the summations since the coupling between these bands is included explicitly in our model.

When the Hamiltonian is expressed in terms of the linear combinations of X, Y and Z, and the spin functions \uparrow and \downarrow [Eqs. (II-1)], which diagonalize the spin-orbit interaction, the parameters in Eqs. (A-2) recombine to form the parameters defined by Luttinger²

$$\gamma_1 = -\frac{2}{3} (A_K + B_K + 2C_K + 2D_K) - 1$$

$$\gamma_2 = -\frac{1}{3} (A_K + B_K - C_K - D_K)$$

$$\gamma_3 = -\frac{1}{3} (A_K - \frac{1}{2}B_K + C_K - D_K)$$

$$\kappa = -\frac{1}{3} (A_K - \frac{1}{2}B_K - C_K + D_K) - \frac{1}{3}$$
(A-5)

The spin-orbit interaction also allows the linear-k parameters defined by Dresselhaus³

$$C \equiv \frac{\hbar^2}{2\sqrt{3}m^2c^2} \sum_{\Gamma_i'=\Gamma_4',\Gamma_5'} \frac{\langle Y^\dagger | \mathcal{H}_{so} | \Gamma_i' \rangle \langle \Gamma_i' | p_y | Z^\dagger \rangle}{E_0 - E(\Gamma_i')} \quad (\text{A-6})$$

Including the spin-orbit splitting of higher Γ_4 bands ($\Gamma_4 \rightarrow \Gamma_7', \Gamma_8'$), we obtain the other four parameters in Table II-2:

$$\begin{aligned} q &\equiv \frac{8}{27} \frac{i}{m} \sum_{\Gamma_8'} \frac{\langle \psi_{3/2}^8 | p_x | \Gamma_8' \rangle \langle \Gamma_8' | p_y | \psi_{3/2}^8 \rangle}{E_0 - E(\Gamma_8')} \\ N_1 &\equiv - \frac{i}{m} \sum_{\Gamma_8'} \frac{\langle \psi_{1/2}^6 | p_x | \Gamma_8' \rangle \langle \Gamma_8' | p_y | \psi_{1/2}^6 \rangle}{E_0 - E(\Gamma_8')} \\ N_2 &\equiv \frac{1}{m} \sum_{\Gamma_8'} \frac{\langle \psi_{1/2}^6 | p_x | \Gamma_8' \rangle \langle \Gamma_8' | p_x | \psi_{-3/2}^8 \rangle}{E_0 - E(\Gamma_8')} \\ N_3 &\equiv - \frac{i}{m} \sum_{\Gamma_8'} \frac{\langle \psi_{1/2}^6 | p_x | \Gamma_8' \rangle \langle \Gamma_8' | p_y | \psi_{-3/2}^8 \rangle}{E_0 - E(\Gamma_8')} \end{aligned} \quad (\text{A-7})$$

We estimate these last four parameters for one higher band (X' , Y' , Z'). Carrying out the spin-orbit transformation on both this and the (X , Y , Z) valence band, we find

$$\begin{aligned}
 q &\approx -\frac{4}{9} \sum_{\Gamma_4'} \frac{\Delta' \langle X | p_y | \Gamma_4' \rangle \langle \Gamma_4' | p_y | X \rangle}{[E_0 - E(\Gamma_4')]^2} \\
 N_1 &\approx \frac{1}{3} \sum_{\Gamma_4'} \frac{\Delta' |\langle S | p_x | \Gamma_4' \rangle|^2}{[E_0 - E(\Gamma_4')]^2} \\
 N_2 \approx N_3 &\approx -\frac{1}{3\sqrt{2}} \sum_{\Gamma_4'} \frac{\Delta' \langle S | p_x | \Gamma_4' \rangle \langle \Gamma_4' | p_y | Z \rangle}{[E_0 - E(\Gamma_4')]^2}
 \end{aligned} \tag{A-8}$$

where Δ' is the spin-orbit splitting of the higher band. This gives

$$\begin{aligned}
 q &\approx -\frac{4}{9} \frac{\Delta'}{E_0'} C_K \\
 N_1 &\approx \frac{1}{3} \frac{\Delta'}{E_0'} F \\
 N_2 \approx N_3 &\approx -\frac{1}{3\sqrt{2}} \frac{\Delta'}{E_0'} G
 \end{aligned} \tag{A-9}$$

where $E_0' \equiv E(\Gamma_4') - E_0$. This result for q is the same as that given by Hensel and Suzuki.⁴

For InSb, the parameters P , γ_1 , γ_2 , γ_3 and κ were obtained from magneto-optical experiments by Pidgeon and Brown⁵:

$$E_p \equiv 2P^2/m \approx 21.9 \text{ eV}$$

$$\gamma_1 = 1.5$$

$$\gamma_2 = -1.2 \tag{A-10}$$

$$\gamma_3 = -0.1$$

$$\kappa = -2.1$$

neglecting the other parameters F , G , C , q , N_1 , N_2 and N_3 . Somewhat different values were obtained by Pidgeon and Groves,⁶ who also found

$$q = 0.39 \tag{A-11}$$

$$C = 9.3 \times 10^{-11} \text{ eV-cm}$$

The results in Eq. (A-10) imply, from Eq. (A-4)

$$A_K \approx 1.4$$

$$B_K \approx -1.1$$

$$C_K \approx -2.5$$

$$D_K \approx 0.0$$

(A-12)

The results for q and C_K imply

$$\frac{\Delta'}{E_0'} \approx 0.35 \tag{A-13}$$

which is approximately satisfied using $\Delta' \approx 1 \text{ eV}$ and $E_0' \approx 3 \text{ eV}$. However,

Glosser, Fischer and Seraphin⁷ have observed electroreflection structure in n-type InSb at 3.1 and 3.5 eV which they attribute to transitions from the Γ_6 to the spin-split Γ_4' band, giving $E_0' \approx 3.3$ eV and $\Delta' \approx 0.4$ eV with $\Delta'/E_0' \approx 0.12$. This value of Δ' is about half that calculated by Varea de Alvarez et al.,⁸ but agrees with a calculation by Bloom and Bergstresser.⁹ The ratio Δ'/E_0' implies

$$q \approx 0.13 \quad (\text{A-14})$$

rather than 0.39, which is close to the value 0.15 estimated by Lawaetz.¹⁰ Using $C_K = -0.25$ and $E_0' = 3.3$ eV gives, from Eq. (A-2),

$$|\langle X | p_y | \Gamma_4' \rangle|^2 / m \approx 8.3 \text{ eV} \quad (\text{A-15})$$

This, with the estimate of Lawaetz

$$E_p' \equiv 2|\langle S | p_x | X' \rangle|^2 / m \approx 15 \text{ eV} \quad (\text{A-16})$$

gives, from Eqs. (A-5)

$$F \approx -2.3 \quad (\text{A-17})$$

$$|G| \approx 2.4$$

Then Eqs. (A-9) give

$$N_1 \approx -0.1 \quad (\text{A-18})$$

$$|N_2| \approx |N_3| \approx 0.09$$

For the case of $\text{Hg}_{1-x}\text{Cd}_x\text{Te}$, Lawaetz¹⁰ estimates, for HgTe and CdTe, $\Delta \approx 1$ eV, $\Delta' \approx 0.6$ eV, and $E_0' \approx 5.8$ eV. He also estimates $B_K \approx -0.5$ and $C_K \approx -1.2$, with $A_K \approx D_K \approx 0$, and $q \approx 0.06$, $E_p' \approx 14$ eV. These give

$$F \approx -1.2$$

$$|G| \approx 1.4$$

(A-19)

$$N_1 \approx -0.4$$

$$|N_2| \approx |N_3| \approx 0.03$$

These results for N_1 , N_2 and N_3 , as well as for q , are even smaller in comparison to the other parameters, than is the case for InSb. These estimates are further decreased if we used the recently calculated results $\Delta' \approx 0.13$, $E_0' \approx 6$ eV for CdTe or $\Delta' \approx 0.26$, $E_0' \approx 5$ eV for HgTe.¹¹

REFERENCES

1. E.O. Kane, J. Phys. Chem. Solids 1, 249 (1957).
2. J.M. Luttinger, Phys. Rev. 102, 1030 (1956).
3. G. Dresselhaus, Phys. Rev. 100, 580 (1955).
4. J.C. Hensel and K. Suzuki, Phys. Rev. Letters 22, 838 (1969).
5. C.R. Pidgeon and R.N. Brown, Phys. Rev. 146, 575 (1966).
6. C.R. Pidgeon and S.H. Groves, Phys. Rev. 186, 824 (1969).
7. R. Glosser, J.E. Fischer and B.O. Seraphin, Phys. Rev. B1, 1607 (1970).
8. C. Varea de Alvarez, J.P. Walter, R.W. Boyd and M.L. Cohen,
J. Phys. Chem. Solids 34, 337 (1973).
9. S. Bloom and T.K. Bergstresser, Sol. State Commun. 6, 465 (1968).
10. P. Lawaetz, Phys. Rev. B4, 3460 (1971).
11. D.J. Chadi, J.P. Walter, M.L. Cohen, Y. Petroff and M. Balkanski,
Phys. Rev. B5, 3058 (1972).

APPENDIX B. DERIVATIVES OF TRANSITION ENERGIES

The system of equations (V-3) for the corrections $\delta\alpha_j$ to the set of parameters α_j involves the derivatives $\partial E(H)/\partial\alpha_j$ of the transition energies $E(H)$ with respect to each parameter. Each transition energy is given by $E(H) = E^C(H) - E^V(H)$, where $E^C(H)$ and $E^V(H)$ are the conduction and valence band energies in the quasi Ge model Eqs. (II-10). These energies are solutions of the determinantal equation

$$\begin{vmatrix} E_1 & C & D & E \\ C & E_2 & L_3 & F \\ D & L_3 & E_3 & G \\ E & F & G & E_4 \end{vmatrix} = 0 \quad (\text{B-1})$$

where, for a-set energies and $n \geq 1$,

$$\begin{aligned} E_1 &\equiv E_g + 2\beta H[(2n+1)F + N_1 + n + 1] - E(H) \\ E_2 &\equiv -\beta H[(2n-1)(\gamma_1 + \gamma') + 3\kappa] + q_1 - E(H) \\ E_3 &\equiv -\beta H[(2n+3)(\gamma_1 - \gamma') - \kappa] + q_5 - E(H) \\ E_4 &\equiv -\Delta - \beta H[(2n+3)\gamma_1 - 2\kappa - 1] - E(H) \end{aligned} \quad (\text{B-2})$$

where q_1 and q_5 are defined in Eqs. (III-3), and

$$\begin{aligned}
C &\equiv \sqrt{n\beta H E_p} & L_3 &\equiv 2\beta H \sqrt{3n(n+1)} \gamma'' \\
D &\equiv -\sqrt{(n+1)\beta H E_p/3} & F &\equiv -2\beta H \sqrt{6n(n+1)} \gamma'' \\
E &\equiv \sqrt{2(n+1)\beta H E_p} & G &\equiv \sqrt{2}\beta H [(2n+3)\gamma' - \kappa - 1]
\end{aligned} \tag{B-3}$$

For the b-set energies, and $n \geq 1$,

$$\begin{aligned}
E_1 &\equiv E_g + 2\beta H [(2n+1)F - N_1 + n] - E(H) \\
E_2 &\equiv -\beta H [(2n-1)(\gamma_1 - \gamma') + \kappa] - q_5 - E(H) \\
E_3 &\equiv -\beta H [(2n+3)(\gamma_1 + \gamma') - 3\kappa] - q_1 - E(H) \\
E_4 &\equiv -\Delta - \beta H [(2n-1)\gamma_1 + 2\kappa + 1] - E(H)
\end{aligned} \tag{B-4}$$

and

$$\begin{aligned}
C &\equiv \sqrt{n\beta H E_p/3} & L_3 &\equiv 2\beta H \sqrt{3n(n+1)} \gamma'' \\
D &\equiv -\sqrt{(n+1)\beta H E_p} & F &\equiv -\sqrt{2}\beta H [(2n-1)\gamma' + \kappa + 1] \\
E &\equiv \sqrt{2n\beta H E_p/3} & G &\equiv 2\beta H \sqrt{6n(n+1)} \gamma''
\end{aligned} \tag{B-5}$$

Equation (B-1) is

$$\begin{aligned}
&E_1 E_2 E_3 E_4 - E_3 E_4 C^2 - E_2 E_4 D^2 - E_2 E_3 E^2 - E_1 E_3 F^2 - E_1 E_2 G^2 \\
&- E_1 E_4 L_3^2 + 2E_1 F G L_3 + 2E_2 D E G + 2E_3 C E F + 2E_4 C D L_3 \\
&- 2C D F G - 2D E F L_3 - 2C E G L_3 + C^2 G^2 + D^2 F^2 + E^2 L_3^2 = 0
\end{aligned} \tag{B-6}$$

Taking the derivative of this equation with respect to each parameter α_j , we obtain the following expression for the derivatives $\partial E(H)/\partial \alpha_j$:

$$\rho \frac{\partial E(H)}{\partial \alpha_j} = \sum_{i=1}^4 f(E_i) \frac{\partial E_i}{\partial \alpha_j} + f(C) \frac{\partial C}{\partial \alpha_j} + f(D) \frac{\partial D}{\partial \alpha_j} + \dots \quad (B-7)$$

where

$$\begin{aligned} f(E_1) &= -E_2(E_3E_4 - G^2) + E_3F^2 + L_3(E_4L_3 - 2FG) \\ f(E_2) &= -E_1(E_3E_4 - G^2) + E_3E^2 + D(E_4D - 2EG) \\ f(E_3) &= -E_4(E_1E_2 - C^2) + E_2E^2 + F(E_1F - 2CE) \\ f(E_4) &= -E_3(E_1E_2 - C^2) + E_1L_3^2 + D(E_2D - 2CL_3) \end{aligned} \quad (B-8)$$

and

$$\begin{aligned} f(C) &= 2[C(E_3E_4 - G^2) - E(E_3F - GL_3) - D(E_4L_3 - FG)] \\ f(D) &= 2[D(E_2E_4 - F^2) - E(E_2G - FL_3) - C(E_4L_3 - FG)] \\ f(E) &= 2[E(E_2E_3 - L_3^2) - D(E_2G - FL_3) - C(E_3F - GL_3)] \\ f(F) &= 2[F(E_1E_3 - D^2) - G(E_1L_3 - CD) - E(E_3C - DL_3)] \\ f(G) &= 2[G(E_1E_2 - C^2) - F(E_1L_3 - CD) - E(E_2D - CL_3)] \\ f(L_3) &= 2[L_3(E_1E_4 - E^2) - F(E_1G - DE) - C(E_4D - EG)] \end{aligned} \quad (B-9)$$

with

$$\begin{aligned}
 \rho = & - (E_1 + E_2)(E_3 E_4 - G^2) - (E_3 + E_4)(E_1 E_2 - C^2) + (E_1 + E_3)F^2 \\
 & + (E_2 + E_4)D^2 + L_3[(E_1 + E_4)L_3 - 2(CD + FG)] \quad (B-10) \\
 & + E[(E_2 + E_3)E - 2(CF + DG)]
 \end{aligned}$$

Taking the appropriate derivatives $\partial E_1 / \partial \alpha_j$, etc. from Eqs. (B-2, 3) or (B-3, 4), and using Eqs. (B-7) through (B-10), gives the equations used to calculate the derivatives $\partial E(H) / \partial \alpha_j$ in the subroutine DECAL which is in the listings of computer programs in Appendix C. The derivatives for the special cases $n = -1$ and 0 are computed, along with these energies, in the subroutine HCTEDR, which calls DECAL for $n \geq 1$.

APPENDIX C. COMPUTER PROGRAMS

This Appendix includes listings of the computer programs used in this investigation. These were all used on the TSO time-sharing system. Those in the first group were used to calculate (GEDIAG) and print (GEPR) the energy eigenvalues and eigenvectors in the quasi Ge model for a given set of parameters and magnetic field values, and also to calculate the energies and intensities (GEINTEN) of transitions among these levels. The most intense interband transitions were calculated (HCTTR) and plotted (HCTPLT) on copies of our magnetoreflexion data for $\text{Hg}_{1-x}\text{Cd}_x\text{Te}$ using the next two programs. The identified magnetoreflexion peaks were stored (DATACR) in disc datasets, which could be edited using the TSO command EDIT. The data points were fit to the calculated transition energies using variations of the next two programs, which call the subroutine HCTEDR which computes the transition energies and their derivatives with respect to all the parameters (see App. B). The program HCTMIN was used to attempt to fit all of the parameters simultaneously, and HCTMBC reduces the fit to 5 parameters or less by expressing the valence band parameters $\gamma_1, \gamma_2, \gamma_3$ and κ in terms of the Kane parameters B_K and C_K [Eqs. (A-5)].

Each program which requires input from the terminal uses a standard set of conventions. The LABL input provides an opportunity to label the output with the date, for example, and setting the first character to "s" is the "stop" signal. The other input uses the TSO READ* or free-format input: values are delimited by commas, successive commas are used to skip (leave unchanged) a variable, and a "/" terminates the input. In our programs the sample orientation is assumed to be [111] unless $\cos \theta$ is reset on input.

C
C
C
C
C
C
C
C
C
C
C
C
C
C
C
C
C
C
C

```
SUBROUTINE GEDIAG(H,NMIN,NMAX,EG,DEL,EP,F,G1,GP,GPP,KAP,O1,O5,IV, EN,U) 00000010
                                                                                         00000020
                                                                                         00000030
DIAGONALIZES 8*8 GERMANIUM K.P MATRIX USING ROUTINE EIGRS 00000040
  IN 'SYS5.IMSLIB.LOAD' 00000050
                                                                                         00000060
PARAMETERS: H(KILOGAUSS) MAGNETIC FIELD 00000070
              NMIN,NMAX(INTEGER8) RANGE OF N-VALUES TO BE USED 00000080
              EG,DEL(EV) ENERGY GAP AND S-O SPLITTING 00000090
              F,G1,GP,GPP,KAP,O1,O5 CONDUCTION AND VALENCE BAND 00000100
              HIGHER-BAND PARAMETERS 00000110
              IV = 0 FOR NO EIGENVECTORS, 1 FOR VECTORS 00000120
                                                                                         00000130
RETURNS: EN(I,I) ENERGIES(EV) 8*LMAX MATRIX 00000140
         U(J,I,L) EIGENVECTOR FOR EN(I,L) 4*8*LMAX MATRIX 00000150
         LMAX = NMAX - NMIN + 1 00000160
                                                                                         00000170
                                                                                         00000180
SUBROUTINE GEDIAG(H,NMIN,NMAX,EG,DEL,EP,F,G1,GP,GPP,K,O1,O5,IV,EN, 00000190
1 U) 00000200
IMPLICIT REAL*8 (A-Z) 00000210
INTEGER NMIN,NMAX,IV,LMAX,L,I,J,IER,II,JJ 00000220
DIMENSION EN(8,18),U(4,8,18),A(10),B(10),D(4),Z(4,4),WK(4) 00000230
DATA RT2/1.414213562D0/ 00000240
DATA RT3/1.732050808D0/ 00000250
DATA RT6/2.449489743D0/ 00000260
LMAX=NMAX-NMIN+1 00000270
S=1.15767578D-5*H 00000280
S2=S/2D0 00000290
M2A=DSORT(S*EP) 00000300
M4A=M2A/RT6 00000310
M7A=M2A/RT3 00000320
M2A=M2A/RT2 00000330
G1S=G1*S 00000340
GPS=GP*S 00000350
GPL=G1S+GPS 00000360
```


GMI=G1S-GPS	00000370
KS=K*S	00000380
O1S=O1*S	00000390
O5S=O5*S	00000400
M1=(P+5D-1)*S	00000410
M1N=M1*2D0	00000420
M1=M1+3G+S2	00000430
M3A=5D-1*GPL-1.5D0*KS+O1S	00000440
M3B=5D-1*GMI-5D-1*KS-O5S	00000450
M6A=5D-1*KS-1.5D0*GMI+O5S	00000460
M6B=1.5D0*KS-1.5D0*GPL-O1S	00000470
M10A=S2-1.5D0*G1S+KS-DEL	00000480
M10B=5D-1*G1S-S2-KS-DEL	00000490
M5=-RT3*GPP*S	00000500
M9N=RT2*GPS	00000510
M9A=(KS+S-3D0*GPS)/RT2	00000520
M8P=(GPS-KS-S)/RT2	00000530
L=1	00000540
N=NMIN	00000550
IF(NMIN.GP.0) GO TO 30	00000560
A(1)=M6A+GMI	00000570
A(2)=-M9A-M9N	00000580
A(3)=M10A+G1S	00000590
CALL FIGPS(A,2,IV,D,Z,4,WK,IER)	00000600
FN(1,1)=0D0	00000610
FN(2,1)=0D0	00000620
FN(3,1)=D(2)	00000630
FN(4,1)=D(1)	00000640
FN(5,1)=0D0	00000650
FN(6,1)=0D0	00000660
FN(7,1)=M6B+GPL	00000670
FN(8,1)=0D0	00000680
IF(IV.EQ.0) GO TO 20	00000690
DO 10 J=1,4	00000700
DO 10 I=1,8	00000710
U(J,I,1)=0D0	00000720

	U(3,3,1)=Z(1,2)	00000730
	U(4,3,1)=Z(2,2)	00000740
	U(3,4,1)=Z(1,1)	00000750
	U(4,4,1)=Z(2,1)	00000760
	U(3,7,1)=1D0	00000770
20	IF(NMAX.EQ.-1) RETURN	00000780
	L=L+1	00000790
	N=N+1D0	00000800
30	DO 110 I=L,LMAX	00000810
	RTN1=DSORT(N+1D0)	00000820
	A(1)=M1N*N+M1	00000830
	R(1)=A(1)-S	00000840
	A(4)=-M4A*RTN1	00000850
	R(4)=-M2A*RTN1	00000860
	A(6)=M6A-N*GMT	00000870
	R(6)=M6B-N*GPL	00000880
	A(7)=M7A*RTN1	00000890
	A(9)=-M9A+M9N*N	00000900
	A(10)=M10A-G1S*N	00000910
	IF(N.NE.0D0) GO TO 60	00000920
	A(2)=A(4)	00000930
	A(3)=A(6)	00000940
	A(4)=A(7)	00000950
	A(5)=A(9)	00000960
	A(6)=A(10)	00000970
	CALL EIGRS(A,3,IV,D,Z,4,WK,IEP)	00000980
	FN(1,L)=D(3)	00000990
	EN(2,L)=0D0	00001000
	FN(3,L)=D(2)	00001010
	FN(4,L)=D(1)	00001020
	IF(IV.EQ.0) GO TO 40	00001030
	U(1,1,L)=Z(1,3)	00001040
	U(2,1,L)=0D0	00001050
	U(3,1,L)=Z(2,3)	00001060
	U(4,1,L)=Z(3,3)	00001070
	U(1,2,L)=0D0	00001080

	U (2, 2, L) = 0D0	00001090
	U (3, 2, L) = 0D0	00001100
	U (4, 2, L) = 0D0	00001110
	U (1, 3, L) = Z (1, 2)	00001120
	U (2, 3, L) = 0D0	00001130
	U (3, 3, L) = Z (2, 2)	00001140
	U (4, 3, L) = Z (3, 2)	00001150
	U (1, 4, L) = Z (1, 1)	00001160
	U (2, 4, L) = 0D0	00001170
	U (3, 4, L) = Z (2, 1)	00001180
	U (4, 4, L) = Z (3, 1)	00001190
40	R (2) = R (4)	00001200
	B (3) = B (6)	00001210
	CALL BTGRS (B, 2, IV, D, Z, 4, WK, IER)	00001220
	FN (5, L) = D (2)	00001230
	FN (6, L) = 0D0	00001240
	FN (7, L) = D (1)	00001250
	EN (8, L) = 0D0	00001260
	IF (IV.EQ.0) GO TO 110	00001270
	DO 50 J=1, 4	00001280
	DO 50 I=5, 8	00001290
50	U (J, I, L) = 0D0	00001300
	U (1, 5, L) = Z (1, 2)	00001310
	U (3, 5, L) = Z (2, 2)	00001320
	U (1, 7, L) = Z (1, 1)	00001330
	U (3, 7, L) = Z (2, 1)	00001340
	GO TO 110	00001350
60	RTN=DSORT (N)	00001360
	A (2) = RTN*M2A	00001370
	B (2) = RTN*M4A	00001380
	A (3) = M3A-N*GPI	00001390
	B (3) = M3B-N*GMI	00001400
	A (5) = -RTN*RTN1*M5	00001410
	B (5) = A (5)	00001420
	B (7) = RTN*M7A	00001430
	A (8) = -RT2*A (5)	00001440

	R(8)=M8B-N*M9N	00001450
	R(9)=-A(8)	00001460
	R(10)=M10B-N*G1S	00001470
	CALL EIGRS(A,4,IV,D,Z,4,WK,IER)	00001480
	DO 80 I=1,4	00001490
	II=5-I	00001500
	FN(II,L)=D(I)	00001510
	IF(IV.EQ.0) GO TO 80	00001520
	DO 70 J=1,4	00001530
70	U(J,II,L)=Z(J,I)	00001540
80	CONTINUE	00001550
	CALL EIGRS(B,4,1,D,Z,4,WK,IER)	00001560
	DO 100 I=1,4	00001570
	II=9-I	00001580
	FN(II,L)=D(I)	00001590
	IF(IV.EQ.0) GO TO 100	00001600
	DO 90 J=1,4	00001610
90	U(J,II,L)=Z(J,I)	00001620
100	CONTINUE	00001630
110	N=N+100	00001640
	IF(IV.EQ.0) RETURN	00001650
	DO 150 L=1,LMAX	00001660
	DO 150 I=1,4	00001670
	IF(U(I,I,L).GE.0D0) GO TO 130	00001680
	DO 120 J=1,4	00001690
120	U(J,I,L)=-U(J,I,L)	00001700
130	IF(U(I,I+4,L).GE.0D0) GO TO 150	00001710
	DO 140 J=1,4	00001720
140	U(J,I+4,L)=-U(J,I+4,L)	00001730
150	CONTINUE	00001740
	RETURN	00001750
	END	00001760
C		00001770
C		00001780
C		00001790
C		00001800

C	FILE GEPRT.FORT	00000010
C		00000020
C	OBTAINS AND TRANSMITS PARAMETERS FOR GEDIAG ROUTINE	00000030
C		00000040
C	PRINTS ENERGY LEVELS AND EIGENVECTORS	00000050
C		00000060
C	USAGE: LCADGO (GEPRT,GEDIAG) FORTLIB LIB('SYS5.IMSLIB.LOAD')	00000070
C		00000080
	IMPLICIT REAL*8(A-Z)	00000090
	INTEGER*2 LABL,BLANK/' ',STOP/'S'/	00000100
	INTEGER LINE,NMIN,NMAX,LMAX,IH,IMAX,I,L,N,J	00000110
	DIMENSION HI(20),LABL(100),EN(8,18),U(4,8,18)	00000120
	DATA HI/2D1,4D1,6D1,8D1,1D2,12D1,14D1,16D1/	00000130
	DATA NMIN,NMAX/-1,4/,IMAX/8/,C111/.5773502692D0/	00000140
	DATA G1,G2,G3,K,F,Q/0D0,0D0,0D0,0D0,0D0,0D0/	00000150
10	DC 20 I=1,100	00000160
20	LABL(I)=BLANK	00000170
	C=C111	00000180
	PRINT 500	00000190
500	FORMAT(//' ENTER LABEL/EGM,EP,DEL,G1,G2,G3,K,F,Q/',	00000200
	1 'COSINE,NMIN,NMAX,FIELD IMAX,VALUES/'//)	00000210
	READ 600,LABL	00000220
600	FORMAT(100A1)	00000230
	IF(LABL(1).EQ.STOP) CALL EXIT	00000240
	READ *,EGM,EP,DEL,G1,G2,G3,K,F,Q	00000250
	READ *,C,NMIN,NMAX,IMAX,HI	00000260
	EG=EGM*1D-3	00000270
	G3L=EP/3D0/EG	00000280
	G1L=G1+G3L	00000290
	G3L=G3L/2D0	00000300
	G2L=G2+G3L	00000310
	KAPL=K+G3L	00000320
	G3L=G3+G3L	00000330
	GPP=(3D0*C*C-1D0)/2D0	00000340
	GPP=(G2-G3)*GPP*GPP	00000350
	GP=G3+GPP	00000360

	GPP=G2/3D0+G3/1.5D0+GPP/6D0	00000370
	O5=(1D0-1.5D0*C*C)*.75D0*C*C	00000380
	O1=(O5-3D0)*O	00000390
	O5=(3D0*O5+1.25D0)*O	00000400
	LMAX=NMAX-NMIN+1	00000410
	PRINT 510	00000420
510	FORMAT(///)	00000430
	PRINT 520,LABL	00000440
520	FORMAT(//1X,100A1)	00000450
	EGM=EG*1D3	00000460
	DELM=DEL*1D3	00000470
	PRINT 530,EGM,DELM,EP,F,O,G1L,G2L,G3L,KAPL,G1,G2,G3,K,GP,GPP	00000480
530	FORMAT(///// ' EG=' ,F8.2,' MEV, DEL=' ,F8.2,' MEV, EP=' ,F8.2,	00000490
	1 ' FV, F=' ,F6.2,' , O=' ,F6.2///' G1L=' ,F7.3,' , G2L=' ,F7.3,	00000500
	2 ' , G3L=' ,F7.3,' , KAPL=' ,F7.3///' G1=' ,F7.3,' , G2=' ,F7.3,	00000510
	3 ' , G3=' ,F7.3,' , KAP=' ,F7.3///' GP=' ,F7.3,' , GPP=' ,F7.3,	00000520
	4 34(/)	00000530
	IH=1	00000540
30	H=HI(IH)	00000550
	PRINT 520,LABL	00000560
	IINF=3	00000570
	CALL GEDIAG(H,NMIN,NMAX,EG,DEL,EP,F,G1,GP,GPP,K,O1,O5,1,EN,U)	00000580
	PRINT 540,H	00000590
540	FORMAT(///50X,'H=' ,F8.2,' KILOGAUSS'///' N' ,8X,'EA(MEV)' ,	00000600
	1 7X,'S' ,8X,'3/2' ,6X,'-1/2' ,7X,'S-O' ,10X,'EB(MEV)' ,7X,	00000610
	2 'S' ,8X,'1/2' ,6X,'-3/2' ,7X,'S-O')	00000620
	IINF=IINF+7	00000630
	DO 40 L=1,LMAX	00000640
	DO 40 I=1,8	00000650
40	FN(I,L)=EN(I,L)*1D3	00000660
	N=NMIN	00000670
	DO 50 L=1,LMAX	00000680
	IF(LINE.GE.52) CALL NPAGE(LINE,LABL,H)	00000690
	PRINT 550,N,(FN(I,L),(U(J,I,L),J=1,4),EN(I+4,L),	00000700
	1 (U(J,I+4,L),J=1,4),I=1,4)	00000710
550	FORMAT(//I3,F16.4,4F10.5,F16.4,4F10.5,	00000720

	1 3 (/3X,F16.4,4F10.5,F16.4,4F10.5)	00000730
	N=N+1	00000740
	LINE=LINE+6	00000750
50	CONTINUE	00000760
	LINE=(LINE/66)*66-LINE+66	00000770
	DO 60 L=1,LINE	00000780
60	PRINT 70	00000790
70	FORMAT()	00000800
	IF(IH.EQ.IMAX) GO TO 10	00000810
	IH=IH+1	00000820
	GO TO 30	00000830
	END	00000840
	SUBROUTINE NPAGE(LINE,LABL,H)	00000850
	INTEGER*2 LABL(100)	00000860
	REAL*8 H	00000870
	LINE=66-LINE	00000880
	DO 10 L=1,LINE	00000890
10	PRINT 20	00000900
20	FORMAT()	00000910
	PRINT 30,LABL	00000920
30	FORMAT(//1X,100A1)	00000930
	PRINT 40,H	00000940
40	FORMAT(///50X,'H=',F8.2,' KILOGAUSS'///' N',8X,'EA(MEV) ',	00000950
	1 7X,'S',8X,'3/2',6X,'-1/2',7X,'S-O',10X,'EB(MEV) ',7X,	00000960
	2 'S',8X,'1/2',6X,'-3/2',7X,'S-O')	00000970
	LINE=10	00000980
	RETURN	00000990
	END	00001000
C		00001010
C		00001020
C		00001030
C		00001040
C		00001050
C		00001060
C		00001070
C		00001080

C
C
C
C
C
C
C
C

FILE GFINTEN.FORT	00000010
OBTAINS AND TRANSMITS PARAMETERS FOR GEDIAG ROUTINE	00000020
PRINTS INTERBAND ENERGIES AND INTENSITIES FOR GE MODEL	00000030
USAGE: LOADGO (GFINTEN,GEDIAG) FORTLIB LIB('SYS5.IMSLIB.LOAD')	00000040
IMPLICIT REAL*8(A-Z)	00000050
INTEGER*2 LABL(100),BLANK/' '/,STOP/'S'/'	00000060
INTEGER LINE,NMAX,IMAX,IMAX,LM1,I,J,L,	00000070
1 I1,LI,LL1	00000080
DIMENSION HI(8),EN(8,18),U(4,8,18),E(8,18,8),ET(2,8)	00000090
DIMENSION AT(2,8),UU(4,8,18,8)	00000100
DATA HI/2D1,4D1,6D1,8D1,1D2,12D1,14D1,16D1/	00000110
DATA IMAX/8/,NMAX/3/,C111/.5773502692D0/	00000120
DATA G1,G2,G3,K,F,O/0D0,0D0,0D0,0D0,0D0,0D0/	00000130
10 C=C111	00000140
DO 20 L=1,100	00000150
20 LABL(L)=BLANK	00000160
PPRINT 500	00000170
500 FORMAT(//'ENTER LABL/EGM,EP,DEL,G1,G2,G3,KAP,F,O',	00000180
1 'COSINE,NMAX,IMAX,H-VALUES'/')	00000190
READ 700,LABL	00000200
700 FORMAT(100A1)	00000210
IF(LABL(1).EQ.STOP) CALL EXIT	00000220
READ *,EGM,EP,DEL,G1,G2,G3,K,F,O	00000230
EG=EGM*1D-3	00000240
READ *,C,NMAX,IMAX,HI	00000250
GPP=(3D0*C*C-1D0)/2D0	00000260
GPP=(G2-G3)*GPP*GPP	00000270
GP=G3+GPP	00000280
GPP=G2/3D0+G3/1.5D0+GPP/6D0	00000290
O5=(1D0-1.5D0*C*C)*.75D0*C*C	00000300
O1=(O5-3D0)*O	00000310
O5=(3D0*O5+1.25D0)*O	00000320
	00000330
	00000340
	00000350
	00000360

	LMAX=NMAX+2	00000370
	PRINT 750, LABEL	00000380
750	FORMAT ('//1X,100A1')	00000390
	DO 30 I=1, IMAX	00000400
	H=HI(I)	00000410
	CALL GEDIAG(H, -1, NMAX, EG, DEL, EP, F, G1, GP, GPP, K, 01, 05, 1, EN, U)	00000420
	DO 30 LL=1, 8	00000430
	DO 30 L=1, LMAX	00000440
	E(LL, L, I) = (FN(LL, L)) * 1D3	00000450
	DO 30 J=1, 4	00000460
30	UU(J, LL, L, I) = U(J, LL, L)	00000470
	PRINT 530, (HI(I), I=1, IMAX)	00000480
530	FORMAT ('/30X, 'TRANSITION ENERGIES (MEV) / INTENSITIES' /16X, 8F10.1	00000490
	1)	00000500
	IINP=15	00000510
	PPRINT 590	00000520
590	FORMAT (' L+:')	00000530
	LINE=LINE+1	00000540
	LM1=LMAX-1	00000550
	DO 50 LL=1, LM1	00000560
	I=LL+1	00000570
	DO 40 I=1, IMAX	00000580
	AT(1, I) = (HWA(3, LL, 1, L, UU, I)) **2	00000590
	AT(2, I) = (HWB(7, LL, 5, L, UU, I)) **2	00000600
	ET(1, I) = E(1, L, I) - E(3, LL, I)	00000610
40	ET(2, I) = E(5, L, I) - E(7, LL, I)	00000620
	L1=LL-1	00000630
	IF (LINE.GE.54) CALL NPAGE(LINE, LABEL, IMAX, HI)	00000640
	PRINT 540, L1, L1, (ET(1, I), I=1, IMAX)	00000650
	PRINT 710, (AT(1, I), I=1, IMAX)	00000660
	PRINT 550, L1, L1, (ET(2, I), I=1, IMAX)	00000670
	PRINT 710, (AT(2, I), I=1, IMAX)	00000680
540	FORMAT (5X, ' A+', I1, ' - AC', I1, 3X, 8F10.4)	00000690
550	FORMAT (5X, ' B+', I1, ' - BC', I1, 3X, 8F10.4)	00000700
710	FORMAT (17X, 8F10.4)	00000710
	LINE=LINE+4	00000720

50	CONTINUE	00000730
	IF (LINE.GE.54) CALL NPAGE (LINE, LABEL, IMAX, HI)	00000740
	PRINT 600	00000750
600	FORMAT (' I -:')	00000760
	LINE=LINE+1	00000770
	DO 70 LL=3, LM1	00000780
	I=LL+1	00000790
	DO 60 I=1, IMAX	00000800
	AT (1, I) = (HWA (2, LL, 1, L, UU, I)) **2	00000810
	AT (2, I) = (HWR (6, LL, 5, I, UU, I)) **2	00000820
	FT (1, I) = F (1, I, I) - F (2, LL, I)	00000830
60	FT (2, I) = F (5, L, I) - F (6, LL, I)	00000840
	L1=LL-1	00000850
	IF (LINE.GE.54) CALL NPAGE (LINE, LABEL, IMAX, HI)	00000860
	PRINT 560, L1, I1, (FT (1, I), I=1, IMAX)	00000870
	PRINT 710, (AT (1, I), I=1, IMAX)	00000880
	PRINT 570, L1, L1, (FT (2, I), I=1, IMAX)	00000890
	PRINT 710, (AT (2, I), I=1, IMAX)	00000900
560	FORMAT (5X, ' A-', I1, ' - AC', I1, 3X, 8F10.4)	00000910
570	FORMAT (5X, ' B-', I1, ' - BC', I1, 3X, 8F10.4)	00000920
	LINE=LINE+4	00000930
70	CONTINUE	00000940
	IF (LINE.GE.54) CALL NPAGE (LINE, LABEL, IMAX, HI)	00000950
	PRINT 610	00000960
610	FORMAT (' R -:')	00000970
	LINE=LINE+1	00000980
	DO 90 LL=3, LMAX	00000990
	I=LL-1	00001000
	DO 80 I=1, IMAX	00001010
	AT (1, I) = (HWA (1, L, 2, LL, UU, I)) **2	00001020
	AT (2, I) = (HWR (5, L, 6, LL, UU, I)) **2	00001030
	FT (1, I) = F (1, I, I) - F (2, LL, I)	00001040
80	FT (2, I) = F (5, L, I) - F (6, LL, I)	00001050
	L1=L-2	00001060
	I1=L	00001070
	IF (LINE.GE.54) CALL NPAGE (LINE, LABEL, IMAX, HI)	00001080

	PRINT 560, LL1, L1, (ET(1, I), I=1, IMAX)	00001090
	PRINT 710, (AT(1, I), I=1, IMAX)	00001100
	PRINT 570, LL1, L1, (ET(2, I), I=1, IMAX)	00001110
	PRINT 710, (AT(2, I), I=1, IMAX)	00001120
	LINE=LINE+4	00001130
90	CONTINUE	00001140
	IF (LINE.GE.54) CALL NPAGE(LINE, LABL, IMAX, HI)	00001150
	PRINT 620	00001160
620	FORMAT(' R+:')	00001170
	LINE=LINE+1	00001180
	DO 110 LL=3, LMAX	00001190
	L=LL-1	00001200
	DO 100 I=1, IMAX	00001210
	AT(1, I) = (HWA(1, L, 3, LL, UU, I)) **2	00001220
	AT(2, I) = (HWP(5, L, 7, LL, UU, I)) **2	00001230
	ET(1, I) = E(1, L, I) - E(3, LL, I)	00001240
100	ET(2, I) = P(5, L, I) - E(7, LL, I)	00001250
	L1=L-2	00001260
	LL1=L	00001270
	IF (LINE.GE.54) CALL NPAGE(LINE, LABL, IMAX, HI)	00001280
	PRINT 540, LL1, L1, (ET(1, I), I=1, IMAX)	00001290
	PRINT 710, (AT(1, I), I=1, IMAX)	00001300
	PRINT 550, LL1, L1, (ET(2, I), I=1, IMAX)	00001310
	PRINT 710, (AT(2, I), I=1, IMAX)	00001320
	LINE=LINE+4	00001330
110	CONTINUE	00001340
	LINE = (LINE/66) *66 - LINE +66	00001350
	DO 120 L=1, LINE	00001360
120	PRINT 580	00001370
580	FORMAT()	00001380
	GO TO 10	00001390
	END	00001400
	SUBROUTINE NPAGE(LINE, LABL, IMAX, HI)	00001410
	REAL*8 HI(IMAX)	00001420
	INTEGER*2 LABL(100)	00001430
	LINE = (LINE/66) *66 - LINE +66	00001440

```

DO 10 I=1,LINE
10 PRINT 20
20 FORMAT (
PRINT 30, LABEL
30 FORMAT (1X, 100A1)
PRINT 40, (HI (I), I=1, IMAX)
40 FORMAT (///30X, 'TRANSITION ENERGIES (MEV) /INTENSITIES' /16X, 8F10.1
1 )
PRINT 20
LINE=7
RETURN
END
FUNCTION HWZ (I, L, J, M, U, IH)
IMPLICIT REAL*8(A-H, O-Z)
DATA RT2/1.414213562D0/, RT3/1.732050808D0/, RT6/2.449489743D0/
DIMENSION U (4, 8, 18, 8)
HWZ = - (U (1, I, L, IH) * (RT2*U (2, J, M, IH) - U (4, J, M, IH)) + U (1, J, M, IH) *
1 (RT2*U (3, I, L, IH) + U (4, I, L, IH))) /RT3
RETURN
ENTRY HWA (I, L, J, M, U, IH)
HWA = (U (1, J, M, IH) * (-U (3, I, L, IH) + RT2*U (4, I, L, IH)) + RT3*U (2, J, M, IH)
1 *U (1, I, L, IH)) /RT6
RETURN
ENTRY HWB (I, L, J, M, U, IH)
HWB = (U (1, I, L, IH) * (U (2, J, M, IH) + RT2*U (4, J, M, IH)) - RT3*U (1, J, M, IH)
1 *U (3, I, L, IH)) /RT6
RETURN
END

```

```

00001450
00001460
00001470
00001480
00001490
00001500
00001510
00001520
00001530
00001540
00001550
00001560
00001570
00001580
00001590
00001600
00001610
00001620
00001630
00001640
00001650
00001660
00001670
00001680
00001690
00001700
00001710
00001720
00001730
00001740
00001750
00001760
00001770
00001780
00001790
00001800

```

00000000

```

C SUBROUTINES HCINIT(EG,DEL,EP,F,G1,GP,GPP,KAP,01,05,N1,EPS) 00000010
C HCTTR(H,IP,IT,ET) 00000020
C 00000030
C DIAGONALIZES 8*8 GERMANIUM K.P MATRIX USING SUBROUTINES DMHS AND 00000040
C DMESP IN SIMATH, FINDS INTERBAND TRANSITION ENERGY 00000050
C 00000060
C PARAMETERS: H(KILOGAUSS) MAGNETIC FIELD 00000070
C IP (INTEGER) 1 FOR LCP, 2 FOR RCP 00000080
C IT (INTEGER) TRANSITION NUMBER 00000090
C EG,DEL(EV) ENERGY GAP AND S-O SPLITTING 00000100
C F,G1,GP,GPP,KAPM,01,05,N1 CONDUCTION AND VALENCE 00000110
C BAND HIGHER-BAND PARAMETERS 00000120
C EPS ACCURACY OF EIGENVALUES 00000130
C 00000140
C RETURNS: ET TRANSITION ENERGY (EV) 00000150
C 00000160
C 00000170
C SUBROUTINE HCINIT(EG,DEL,EP,F,G1,GP,GPP,K,01,05,N1,EPS) 00000180
C IMPLICIT REAL*8 (A-Z) 00000190
C INTEGER L,I,IER,IP,IT,LC,LCP(20,2),LH,LHP(20,2),IC,ICP(20,2),IH, 00000200
C IHP(20,2),L1,L2,IL,IEP 00000210
C DIMENSION E(2),A(10),B(10),D(4),CD(4),R(1),AUX(8) 00000220
C DATA RT2/1.414213562D0/ 00000230
C DATA ICP/1,5,1,5,5,9,9,9,5,9,9,9,5,9,9,9,5,9,9,9, 00000240
C 1 1,5,1,1,5,1,5,9,1,9,9,9,1,9,9,9,1,9,9,9/ 00000250
C DATA IHP/3,7,2,6,7,2,2,2,7,2,2,2,7,2,2,2,7,2,2,2, 00000260
C 1 2,6,2,3,6,2,6,2,3,2,2,2,3,2,2,2,3,2,2,2/ 00000270
C DATA LCP/2,2,4,4,3,5,6,7,4,8,9,10,5,11,12,13,6,14,15,16, 00000280
C 1 2,2,3,2,3,4,4,5,3,6,7,8,4,9,10,11,5,12,13,14/ 00000290
C DATA LHP/1,1,3,3,2,4,5,6,3,7,8,9,4,10,11,12,5,13,14,15, 00000300
C 1 3,3,4,3,4,5,5,6,4,7,8,9,5,10,11,12,6,13,14,15/ 00000310
C EMIN=-DEL 00000320
C RETURN 00000330
C ENTRY HCTTR(H,IP,IT,ET) 00000340
C S=1.15767578D-5*H 00000350
C S2=S/2D0 00000360

```

	IC=ICP(IT,IP)	00000370
	IH=IHP(IT,IP)	00000380
	LC=LCP(IT,IP)	00000390
	LH=LHP(IT,IP)	00000400
	IF(LH.GT.LC) GO TO 10	00000410
	L1=LH	00000420
	L2=LC	00000430
	GO TO 20	00000440
10	L2=IH	00000450
	I1=LC	00000460
20	IF(IC.EQ.5) GO TO 110	00000470
	IL=1	00000480
	DO 100 L=L1,L2	00000490
	N=L-2	00000500
	IF(N.GE.000) GO TO 30	00000510
C	A-SET N=-1	00000520
	A(1)=(K-G1+GP)*S2+05*S	00000530
	A(2)=(GP-K-1D0)*S/RT2	00000540
	A(3)=K*S+(1D0-G1)*S2-DEL	00000550
	CALL DMHS(A,2,D,CD,IER)	00000560
	CALL DMESP(D,CD,2,2,2,EPS,R,AUX,IER)	00000570
	F(IL)=-R(1)	00000580
	GO TO 100	00000590
30	IF(N.GT.000) GO TO 50	00000600
C	A-SET N=0	00000610
	A(1)=(1D0+F+N1)*S+EG	00000620
	A(2)=-DSORT(EP*S/6D0)	00000630
	A(3)=(K-3D0*(G1-GP))*S2+05*S	00000640
	A(4)=-A(2)*RT2	00000650
	A(5)=(GP*3D0-K-1D0)*S/RT2	00000660
	A(6)=K*S+(1D0-3D0*G1)*S2-DEL	00000670
	CALL DMHS(A,3,D,CD,IER)	00000680
	IF(L.EQ.LC) GO TO 40	00000690
	CALL DMESP(D,CD,3,2,2,EPS,R,AUX,IER)	00000700
	F(IL)=-R(1)	00000710
	GO TO 100	00000720

40	CALL DMESP(D,CD,3,3,3,EPS,R,AUX,IER)	00000730
	F(IL)=R(1)	00000740
	GO TO 100	00000750
C A-SET	N>0	00000760
50	NP1=N+1D0	00000770
	N3=N+1.5D0	00000780
	A(1)=(F*(2D0*N+1D0)+N1+NP1)*S+FG	00000790
	A(2)=DSORT(N*S2*EP)	00000800
	A(3)=- (1.5D0*K+(G1+GP)*(N-.5D0)-Q1)*S	00000810
	A(4)=-DSORT(NP1*S*EP/6D0)	00000820
	A(5)=DSORT(3D0*N*NP1)*GPP*S	00000830
	A(6)=(.5D0*K-(G1-GP)*N3+Q5)*S	00000840
	A(7)=-A(4)*RT2	00000850
	A(8)=-A(5)*RT2	00000860
	A(9)=(GP*N3*S-(K+1D0)*S2)*RT2	00000870
	A(10)=(K+.5D0-G1*N3)*S-DEL	00000880
	CALL DMHS(A,4,D,CD,IER)	00000890
	IF(L.EO.LC) GO TO 80	00000900
	IF(IH.EO.3) GO TO 70	00000910
	CALL DMESP(D,CD,4,3,3,EPS,R,AUX,IER)	00000920
	F(IL)=-R(1)	00000930
	GO TO 100	00000940
70	CALL DMESP(D,CD,4,2,2,EPS,R,AUX,IER)	00000950
	F(IL)=-R(1)	00000960
	GO TO 100	00000970
80	CALL DMESP(D,CD,4,4,4,EPS,R,AUX,IER)	00000980
	F(IL)=R(1)	00000990
100	IL=IL+1	00001000
110	IF(IC.EO.1) GO TO 200	00001010
	IL=1	00001020
	DO 190 L=L1,L2	00001030
	N=L-2	00001040
	IF(N.GE.0D0) GO TO 120	00001050
C B-SET	N=-1	00001060
	F(IL)=- (3D0*K-G1-GP)*S2+Q1*S	00001070
	GO TO 190	00001080

120	IF(N.GT.0D0) GO TO 140	00001090
C	B-SET N=0	00001100
	B(1)=(F-N1)*S+EG	00001110
	B(2)=-DSORT(EP*S2)	00001120
	B(3)=(K-G1-GP)*3D0*S2-01*S	00001130
	CALL DMHS(B,2,D,CD,IER)	00001140
	IF(L.EO.LC) GO TO 130	00001150
	CALL DMESP(D,CD,2,1,1,EPS,R,AUX,IER)	00001160
	E(IL)=-R(1)	00001170
	GO TO 190	00001180
130	CALL DMESP(D,CD,2,2,2,EPS,R,AUX,IER)	00001190
	F(IL)=R(1)	00001200
	GO TO 190	00001210
C	B-SET N>0	00001220
140	NP1=N+1D0	00001230
	N3=.5D0-N	00001240
	B(1)=(F*(2D0*N+1D0)-N1+N)*S+EG	00001250
	B(2)=DSORT(N*S*EP/6D0)	00001260
	B(3)=((G1-GP)*N3-05)*S-K*S2	00001270
	B(4)=-DSORT(NP1*S*EP/2D0)	00001280
	B(5)=DSORT(3D0*N*NP1)*GPP*S	00001290
	B(6)=(1.5D0*K-(G1+GP)*(N+1.5D0)-01)*S	00001300
	B(7)=B(2)*RT2	00001310
	B(8)=(N3*GP*S-(K+1D0)*S2)*RT2	00001320
	B(9)=B(5)*RT2	00001330
	B(10)=(N3*G1-K-.5D0)*S-DEL	00001340
	CALL DMHS(B,4,D,CD,IER)	00001350
	IF(L.EO.LC) GO TO 170	00001360
	IF(IH.EO.7) GO TO 160	00001370
	CALL DMESP(D,CD,4,3,3,EPS,R,AUX,IER)	00001380
	IF(IC.NE.9) GO TO 165	00001390
	E(IL)=(E(IL)-R(1))/2D0	00001400
	GO TO 190	00001410
160	CALL DMESP(D,CD,4,2,2,EPS,R,AUX,IER)	00001420
165	E(IL)=-R(1)	00001430
	GO TO 190	00001440

C	FILE HCTPLT.FORT	00000010
C		00000020
C	OBTAINS AND TRANSMITS PARAMETERS FOR HCTTR ROUTINE	00000030
C		00000040
C	PRINTS AND PLOTS INTERBAND TRANSITION ENERGIES FOR HG(1-X)CD(X)TE	00000050
C		00000060
C	USAGE: LOADGO (HCTPLT,HCTTR,HCTEV) FORTLIB LIB('SYS5.IMSLIB.LOAD',	00000070
C	'U.M4006.P4540.TSP.LOAD')	00000080
C	IMPLICIT REAL*8(A-Z)	00000090
	INTEGER LINE,TMAX,IT,I,L,IPLT,NML	00000100
	INTEGER*2 LABL(100),BLANK/' '/,STOP/'S'/	00000110
	DIMENSION HI(75),ET(20,75)	00000120
	DATA TMAX/18/,C111/.5773502692D0/,FO,F1,H0,H1/5D1,27D1,0D0,15D1/	00000130
	DATA G1,G2,G3,K,F,0/2.5,-.3,.5,-1.2,-.7,0D0/	00000140
	DATA DEL/1D0/,EPS/1D-5/,N1/0D0/	00000150
	DO 5 I=1,75	00000160
5	HI(I)=I*2D0	00000170
10	C=C111	00000180
	DO 15 L=1,100	00000190
15	LABL(L)=BLANK	00000200
	PRINT 500	00000210
500	FORMAT(//' ENTER LABL/EGM,EP,DEL,G1,G2,G3,KAP,F,O,N1/')	00000220
	1 'COSINE,TMAX,FO,F1,H0,H1,EPS/'/)	00000230
	READ 600,LABL	00000240
600	FORMAT(100A1)	00000250
	IF(LABL(1).EQ.STOP) CALL EXIT	00000260
	READ *,EGM,EP,DEL,G1,G2,G3,K,F,O,N1	00000270
	EG=EGM*1D-3	00000280
	READ *,C,TMAX,FO,E1,H0,H1,EPS	00000290
	GPP=(3D0*C*C-1D0)/2D0	00000300
	GPP=(G2-G3)*GPP*GPP	00000310
	GP=G3+GPP	00000320
	GPP=G2/3D0+G3/1.5D0+GPP/6D0	00000330
	O5=(1D0-1.5D0*C*C)*.75D0*C*C	00000340
	O1=(O5-3D0)*O	00000350
	O5=(3D0*O5+1.25D0)*O	00000360

	CALL HCINIT (EG,DFL,FP,F,G1,GP,GPP,K,01,05,N1,EPS)	00000370
	PRINT 510,LAB1	00000380
610	FORMAT (//1X,100A1)	00000390
	PRINT 530, (HI (I), I=20,70,10)	00000400
530	FORMAT (/20Y, 'TRANSITION ENERGIES (MEV) '/3X,6F10.1	00000410
	1, ' KILOGAUSS')	00000420
	LINE=15	00000430
	PRINT 590	00000440
590	FORMAT (' L:')	00000450
	LINE=LINE+1	00000460
	DO 30 IT=1, TMAX	00000470
	DO 20 I=1, 75	00000480
	CALL HCTTP (HI (I), 1, IT, E)	00000490
20	FT (IT, I)=F*1D3	00000500
	IF (LINE.GE.57) CALL NPAGE (LINE, LAB1, HI)	00000510
	PRINT 540, IT, (FT (IT, I), I=20,70,10)	00000520
	LINE=LINE+1	00000530
540	FORMAT (3X, I2, 6F10.4)	00000540
30	CONTINUE	00000550
	CALL ETPL0T (ET, E0, E1, H0, H1)	00000560
	IF (LINE.GE.52) CALL NPAGE (LINE, LAB1, HI)	00000570
	PRINT 550	00000580
550	FORMAT (' R:')	00000590
	LINE=LINE+4	00000600
	DO 50 IT=1, TMAX	00000610
	DO 40 I=1, 75	00000620
	CALL HCTTP (HI (I), 2, IT, E)	00000630
40	FT (IT, I)=F*1D3	00000640
	IF (LINE.GE.57) CALL NPAGE (LINE, LAB1, HI)	00000650
	PRINT 540, IT, (FT (IT, I), I=20,70,10)	00000660
	LINE=LINE+1	00000670
50	CONTINUE	00000680
	CALL ETPL0T (ET, E0, E1, H0, H1)	00000690
	LINE=LINE+3	00000700
	LINE=66-LINE	00000710
	DO 210 L=1, LINE	00000720

210	PRINT 580	00000730
580	FORMAT()	00000740
	GO TO 10	00000750
	END	00000760
	SUBROUTINE NPAGE(LINE, LABL, HI)	00000770
	INTEGER*2 LABL(100)	00000780
	REAL*8 HI(75)	00000790
	LINE=66-LINE	00000800
	DO 910 L=1, LINE	00000810
910	PRINT 580	00000820
580	FORMAT()	00000830
	PRINT 920, LABL	00000840
920	FORMAT(1X, 100A1)	00000850
	PRINT 530, (HI(I), I=20, 70, 10)	00000860
530	FORMAT(/20X, 'TRANSITION ENERGIES(MEV)'/3X, 6F10.1	00000870
	1, ' KILOGAUSS')	00000880
	PRINT 580	00000890
	LINE=5	00000900
	RETURN	00000910
	END	00000920
	SUBROUTINE RTPLOT(ET, E0, E1, H0, H1)	00000930
	REAL*8 ET, E0, E1, H0, H1	00000940
	DIMENSION ET(20, 75), HI(75), EP(75)	00000950
	DO 5 I=1, 75	00000960
5	HI(I)=I*2.	00000970
	E0S=E0	00000980
	E1S=E1	00000990
	H0S=H0	00001000
	H1S=H1	00001010
	NMAX=0	00001020
	PEAD *, NMAX	00001030
	IF(NMAX.GT.0) GO TO 20	00001040
	PRINT 10	00001050
10	FORMAT()	00001060
	RETURN	00001070
20	CALL SPEED(30)	00001080

	DO 50 I=1,75	00001090
50	EP(I)=EOS	00001100
	CALL TSPLP(75,HI,FP,0.,10.,0.,10.,H0S,H1S,E0S,E1S)	00001110
	DO 40 N=1,NMAX	00001120
	DO 30 I=1,75	00001130
	IF(ET(N,I).LE.E1) GO TO 30	00001140
	I=I-1	00001150
	GO TO 40	00001160
30	EP(I)=ET(N,I)	00001170
40	CALL TSPLP(I,HI,FP,0.,10.,0.,10.,H0S,H1S,E0S,E1S)	00001180
	CALL TTY	00001190
	END	00001200
C		00001210
C		00001220
C		00001230
C		00001240
C		00001250
C		00001260
C		00001270
C		00001280
C		00001290
C		00001300
C		00001310
C		00001320
C		00001330
C		00001340
C		00001350
C		00001360
C		00001370
C		00001380
C		00001390
C		00001400
C		00001410
C		00001420
C		00001430
C		00001440

C FILE: DATACR.POPM

C

	DIMENSION ITS(2,14,20)	00000010
	DATA HT/560*0./	00000020
	PRINT 600	00000030
600	FORMAT(// ' ENTER IPOL,IT,H,E,IT1/')	00000040
10	CONTINUE	00000050
	READ *,IP,IT,H,E,IT1	00000060
	IF(IT.LE.0) GO TO 10	00000070
	IF(IT.GT.20) GO TO 10	00000080
	IF(IP.LE.0) GO TO 40	00000090
	IF(IP.GT.2) GO TO 10	00000100
	WRITE (2,500) IP,IT,IT1,H,E	00000110
	DO 20 ID=1,14	00000120
	IF(HT(IP,ID,IT).EQ.0.) GO TO 30	00000130
20	CONTINUE	00000140
	GO TO 10	00000150
30	HT(IP,ID,IT)=H	00000160
	ET(IP,ID,IT)=E	00000170
	ITS(IP,ID,IT)=IT1	00000180
	GO TO 10	00000190
40	DO 60 IP=1,2	00000200
	DO 60 IT=1,20	00000210
	DO 50 ID=1,14	00000220
	IF(HT(IP,ID,IT).EQ.0.) GO TO 60	00000230
50	WRITE(1,500) IP,IT,ITS(IP,ID,IT),HT(IP,ID,IT),ET(IP,ID,IT)	00000240
60	CONTINUE	00000250
	IP=0	00000260
	WRITE(1,500) IP	00000270
	WRITE (2,500) IP	00000280
	PRINT 610	00000290
610	FORMAT(/ ' REMEMBER TO DELETE BACKUP DATASET')	00000300
	CALL EXIT	00000310
500	FORMAT (I1,I2,I2,2F5.1)	00000320
	END	00000330
C		00000340
		00000350
		00000360

C	TO USE DATACR, TYPE EX DATACR 'FILE' WHICH EXECUTES	00000370
C	THE FOLLOWING CLIST TO CREATE A DATASET FILE.DATA	00000380
C	DATACR.CLIST	00000390
C	PROC 1 NAME	00000400
C	FREEQ ATTR(FB15) FI(FT01F001) DA(&NAME..DATA)	00000410
C	FREEQ DA(BACKUP.DATA)	00000420
C	DELETE &NAME..DATA	00000430
C	DELETE BACKUP.DATA	00000440
C	ATTRIB FB15 REC(F,F) LRE(15) BLK(2040)	00000450
C	ALLOC FI(FT01F001) DA(&NAME..DATA) US(FB15) BLO(2040) SP(6,6)	00000460
C	ALLOC FI(FT02F001) DA(BACKUP.DATA) US(FB15) BLO(2040) SE(6,6)	00000470
C	LOAD DATACR FORTLIB	00000480
C	FREE FI(FT01F001)	00000490
C	FREE FI(FT02F001)	00000500

	RETURN	00000370
	PNTRY HCTEDR(H,IP,IT,ET,DE)	00000380
	S=1.15767578D-5*H	00000390
	S2=S/2D0	00000400
	DO 5 I=1,10	00000410
5	DE(I)=D00	00000420
	TC=ICP(IT,IP)	00000430
	TH=IHP(IT,IP)	00000440
	LC=LCP(IT,IP)	00000450
	LH=LHP(IT,IP)	00000460
	IF(LH.GT.LC) GO TO 10	00000470
	I1=LH	00000480
	I2=LC	00000490
	GO TO 20	00000500
10	L2=LH	00000510
	I1=LC	00000520
20	IF(IC.EQ.5) GO TO 110	00000530
	II=1	00000540
	DO 100 L=L1,L2	00000550
	N=L-2	00000560
	IF(N.GE.0D0) GO TO 30	00000570
C	A-SET N=-1	00000580
	A(1)=(K-G1+GP)*S2+05*S	00000590
	A(2)=(GP-K-1D0)*S/RT2	00000600
	A(3)=K*S+(1D0-G1)*S2-DEL	00000610
	DO 25 I=1,3	00000620
25	B(I)=A(I)	00000630
	CALL DMHS(B,2,D,CD,IER)	00000640
	CALL DMESP(D,CD,2,2,2,EPS,R,AUX,IER)	00000650
	F(IL)=-R(1)	00000660
	F3=F(1)-A(1)	00000670
	F4=F(1)-A(3)	00000680
	RHO=E3+E4	00000690
	IF(DABS(RHO).LT.1D-15) PHO=1D-15	00000700
	DE(10)=DE(10)+E3/RHO	00000710
	DE(3)=DE(3)+S2	00000720

	P1=(RT2*S*A(2)+S2*P4)/RHO	00000730
	DE(4)=DE(4)-P1	00000740
	DE(6)=DE(6)+P1-S	00000750
	DE(8)=DE(8)-005*S*P4/RHO	00000760
	GO TO 100	00000770
30	IF(N.GT.0D0) GO TO 50	00000780
C A-SET	N=0	00000790
	A(1)=(1D0+F+N1)*S+FC	00000800
	A(2)=-DSQRT(EP*S/6D0)	00000810
	A(3)=(K-2D0*(G1-GP))*S2+05*S	00000820
	A(4)=-A(2)*RT2	00000830
	A(5)=(GP*3D0-K-1D0)*S/RT2	00000840
	A(6)=K*S+(1D0-3D0*G1)*S2-DEL	00000850
	DO 35 I=1,6	00000860
35	B(I)=A(I)	00000870
	CALL DMHS(B,3,D,CD,IER)	00000880
	IF(I.EO.IC) GO TO 40	00000890
	CALL DMESP(D,CD,3,2,2,EPS,P,AUX,IER)	00000900
	FC=P(1)	00000910
	F(IL)=-FC	00000920
	SGN=-1D0	00000930
	GO TO 45	00000940
40	CALL DMESP(D,CD,3,3,3,EPS,P,AUX,IER)	00000950
	FC=P(1)	00000960
	F(IL)=FC	00000970
	SGN=1D0	00000980
45	E1=FC-A(1)	00000990
	E3=FC-A(3)	00001000
	E4=FC-A(6)	00001010
	F1=E3*E4-A(5)*A(5)	00001020
	F2=E1*E3-A(2)*A(2)	00001030
	F3=E1*E4-A(4)*A(4)	00001040
	RHO=(F1+F2+F3)*SGN	00001050
	IF(DABS(RHO).LT.1D-15) RHO=1D-15	00001060
	F1=F1/RHO	00001070
	DE(1)=DE(1)+F1	00001080

	F2=F2/RHO	00001090
	DE(10)=DE(10)-F2	00001100
	DE(2)=DE(2)+(A(2)*(F4*A(2)+2D0*A(4)*A(5))+A(4)*A(4)*E3)/EP/RHO	00001110
	DE(7)=DE(7)+S*F1	00001120
	DE(9)=DE(9)+S*F1	00001130
	F3=F3*S2*3D0/RHO	00001140
	F2=F2*S	00001150
	DE(3)=DE(3)-F3-1.5D0*F2	00001160
	F1=(A(5)*E1+A(2)*A(4))*S*RT2/RHO	00001170
	DE(4)=DE(4)+F3+F1*3D0	00001180
	DE(6)=DE(6)+F3/3D0-F1+F2	00001190
	DE(8)=DE(8)+F3*C05/1.5D0	00001200
	GO TO 100	00001210
C	A-SET N>0	00001220
50	NP1=N+1D0	00001230
	N3=N+1.5D0	00001240
	A(1)=(F*(2D0*N+1D0)+N1+NP1)*S+EG	00001250
	A(2)=DSORT(N*S2*EP)	00001260
	A(3)=- (1.5D0*K+(G1+GP)*(N-.5D0)-O1)*S	00001270
	A(4)=-DSORT(NP1*S*EP/6D0)	00001280
	A(5)=DSORT(3D0*N*NP1)*GPP*S	00001290
	A(6)=(.5D0*K-(G1-GP)*N3+O5)*S	00001300
	A(7)=-A(4)*RT2	00001310
	A(8)=-A(5)*PT2	00001320
	A(9)=(GP*N3*S-(K+1D0)*S2)*PT2	00001330
	A(10)=(K+.5D0-G1*N3)*S-DEL	00001340
	DO 55 I=1,10	00001350
55	B(I)=A(I)	00001360
	CALL DMHS(B,4,D,CD,IER)	00001370
	SA=1D0	00001380
	IF(L.EQ.LC) GO TO 80	00001390
	IF(IH.EQ.3) GO TO 70	00001400
	CALL DMFSP(D,CD,4,3,3,EPS,R,AUX,IER)	00001410
	EC=R(1)	00001420
	E(IL)=-EC	00001430
	SGN=-1D0	00001440

	IF (IC.EQ.9) SGN=-2D0	00001450
	GO TO 85	00001460
70	CALL DMESP (D,CD,4,2,2,EPS,R,AUX,IER)	00001470
	FC=R(1)	00001480
	F(IL)=-EC	00001490
	SGN=-1D0	00001500
	GO TO 85	00001510
80	CALL DMESP (D,CD,4,4,4,EPS,R,AUX,IER)	00001520
	FC=R(1)	00001530
	F(IL)=EC	00001540
	SGN=1D0	00001550
	IF (IC.EQ.9) SGN=2D0	00001560
85	CALL DECAL (EC,SGN,SA,A,N,S,EP,DE)	00001570
100	IL=IL+1	00001580
110	IF (IC.EQ.1) GO TO 200	00001590
	IL=1	00001600
	DO 190 L=L1,L2	00001610
	N=L-2	00001620
	IF (N.GE.0D0) GO TO 120	00001630
C R-SET	N=-1	00001640
	F(IL)=- (3D0*K-G1-GP) *S2+S*Q1	00001650
	DE(3)=DE(3)+S2	00001660
	DE(4)=DE(4)+S2	00001670
	DE(6)=DE(6)-3D0*S2	00001680
	DE(8)=DE(8)+S*CO1	00001690
	GO TO 190	00001700
120	IF (N.GT.0D0) GO TO 140	00001710
C R-SET	N=0	00001720
	R(1)=(P-N1)*S+EG	00001730
	R(2)=-DSORT (EP*S2)	00001740
	R(3)=(K-G1-GP) *3D0*S2-S*Q1	00001750
	DO 125 I=1,3	00001760
125	A(I)=B(I)	00001770
	CALL DMHS (A,2,D,CD,IER)	00001780
	IF (L.EQ.LC) GO TO 130	00001790
	CALL DMESP (D,CD,2,1,1,EPS,R,AUX,IER)	00001800

	FC=P(1)	00001810
	F(IL)=-FC	00001820
	SGN=-1D0	00001830
	GO TO 135	00001840
130	CALL DMESP(D,CD,2,2,2,EPS,R,AUX,IER)	00001850
	FC=P(1)	00001860
	F(IL)=FC	00001870
	SGN=1D0	00001880
135	F1=FC-R(1)	00001890
	F3=FC-R(3)	00001900
	RHO=(F1+F3)*SGN	00001910
	IF(DABS(RHO).LT.1D-15) RHO=1D-15	00001920
	F1=F3/RHO	00001930
	DE(1)=DE(1)+F1	00001940
	DE(7)=DE(7)+F1*S	00001950
	DE(9)=DE(9)-F1*S	00001960
	DE(2)=DE(2)+R(2)*R(2)/FP/RHO	00001970
	F1=F1*S2*3D0/RHO	00001980
	DE(3)=DE(3)-F1	00001990
	DE(4)=DE(4)-F1	00002000
	DE(6)=DE(6)+F1	00002010
	DE(8)=DE(8)-C01*F1/1.5D0	00002020
	GO TO 190	00002030
	C R-SET N>0	00002040
140	NP1=N+1D0	00002050
	N3=.5D0-N	00002060
	R(1)=(F*(2D0*N+1D0)-N1+N)*S+EG	00002070
	R(2)=DSORT(N*S*EP/6D0)	00002080
	R(3)=((G1-GP)*N3-Q5)*S-K*S2	00002090
	R(4)=-DSORT(NP1*S*EP/2D0)	00002100
	R(5)=DSORT(3D0*N*NP1)*GPP*S	00002110
	R(6)=(1.5D0*K-(G1+GP)*(N+1.5D0)-Q1)*S	00002120
	R(7)=R(2)*RT2	00002130
	R(8)=(N3*GP*S-(K+1D0)*S2)*RT2	00002140
	R(9)=R(5)*RT2	00002150
	R(10)=(N3*G1-K-.5D0)*S-DEL	00002160

	DO 145 I=1,10	00002170
145	A(I)=R(I)	00002180
	CALL DMHS(A,4,D,CD,IER)	00002190
	SA=-1D0	00002200
	IF(L.FO.LC) GO TO 170	00002210
	IF(IH.EO.7) GO TO 160	00002220
	CALL DMESP(D,CD,4,3,3,EPS,R,AUX,IER)	00002230
	FC=R(1)	00002240
	IF(IC.NE.9) GO TO 165	00002250
	F(IL)=(F(IL)-FC)/2D0	00002260
	SGN=-2D0	00002270
	GO TO 188	00002280
160	CALL DMESP(D,CD,4,2,2,EPS,P,AUX,IER)	00002290
	FC=F(1)	00002300
165	F(IL)=-FC	00002310
	SGN=-1D0	00002320
	GO TO 188	00002330
170	CALL DMESP(D,CD,4,4,4,EPS,R,AUX,IER)	00002340
	FC=R(1)	00002350
	IF(IC.NE.9) GO TO 185	00002360
	F(IL)=(F(IL)+FC)/2D0	00002370
	SGN=2D0	00002380
	GO TO 188	00002390
185	F(IL)=FC	00002400
	SGN=1D0	00002410
188	CALL DECAL(FC,SGN,SA,B,N,S,EP,DE)	00002420
190	II=IL+1	00002430
200	ET=F(1)+F(2)	00002440
	F1=DE(4)	00002450
	DE(4)=CGP2*E1+CGPP2*DE(5)	00002460
	DE(5)=CGP3*F1+CGPP3*DE(5)	00002470
	RETURN	00002480
	END	00002490
	SUBROUTINE DECAL(FC,SGN,SA,A,N,S,EP,DE)	00002500
	IMPLICIT REAL*8(A-Z)	00002510
	COMMON C01,C05	00002520

DIMENSION A(10),DE(10)	00002530
DATA RT2/1.414213562D0/	00002540
E1=EC-A(1)	00002550
E2=EC-A(3)	00002560
E3=EC-A(6)	00002570
E4=EC-A(10)	00002580
F1=E1*E2-A(2)*A(2)	00002590
F2=E3*E4-A(9)*A(9)	00002600
RHO=(F1*(E3+E4)+F2*(E1+E2)-A(4)*A(4)*(E2+E4)-A(8)*A(8)*(E1+E3)	00002610
1 -A(5)*(A(5)*(E1+E4)+2D0*(A(2)*A(4)+A(8)*A(9)))	00002620
2 -A(7)*(A(7)*(E2+E3)+2D0*(A(2)*A(8)+A(4)*A(9))))*SGN	00002630
IP(DABS(RHO).LT.1D-15) RHO=1D-15	00002640
F3=(F2*E2-A(5)*(A(5)*E4+2D0*A(8)*A(9))-A(8)*A(8)*E3)/RHO	00002650
DE(1)=DE(1)+F3	00002660
DE(7)=DE(7)+(2D0*N+1D0)*S*F3	00002670
DE(9)=DE(9)+SA*S*F3	00002680
F3=(F1*E3-A(4)*(A(4)*E2+2D0*A(2)*A(5))-A(5)*A(5)*E1)/RHO	00002690
DE(10)=DE(10)-F3	00002700
NAS=(N+SA+.5D0)*S	00002710
DE(3)=DE(3)-F3*NAS	00002720
DE(6)=DE(6)+F3*SA*S	00002730
F3=E2*E3-A(5)*A(5)	00002740
F4=E2*E4-A(8)*A(8)	00002750
DE(2)=DE(2)+(A(2)*(A(2)*F2+2D0*A(4)*(A(5)*E4+A(8)*A(9)))	00002760
1 +A(4)*A(4)*F4+A(7)*(A(7)*F3+2D0*(A(4)*A(9)*E2+A(2)*A(8)*E3	00002770
2 +A(5)*(A(2)*A(9)+A(4)*A(8))))/EP/RHO	00002780
F5=(F2*E1-A(4)*(A(4)*E4+2D0*A(7)*A(9))-A(7)*A(7)*E3)*S/RHO	00002790
F6=(F1*E4-A(8)*(A(8)*E1+2D0*A(2)*A(7))-A(7)*A(7)*E2)*S/RHO	00002800
DE(6)=DE(6)-((2D0+SA)*F5-(2D0-SA)*F6)*.5D0	00002810
IF(SA.GT.0D0) DE(8)=DE(8)+CQ1*F5+CQ5*F6	00002820
IF(SA.LT.0D0) DE(8)=DE(8)-CQ5*F5-CQ1*F6	00002830
F5=F5*(N-.5D0)	00002840
F6=F6*(N+1.5D0)	00002850
DE(3)=DE(3)-F5-F6	00002860
DE(4)=DE(4)-(F5-F6)*SA	00002870
F5=((E1*E3-A(4)*A(4))*A(8)+(E1*A(5)+A(2)*A(4))*A(9)	00002880

	1 + (E3*A(2) + A(4)*A(5)) * A(7) * RT2 / RHO	00002890
	P6 = (P1*A(9) + (E1*A(5) + A(2)*A(4)) * A(8)	00002900
	1 + (E2*A(4) + A(2)*A(5)) * A(7) * RT2 / RHO	00002910
	P4 = (P1*E4 - A(7)*A(7)) * A(5) + (P1*A(8) + A(2)*A(7)) * A(9)	00002920
	1 + (P4*A(2) + A(7)*A(8)) * A(4) / RHO	00002930
	IF(SA.LT.0D0) GO TO 10	00002940
	P1 = P6	00002950
	P2 = P4 - P5	00002960
	P3 = P6	00002970
	GO TO 20	00002980
10	P1 = -P5	00002990
	P2 = P4 + P5	00003000
	P3 = P5	00003010
20	DE(4) = DE(4) + NAS*2D0*P1	00003020
	DE(5) = DE(5) + DSQRT((N+1D0)*N*12D0)*S*P2	00003030
	DE(6) = DE(6) - S*P3	00003040
	RETURN	00003050
	END	00003060
		00003070
		00003080
		00003090
		00003100
		00003110
		00003120
		00003130
		00003140
		00003150
		00003160
		00003170
		00003180
		00003190
		00003200
		00003210
		00003220
		00003230
		00003240

C	FILE: HCTMIN.FOR	00000010
C		00000020
C	MINIMIZES MEAN SQUARE DEVIATION WITH RESPECT TO: 1-EG, 2-EP,	00000030
C	3-G1, 4-G2, 5-G3, 6-KAP, 7-F, 8-O, 9-N1, 10-DELTA	00000040
C		00000050
	IMPLICIT REAL*8(A-Z)	00000060
	INTEGER LINE, IP, IT, IPOL(280), ITRN(280), I, IDAT,	00000070
1	J, L, IPR(8), IS, IEP, NP, IT1(280)	00000080
	INTEGER*2 LABL(100), STOP/'S'//, BL/' '/	00000090
	DIMENSION HTRN(280), FTRN(280)	00000100
	DIMENSION X(10), A(10,10), B(10), DE(10), DE2(10)	00000110
	COMMON C01, C05, CGP2, CGP3, CGPP2, CGPP3	00000120
	DATA C111/.5773502692D0/	00000130
	DATA X/10*0D0/	00000140
	DATA EPS/1D-6/, NP/10/	00000150
	IDAT=0	00000160
10	READ (1,600) IP, IT, J, H, E	00000170
600	FORMAT (I1, I2, I2, 2F5.1)	00000180
	IF (IP.EQ.0) GO TO 20	00000190
	IDAT=IDAT+1	00000200
	IPOL (IDAT)=IP	00000210
	ITRN (IDAT)=IT	00000220
	IT1 (IDAT)=J	00000230
	FTRN (IDAT)=E*1D-3	00000240
	HTRN (IDAT)=H	00000250
	IF (IDAT.EQ.280) GO TO 20	00000260
	GO TO 10	00000270
20	C=C111	00000280
	DO 30 I=1,100	00000290
30	LABL (I)=BL	00000300
	PRINT 500, IDAT	00000310
500	FORMAT (/1X, I3, ' DATA POINTS, ENTER LABL/COSINE, EPS, NP/')	00000320
	READ 610, LABL	00000330
610	FORMAT (100A1)	00000340
	IF (LABL (1).EQ.STOP) STOP	00000350
	READ *, C, EPS, NP	00000360

	FC = ((3D0*C*C-1D0)/2D0)**2	00000370
	CGP2=FC	00000380
	CGP3=1D0-FC	00000390
	CGPP2=(2D0+FC)/6D0	00000400
	CGPP3=(4D0-FC)/6D0	00000410
	O5=(1D0-1.5D0*C*C)*.75D0*C*C	00000420
	C01=(O5-3D0)	00000430
	C05=(3D0*O5+1.25D0)	00000440
	PPRINT 510,IAB1	00000450
510	FORMAT(//1Y,100A1)	00000460
	LINE=8	00000470
40	PRINT 520	00000480
520	FORMAT('/' ENTER EGM,EP,DEL,G1,G2,G3,KAP,P,O,N1')	00000490
	PFAD *,EGM,X(2),Y(10),(X(I),I=3,9)	00000500
	X(1)=EGM*1D-3	00000510
	LINE=LINE+4	00000520
	IF(EGM.EO.OO0) GO TO 90	00000530
	GP=CGP2*Y(4)+CGP3*Y(5)	00000540
	GPP=CGPP2*Y(4)+CGPP3*Y(5)	00000550
	PPRINT 530,EGM,X(2),Y(10),(X(I),I=3,9),GP,GPP	00000560
530	FORMAT(//' EG(MEV) EP(FV) DEL(FV)',4X,'G1',6X,'G2',5X,	00000570
	1 'G3',5X,'KAP',6X,'P',7X,'O',7X,'N1',6X,'GP',6X,'GPP'/	00000580
	2 F8.3,F8.4,F8.5,9P8.4)	00000590
	LINE=LINE+4	00000600
50	O1=C01*X(8)	00000610
	O5=C05*X(8)	00000620
	CALL H0INIT(X(1),X(10),Y(2),X(7),X(3),GP,GPP,X(6),	00000630
	1 O1,O5,X(9),EPS)	00000640
	DEV=0D0	00000650
	DO 60 J=1,NP	00000660
	R(J)=0D0	00000670
	DO 60 L=1,NP	00000680
60	R(J,L)=0D0	00000690
	DO 80 I=1,IDAT	00000700
	CALL HCTEDR(HTRN(I),IPOL(I),ITRN(I),FCAL,DE)	00000710
	IF(IT1(I).EO.0) GO TO 65	00000720

	CALL HCTEDR (HTRN (I) , IPOL (I) , IT1 (I) , EC2 , DE2)	00000730
	FCAL=(FCAL+EC2)/2D0	00000740
	DO 64 J=1, NP	00000750
64	DE (J) = (DE (J) +DE2 (J)) /2D0	00000760
65	DELE=ETR (I) -FCAL	00000770
	DO 70 J=1, NP	00000780
	R (J) =R (J) +DELE*DE (J)	00000790
	DO 70 L=1, NP	00000800
70	A (J, L) =A (J, L) +DE (J) *DE (L)	00000810
80	DEV=DELE*DELE+DEV	00000820
	DRMS=DSQR (DEV/IDAT) *1D3	00000830
	T=1	00000840
	PRINT 540, DRMS	00000850
540	FORMAT (/ ' DRMS=' , 1PD10.3, ' MEV: ENTER 0 TO STOP')	00000860
	READ *, I	00000870
	IINF=IINF+4	00000880
	IF (T.FO.0) GO TO 90	00000890
	CALL DMFG (A, 10, NP, IPER, IS, IER)	00000900
	CALL DMSG (A, 10, IPER, NP, C, R, IPR)	00000910
	DO 85 J=1, NP	00000920
85	X (J) =X (J) +R (J)	00000930
	EGM=X (1) *1D3	00000940
	GP=CGP2*X (4) +CGP3*X (5)	00000950
	GPP=CGPP2*X (4) +CGPP3*X (5)	00000960
	IF (LINE.GE.50) CALL NPAGE (LINE, LABEL)	00000970
	PRINT 530, EGM, X (2) , X (10) , (X (I) , I=3, 9) , GP, GPP	00000980
	LINE=LINE+4	00000990
	GO TO 50	0001000
90	IF (X (1) .EQ.0D0) GO TO 95	0001010
	G0=X (2) /3D0/X (1)	0001020
	GC=X (1) / (X (1) +X (10))	0001030
	MC=1D0 / ((GC+2D0) *G0+X (7) *2D0+1D0)	0001040
	GC= ((GC-1D0) *G0+1D0+2D0*X (9)) *2D0	0001050
	MP=X (3) +G0	0001060
	G0=G0/2D0	0001070
	T1=DSQR ((G0+X (4)) **2+3D0* (G0+ (X (4) +X (5)) /2D0) **2)	0001080

	M2=DSORT ((G0+(X(4)+3D0*Y(5))/4D0)**2	00001090
	1 +3D0*(G0+(3D0*X(4)+5D0*X(5))/8D0)**2)	00001100
	M3=DSORT ((G0+X(5))**2+3D0*(G0+(X(4)+2D0*X(5))/3D0)**2)	00001110
	M1=1D0/(MP-T1)	00001120
	M2=1D0/(MP-M2)	00001130
	M3=1D0/(MP-M3)	00001140
	MP=1D0/(MP+T1)	00001150
	PPRINT 580,MC,GC,MP,M1,M2,M3	00001160
580	FORMAT ('/ MC,GC,MP(001),M-(001),(110),(111) =',1P6D12.3)	00001170
	LINE=LINE+2	00001180
95	LINE=66-LINE	00001190
	DO 100 J=1,LINE	00001200
100	PPRINT 570	00001210
570	FORMAT ()	00001220
	GO TO 20	00001230
	END	00001240
	SUBROUTINE NPAGE(LINE,LABL)	00001250
	INTEGER*2 LABL(100)	00001260
	LINE=66-LINE	00001270
	DO 10 L=1,LINE	00001280
10	PPRINT 20	00001290
20	FORMAT ()	00001300
	PPRINT 30,LABL	00001310
30	FORMAT (1X,100A1)	00001320
	PPRINT 20	00001330
	LINE=2	00001340
	RETURN	00001350
	END	00001360
		00001370
		00001380
		00001390
		00001400
		00001410
		00001420
		00001430
		00001440

C	FILE: HCTMBC.FOFT	00000010
C		00000020
C	MINIMIZES MEAN SQUARE DEVIATION WITH RESPECT TO: 1-EG, 2-EP,	00000030
C	3-CK, 4-BK, 5-F, 6-O, 7-N1	00000040
C		00000050
	IMPLICIT REAL*8(A-Z)	00000060
	INTEGER LINE,IP,IT,IPOL(280),ITRN(280),I,IDAT,	00000070
1	J,L,IPRF(8),IS,IFR,NP,IT1(280)	00000080
	INTEGER*2 LABL(100),STOP/'S'//,BL/' '/	00000090
	DIMENSION HTRN(280),FTRN(280)	00000100
	DIMENSION A(10,10),B(10),DE(10),DE2(10),DB(7)	00000110
	COMMON C01,C05,CGP2,CGP3,CGPP2,CGPP3	00000120
	DATA TTH,FTH,OTH,OSX/.666666667D0,1.333333333D0,	00000130
1	.333333333D0,.1666666667D0/	00000140
	DATA C111/.5773502692D0/	00000150
	DATA BK,CK,F,O,N1/5*0D0/	00000160
	DATA EPS/1D-6/,NP/2/	00000170
	IDAT=0	00000180
10	READ (1,600) IP,IT,J,H,E	00000190
600	FORMAT(I1,I2,I2,2F5.1)	00000200
	IF(IP.EQ.0) GO TO 20	00000210
	IDAT=IDAT+1	00000220
	IPOL(IDAT)=IP	00000230
	ITRN(IDAT)=IT	00000240
	IT1(IDAT)=J	00000250
	FTRN(IDAT)=F*1D-3	00000260
	HTRN(IDAT)=H	00000270
	IF(IDAT.EQ.280) GO TO 20	00000280
	GO TO 10	00000290
20	C=C111	00000300
	DO 30 I=1,100	00000310
30	LABL(I)=BL	00000320
	PRINT 500,IDAT	00000330
500	FORMAT(/1X,I3,' DATA POINTS, ENTER LABL/DEL,COSINE,EPS,NP/')	00000340
	READ 610,LABL	00000350
610	FORMAT(100A1)	00000360

	IF (LABL(1) .EQ. STOP) STOP	00000370
	READ *, DEL, C, FPS, NP	00000380
	PRINT 510, LABL	00000390
510	FORMAT (//1X, 100A1)	00000400
	LINE=8	00000410
40	PRINT 520	00000420
520	FORMAT (/' ENTER EGM, EP, CK, BK, F, O, N1')	00000430
	READ *, EGM, EP, CK, BK, F, O, N1	00000440
	LINE=LINE+4	00000450
	IF (EGM .EQ. 0D0) GO TO 90	00000460
	G1=-TTH*BK-PTH*CK-1D0	00000470
	G2=(CK-BK)*OTH	00000480
	G3=OSX*BK-OTH*CK	00000490
	K=OSX*BK+OTH*CK-OTH	00000500
	FC=((3D0*C*C-1D0)/2D0)**2	00000510
	GPP=(G2-G3)*FC	00000520
	GP=G3+GPP	00000530
	GPP=G2/3D0+G3/1.5D0+GPP/6D0	00000540
	O5=(1D0-1.5D0*C*C)*.75D0*C*C	00000550
	C01=(O5-3D0)	00000560
	C05=(3D0*O5+1.25D0)	00000570
	CGP2=FC	00000580
	CGP3=1D0-FC	00000590
	CGPP2=(2D0+FC)/6D0	00000600
	CGPP3=(4D0-FC)/6D0	00000610
	PRINT 530, EGM, EP, DEL, G1, G2, G3, K, F, O, N1, GP, GPP	00000620
530	FORMAT (//' EG (MEV) EP (EV) DEL (EV) ', 4X, 'G1', 6X, 'G2', 5X,	00000630
	1 'G3 ', 5X, 'KAP', 6X, 'F', 7X, 'O', 7X, 'N1', 6X, 'GP', 6X, 'GPP' /	00000640
	2 F8.3, F8.4, F8.5, 9F8.4)	00000650
	LINE=LINE+4	00000660
	EG=EGM*1D-3	00000670
50	O1=C01*O	00000680
	O5=C05*O	00000690
	CALL HCINIT (EG, DEL, EP, F, G1, GP, GPP, K, O1, O5, N1, EPS)	00000700
	DEV=0D0	00000710
	DO 60 J=1, NP	00000720

	R(J)=0D0	00000730
	DO 60 L=1,NP	00000740
60	A(J,L)=0D0	00000750
	DO 70 I=1,IDAT	00000760
	CALL HCTEDR(HTRN(I),IPOL(I),ITPN(I),ECAL,DE)	00000770
	IF(IT1(I).EQ.0) GO TO 65	00000780
	CALL HCTEDR(HTRN(I),IPOL(I),IT1(I),EC2,DE2)	00000790
	ECAL=(ECAL+EC2)/2D0	00000800
	DO 64 J=1,2	00000810
64	DE(J)=(DE(J)+DE2(J))/2D0	00000820
65	DELE=PTRN(I)-PCAL	00000830
	DEV=DELE*DELE+DEV	00000840
	DB(1)=DE(1)	00000850
	DB(2)=DE(2)	00000860
	DB(4)=OSX*(DE(5)+DE(6))-TTH*DE(3)-OTH*DE(4)	00000870
	DB(3)=OTH*(DE(4)-DE(5)+DE(6))-PTH*DE(3)	00000880
	DB(5)=DE(7)	00000890
	DB(6)=DE(8)	00000900
	DB(7)=DE(9)	00000910
	DO 70 J=1,NP	00000920
	B(J)=B(J)+DELE*DB(J)	00000930
	DO 70 L=1,NP	00000940
70	A(J,L)=A(J,L)+DB(J)*DB(L)	00000950
	DRMS=DSORT(DEV/IDAT)*1D3	00000960
	I=1	00000970
	PRINT 540,CK,BK,DRMS	00000980
540	FORMAT(/' CK,BK=',F8.4,' ',F8.4,' DRMS=',1PD10.3,	00000990
	1 ' MEV: ENTER 0 TO STOP')	00001000
	READ *,I	00001010
	LINE=LINE+4	00001020
	IF(I.EQ.0) GO TO 90	00001030
	CALL DMPG(A,10,NP,IPER,IS,IEP)	00001040
	CALL DMSG(A,10,IPER,NP,0,R,IER)	00001050
	EG=EG+B(1)	00001060
	EP=EP+B(2)	00001070
	IF(NP.LT.3) GO TO 82	00001080

	IF (NP.LT.4) R(4)=0D0	00001090
	G1=G1-PTH*B(4)-PTH*B(3)	00001100
	G2=G2-OTH*(R(4)-B(3))	00001110
	G3=G3+OSX*B(4)-OTH*B(3)	00001120
	K=K+OSX*B(4)+OTH*B(3)	00001130
	GPP=(G2-G3)*FC	00001140
	GP=G3+GPP	00001150
	GPP=G2/3D0+G3/1.5D0+GPP/6D0	00001160
	IF (NP.GE.5) F=F+B(5)	00001170
	IF (NP.GE.6) O=O+B(6)	00001180
	IF (NP.GE.7) N1=N1+B(7)	00001190
82	FGM=FG*1D3	00001200
	IF (LINE.GE.50) CALL NPAGE (LINE, LABEL)	00001210
	PRINT 530, FGM, FP, DEL, G1, G2, G3, K, F, O, N1, GP, GPP	00001220
	LINE=LINE+4	00001230
	IF (NP.GE.4) BK=BK+B(4)	00001240
	IF (NP.GE.3) CK=CK+B(3)	00001250
	GO TO 50	00001260
90	IF (EG.EQ.0D0) GO TO 95	00001270
	G0=EP/3D0/EG	00001280
	GC=EG/(EG+DEL)	00001290
	MC=1D0/((GC+2D0)*G0+F*2D0+1D0)	00001300
	GC=((GC-1D0)*G0+1D0+2D0*N1)*2D0	00001310
	MP=G1+G0	00001320
	G0=G0/2D0	00001330
	T1=DSORT((G0+G2)**2+3D0*(G0+(G2+G3)/2D0)**2)	00001340
	M2=DSORT((G0+(G2+3D0*G3)/4D0)**2	00001350
	+3D0*(G0+(3D0*G2+5D0*G3)/8D0)**2)	00001360
	M3=DSORT((G0+G3)**2+3D0*(G0+(G2+2D0*G3)/3D0)**2)	00001370
	M1=1D0/(MP-T1)	00001380
	M2=1D0/(MP-M2)	00001390
	M3=1D0/(MP-M3)	00001400
	MP=1D0/(MP+T1)	00001410
	PRINT 580, MC, GC, M1, M2, M3	00001420
580	FORMAT(/' MC, GC, M+(001), M-(001), (110), (111) =' , 1P6D12.3)	00001430
	LINE=LINE+2	00001440

95	LINE=66-LINE	00001450
	DO 100 J=1,LINE	00001460
100	PRINT 570	00001470
570	FORMAT()	00001480
	GO TO 20	00001490
	FND	00001500
	SUBROUTINE NPAGE(LINE,LABL)	00001510
	INTEGER*2 LABL(100)	00001520
	LINE=66-LINE	00001530
	DO 10 L=1,LINE	00001540
10	PRINT 20	00001550
20	FORMAT()	00001560
	PRINT 30,LABL	00001570
30	FORMAT(1X,100A1)	00001580
	PRINT 20	00001590
	LINE=2	00001600
	RETURN	00001610
	FND	00001620
C		00001630
C		00001640
C		00001650
C		00001660
C		00001670
C		00001680
C		00001690
C		00001700
C		00001710
C		00001720
C		00001730
C		00001740
C		00001750
C		00001760
C		00001770
C		00001780
C		00001790
C		00001800

ACKNOWLEDGEMENTS

I gratefully acknowledge the guidance and support of Dr. R.L. Aggarwal and Prof. B. Lax during the years I have spent at the Francis Bitter National Magnet Laboratory as a staff member and student. I am particularly grateful to them for their guidance of this thesis investigation, and for their support and patience during the years when my time was divided between physics and child care.

I wish to thank L. Sousa for his assistance with the experiments, E.J. Alexander for the sample preparation and orientation measurements, D. Nelson for advice on computer techniques, and L. Rubin for assistance with instrumentation. I am grateful to Mary Finn of Lincoln Laboratory for performing the microprobe measurements on the $\text{Hg}_{1-x}\text{Cd}_x\text{Te}$ samples, and to W. Zawadzki for sending me his results prior to publication. I acknowledge helpful discussions with Drs. S.H. Groves and G. Dresselhaus about the zincblende $\vec{k}\cdot\vec{p}$ Hamiltonian. I wish to thank M. McDowell for typing this manuscript.

Finally, I wish to express my gratitude to my husband and children for their patience and support during my student years and, particularly, during this thesis investigation.

BIOGRAPHICAL NOTE

Margaret Horton Weiler was born on April 30, 1941, in Sewickley, Pennsylvania, where she attended Sewickley Academy until 1956. She graduated with distinction from Milton Academy, Milton, Massachusetts, in 1959. She received the A.B. degree, Summa Cum Laude in Physics, from Radcliffe College in 1962, having been elected to Phi Beta Kappa in her junior (and final) year. She was married to William M. Weiler in June, 1962. She received the M.S. degree in Physics from the University of Maine in June, 1964, and was an Instructor in Physics there in 1964-5. While a student there she was elected to Phi Kappa Phi, Sigma Pi Sigma and Sigma Xi. She became a Staff Member of the Francis Bitter National Magnet Laboratory in 1965, working half time after the birth of her first son, Christopher, in November, 1968; her second son, Theodore, was born in January, 1972. She became a full-time graduate student and Research Assistant at M.I.T. in 1974.